MAX-PLANCK-INSTITUT
FÜR METEOROLOGIE

Understanding the dynamics of late Quaternary African humid periods

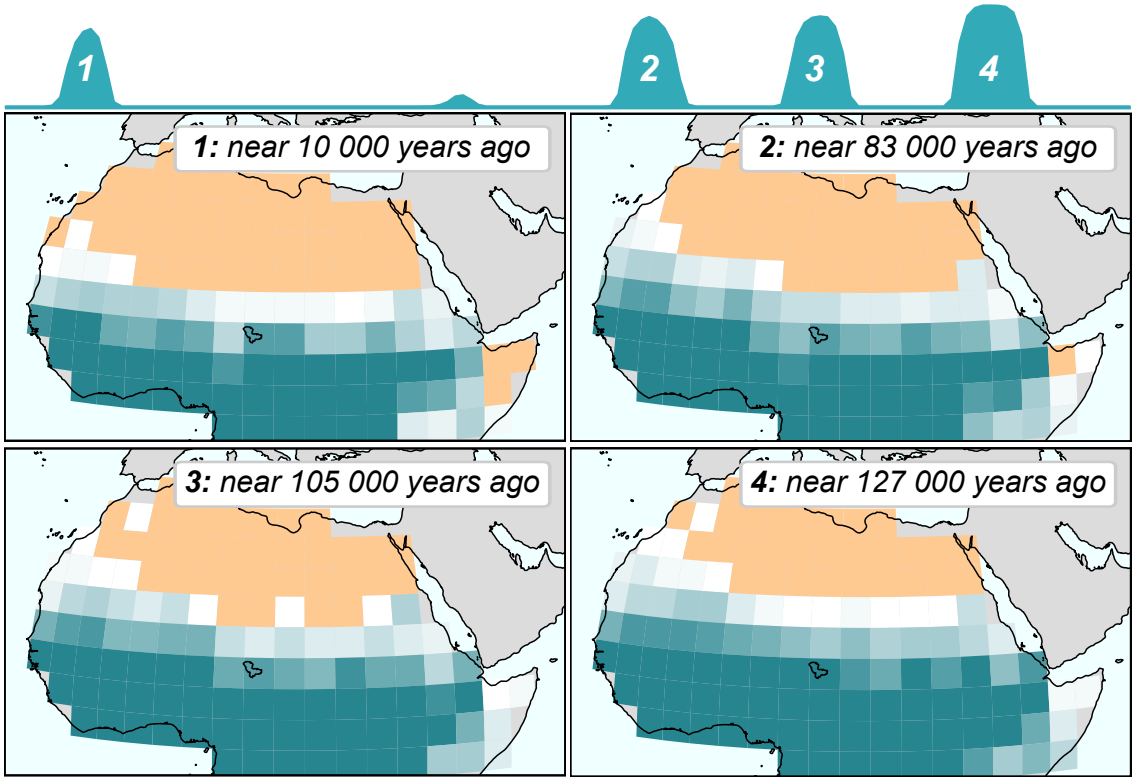

Mateo Duque-Villegas

Hamburg 2023

Berichte zur Erdsystemforschung 272
Reports on Earth System Science 2023

Hinweis

Die Berichte zur Erdsystemforschung werden vom Max-Planck-Institut für Meteorologie in Hamburg in unregelmäßiger Abfolge herausgegeben.

Sie enthalten wissenschaftliche und technische Beiträge, inklusive Dissertationen.

Die Beiträge geben nicht notwendigerweise die Auffassung des Instituts wieder.

Die "Berichte zur Erdsystemforschung" führen die vorherigen Reihen "Reports" und "Examensarbeiten" weiter.

Anschrift / Address

Max-Planck-Institut für Meteorologie
Bundesstrasse 53
20146 Hamburg
Deutschland

Tel./Phone: +49 (0)40 4 11 73 - 0
Fax: +49 (0)40 4 11 73 - 298

name.surname@mpimet.mpg.de
www.mpimet.mpg.de

Notice

The Reports on Earth System Science are published by the Max Planck Institute for Meteorology in Hamburg. They appear in irregular intervals.

They contain scientific and technical contributions, including PhD theses.

The Reports do not necessarily reflect the opinion of the Institute.

The "Reports on Earth System Science" continue the former "Reports" and "Examensarbeiten" of the Max Planck Institute.

Layout

Bettina Diallo and Norbert P. Noreiks
Communication

Copyright

Understanding the dynamics of late Quaternary African humid periods

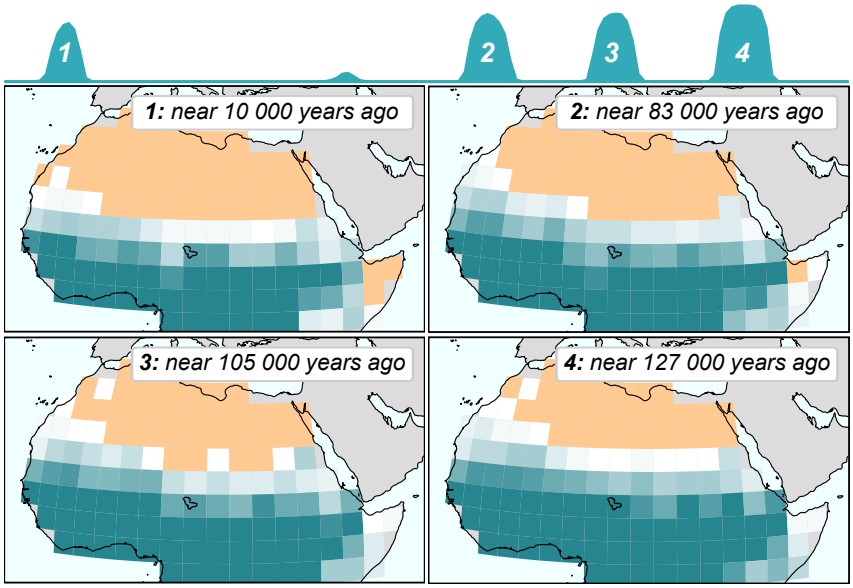

Mateo Duque-Villegas

Hamburg 2023

Mateo Duque-Villegas
aus Medellín, Kolumbien

Max-Planck-Institut für Meteorologie
The International Max Planck Research School on Earth System Modelling
(IMPRS-ESM)
Bundesstrasse 53
20146 Hamburg

Tag der Disputation: 21. November 2023

Folgende Gutachter empfehlen die Annahme der Dissertation:
Prof. Dr. Martin Claußen
Prof. Dr. Victor Brovkin

Vorsitzender des Promotionsausschusses:
Prof. Dr. Hermann Held

Dekan der MIN-Fakultät:
Prof. Dr.-Ing. Norbert Ritter

Titelgrafik: *Peaks in simulated vegetation fraction in the Sahara and related vegetation cover patterns in North Africa during the last four African humid periods of the late Quaternary. Credit: Mateo Duque-Villegas*

Berichte zur Erdsystemforschung / Max-Planck-Institut für Meteorologie 272
Reports on Earth System Science / Max Planck Institute for Meteorology 2023

ISSN 1614-1199 - doi: 10.17617/2.3556280

Mateo Duque-Villegas

Understanding the dynamics of late Quaternary African humid periods

ABSTRACT

Geological records reveal broad swings in hydro-climatology of North Africa in the late Quaternary (about the last million years), characterized by repeated expansion of water resources and vegetation cover deep into the Sahara. Episodes of Saharan greening and extensive humid climate in North Africa are known as African humid periods (AHPs). The best known AHP case is the latest event, happening roughly between 11 700 to 4200 years ago. Although it has been thoroughly examined with available evidence, uncertainty about its full extent and causes still clouds AHP understanding. More uncertain is what happened during AHPs before the last one. A complete AHP theory is key to explain, for instance, regional geomorphology, hominin evolution, and the climate–land surface interactions driving the land cover changes. Advances in climate proxies and models offer now the possibility to examine in more detail several ancient AHPs of the late Quaternary. That is the major goal of the work in this thesis. The dissertation includes research that uses two climate models of different complexity to resolve temporal and spatial climate patterns of at least four distinct past AHPs. One study disentangles contributions from three known AHP forcing factors: Earth's orbital parameters, greenhouse gases (GHGs) and ice sheets. Unprecedented factor separation analyses highlight the dominance of the orbital forcing and quantify it as sole contributor of about 80 % of vegetation cover changes during AHPs. GHGs and ice sheets have far smaller contributions, being only considerably effective when in synergy with the orbital forcing. Remarkable is the discovery of an insolation threshold for simulated Saharan greening that agrees with a threshold for humidity signals in Mediterranean marine sediments. Moreover, the insolation threshold appears clearly sensitive to levels of GHGs. A follow-up study evaluates such forcing–AHP relationships in simulated vegetation cover patterns of North Africa over the last glacial cycle. For this, an exceptionally long climate simulation is run at enough spatial resolution to include patterns of four AHPs. All simulated AHPs show a northwest–southeast tilted front of northward push of vegetation cover, which scales in intensity proportionally to climatic forcing. Pattern scaling is used to estimate roughly vegetation cover in North Africa of the last 800 000 years. These studies contain also simulated future AHPs, which stress the lesson that AHP past differs from AHP future, since scenarios of GHGs-induced warming predict new kinds of AHPs. Altogether this dissertation expands AHP theory towards more ancient and future events, and identifies AHP patterns that seem to be preserved along glacial cycles.

ZUSAMMENFASSUNG

Klimaarchive zeigen, dass es große Schwankungen in den Umweltbedingungen Nordafrikas im späten Quartär (etwa die letzte Million Jahre) gab, die durch mehrmalige Ausbreitung der Wasserquellen und Vegetationsdecke bis tief hinein in die Sahara gekennzeichnet sind. Das wiederholte Auftreten einer grünen Sahara und eines sehr feuchten Klima Nordafrikas sind als afrikanische Feuchtperioden bekannt. Der bekannteste Fall ist der letzte, der um 11 700 bis 4200 geschah. Obwohl die letzte Feuchtperiode auf Basis der vorhandenen Daten erforscht wurde, sind die volle Ausbreitung und Ursachen noch unklar. Noch unsicherer ist das Wissen um die vorherigen Feuchtperioden. Eine vollständige Theorie der Feuchtperioden ist besonders wichtig, um, zum Beispiel, Regionalgeomorphologie, Menschheitsevolution und die die Änderungen der Landbedeckung antreibenden Wechselwirkungen zwischen Klima und Landoberfläche zu erklären. Fortschritte in den Klimaarchiven und Klimamodellen ermöglichen es jetzt, mehrere ältere Feuchtperioden des späten Quartärs detaillierter zu forschen. Das ist das Hauptziel dieser Arbeit. Die Dissertation umfasst Studien, die mit zwei Klimamodellen verschiedener Komplexität erstellt wurden, um temporale und räumliche Klimamuster von mindestens vier Feuchtperioden der Vergangenheit zu analysieren. Eine Studie entwirrt die Beiträge von drei bekannten Klimaantreibern der Feuchtperioden: Erdbahnparameter, Treibhausgaskonzentrationen und Eisschilder. Neue Faktor-Trennungsanalysen zeigen, dass die Änderungen der Erdbahn der dominierende Faktor ist, und quantifizieren ihn als alleiniger Treiber von rund 80 % der Änderungen der Vegetationsdecke während der Feuchtperioden. Treibhausgaskonzentrationen und Eisschilder zeigen viel kleinere Beiträge, und sind nur zusammen mit Änderungen der Erdbahn deutlich wirksam. Bemerkenswert ist die Entdeckung eines Schwellenwerts der Sonneneinstrahlung für die Simulation einer grünen Sahara, der mit dem Schwellenwert für Feuchtigkeitssignale in Meeressedimenten des Mittelmeers übereinstimmt. Der Schwellenwert ist außerdem eindeutig empfindlich gegen Treibhausgaskonzentrationen. Eine nachfolgende Studie bewertet solche Beziehungen zwischen Antrieb und Feuchtperioden in Mustern der simulierten Vegetationsdecke Nordafrikas des letzten glazialen Zyklus. Dafür wird eine außergewöhnlich lange Klimasimulation mit genügender räumlicher Auslösung gerechnet, um Muster von vier Feuchtperioden einzubeziehen. Alle simulierten Feuchtperioden zeigen eine nordwest-südost geneigte Front einer Verschiebung der Vegetationsdecke nach Norden, die mit der Intensität des Klimaantriebs proportional skalierbar ist. Musterskalierung wird

benutzt, um grobe Schätzungen der Vegetationsdecke in Nordafrika der letzten 800 000 Jahren zu erstellen. Diese Studien enthalten auch simulierte zukünftige Feuchtperioden, die betonen, dass die Zukunft der Feuchtperioden anders aussieht als ihre Vergangenheit, denn Szenarien von durch Treibhausgaskonzentrationen verursachte globale Erwärmung sagen neue Arten von Feuchtperioden vorher. Insgesamt wird in dieser Dissertation die AHP-Theorie auf ältere und zukünftige Ereignisse ausgeweitet und es werden AHP-Muster identifiziert, die entlang von glazialen Zyklen erhalten zu bleiben scheinen.

PUBLICATIONS RELATED TO THIS DISSERTATION

APPENDIX A

Duque-Villegas, M., Claussen, M., Brovkin, V., & Kleinen, T. (2022). Effects of orbital forcing, greenhouse gases and ice sheets on Saharan greening in past and future multi-millennia. *Climate of the Past*, *18*(8), 1897–1914. DOI: 10.5194/cp-18-1897-2022.

APPENDIX B

Duque-Villegas, M., Claussen, M., Kleinen, T., Bader, J., & Reick, C. H. (2023). Vegetation cover changes in North Africa scaled with climatic forcing across glacial cycles. *In preparation*, 1–20.

CONTENTS

UNIFYING ESSAY

1 INTRODUCTION

Past climate change was recorded around the globe in preserved geological features. Examination of the geological record often yields clues about formerly possible environmental conditions. Some alternative past environments appear so contrasting with current landscapes that explaining their origin becomes a fascinating scientific challenge. How diverse is the set of patterns that climate on Earth can adopt? Understanding how such different environments came about and transformed is a key part of Earth system science, and may even offer insight into potential future climate change.

This dissertation is concerned with climate modelling of past environmental changes in North Africa, which repeatedly vegetated much of the Sahara, in the course of millennia, while the Earth system underwent the latest set of glacial cycles. The structure of this cumulative thesis comprises this opening synthesis essay and an appendix with two first-authored manuscripts. The goal of this unifying essay is, first, to expose the motivation and scientific context that led to specific research questions, and second, to condense the key findings of the manuscripts in the appendix. It closes with a summary of their implications and the way forward.

1.1 MOTIVATION

This thesis investigates changes in the climate of North Africa during the late Quaternary, when the last several glacial cycles developed at orbital (multi-millennial) pacing. While global temperature averages undulated during these cycles, North Africa experienced drastic periodic changes in hydrology and land cover that saw repeated expansion and contraction of the hyper-arid ecosystems found today only within the Sahara (Claussen et al., 2017). Evidence of such large regional environmental changes not only abounds in surrounding geological records, but also agrees with results from a diverse suite of numerical climate models (Pausata et al., 2020).

The continental scale of hydro-climatological change makes it already a compelling research field within the geosciences: What forces are able to transform periodically the Sahara into a hospitable environment for widespread vegetation? Furthermore, as an instance of recorded extensive climate change, North Africa opens a possibility for testing the physical understanding behind numerical climate models (e.g. climate–land surface interactions). Although models in many

cases agree with field data, enduring discrepancies point to missing parts in current theory (Brierley et al., 2020). Moreover, another compelling fact about past climate in North Africa is that it most likely influenced some outcomes of hominin evolution (Blome et al., 2012).

Similar reasons have motivated much previous science about palaeoclimatology of North Africa (e.g. Grove & Warren, 1968; Street & Grove, 1976; Ritchie et al., 1985; deMenocal, 1995; Tuenter et al., 2003; Shanahan et al., 2015; Yacoub et al., 2023). Especially as a testing ground for climate models, where field data consistently suggest there is room for improvement (Braconnot et al., 2012; Harrison et al., 2015). However, many former studies are tied to evaluation of a single event: the Holocene environmental change in North Africa (e.g. Tierney et al., 2017b; Gaetani et al., 2017), spanning roughly between 11.7 ka to 4.2 ka (ka: age of a thousand years ago). Because this is not far on the geological timescale, plenty of evidence survives which is amply descriptive and opens the door for modellers to evaluate climate simulations. But how representative is a single event? What preceded it?

How did climate change in North Africa before the Holocene? Scarce field data suggest earlier times had more intense changes (minimum Sahara), like during the previous interglacial, roughly around 125 ka (Larrasoaña et al., 2013). However, the extent of the previous interglacial changes is contested (Scerri et al., 2014). Similarly, it is unclear what happens during the over 100 kyr (kyr: duration of a thousand years)[1] between the previous and Holocene interglacials (Drake et al., 2013). Unfortunately, the cyclical nature of such climate change, its spatial scale and concomitant geological processes, erased much of the oldest traces (Drake et al., 2018). Moreover, climate modelling of such ancient times is restricted in terms of model complexity and spatio-temporal resolution. Hence, field and modelling approaches both face considerable limitations when studying pre-Holocene North African climate.

Much insight comes from deep-sea sediments nearby (e.g. McGee et al., 2013; Ehrmann et al., 2017). The underlying assumption is that the amount of sediments that accumulate at the seafloor must be proportional to the amount of terrigenous material over North Africa available for transport (Rea, 1994). Certain land cover types will provide more sediment material to surrounding seas, and also the geochemical composition of the transported material can be analysed for provenance. Because sediments can accumulate (mostly) undisturbed for long periods, they provide a rich stacked archive that usually reaches deep back in time. Such kind of data reveals, for instance, the periodic nature of the environmental changes in North Africa, which

1 About time units: ka is a date or time location in the past, while kyr is a duration or time difference; estimates in thousand of years. Similar for Ma and Myr with million years. Future times are presented as kyr after present (AP).

seem to be taking place since 11 Ma (Ma: age of a million years ago) at least (Crocker et al., 2022). Nevertheless, there are limits to what can be inferred is happening on land, and therefore other means of verification are called for. Given a severe lack of relevant continental data extending until the previous interglacial, climate modelling remains a viable option despite limitations.

This thesis aims at understanding environmental changes in North Africa over the last 200 kyr. It is a time of large swings in global climate variability, when superimposed local and remote effects likely influenced North African conditions. From a climate modelling approach, this study relies on two different models of varying complexity, in order to address different kinds of research questions within sensible computing times. A strong focus is on the influence of the main forces that drive changes in North Africa across the glacial cycles. The following sections provide an overview of relevant scientific background.

1.2 AFRICAN HUMID PERIODS

Many landforms in North Africa reveal a wet past: ancient river networks, palaeolake shorelines, calcareous deposits and speleothems are features around the Sahara that required abundant water to originate (Gasse et al., 1990; Cremaschi et al., 2010; Drake et al., 2011; El-Shenawy et al., 2018). Archaeological explorations also collected evidence for ancient life-sustaining hydrology, including fossil flora and fauna, artefacts and other signs of prehistoric settlements, all in places that today are so arid they are almost life-averse (Kowalski et al., 1989; Pachur & Hoelzmann, 1991; Nicoll, 2004; Scerri, 2017).

Stratigraphy and age estimates at North African sites indicated water levels fluctuated multiple times during glacial cycles of the late Quaternary (Gaven et al., 1981; Armitage et al., 2007; Causse et al., 2003; Smith et al., 2004). Humidity variations were also clearly marked in colour and geochemical gradients in sediment cores drilled from nearby seafloors (Rossignol-Strick, 1983, 1985). Pollen assemblages from sediments showed changes in terrestrial plants tracking the humidity fluctuations (Lézine & Casanova, 1991; L. M. Dupont, 1993). Further analyses resulted in long chronologies of a few million years of regional climate change, with distinct relatively arid and humid phases (Larrasoaña et al., 2003; Grant et al., 2017). Arid phases would align with current conditions, though more extreme aridity and a larger Sahara were also possible near glacial maxima (Sarnthein, 1978). In contrast, humid phases would periodically promote invasion of vegetation and wildlife into the Sahara (Pachur & Hoelzmann, 2000).

The last humid phase developed from about 11.7 ka until 4.2 ka (Tierney et al., 2017b). Its humidity signal is frequently recognized in diverse data sources from the Holocene epoch in North Africa, albeit

with spatially varying degrees of intensity (Shanahan et al., 2015). Records indicate the appearance of freshwater bodies deep inside the Sahara (Lézine et al., 2011), surrounded by gallery forests and wooded grasslands (Watrin et al., 2009), including some tropical species that migrated northward (Hély et al., 2014). Vegetation cover stabilized soils and greatly reduced dust output onto surrounding seas (McGee et al., 2013). Water and plant resources then harboured wildlife and prehistoric populations (Kuper & Kröpelin, 2006; Manning & Timpson, 2014). These events broadly describe what is commonly known as the "African Humid Period" (AHP) of the Holocene (deMenocal et al., 2000), even though such changes may not represent whole Africa (Chase et al., 2022; L. A. Dupont et al., 2022). Alternatively, "green Sahara" or "Sahara(n) greening" of the Holocene, likewise denote this humid phase (Kröpelin et al., 2008).

Decades of interdisciplinary research provided deep understanding of what unfolded in North Africa during the Holocene AHP (Claussen et al., 2017; Holmes & Hoelzmann, 2017; Lézine, 2017; McGee & deMenocal, 2017; Yacoub et al., 2023). Nevertheless, questions remain about driving mechanisms, seasonality, extent and timing of the changes (Pausata et al., 2020). Some issues relate to evaluation of current physical theory (i.e. climate models) against available field data (Brierley et al., 2020). It may seem overly optimistic to expect all lines of evidence to completely agree for a region as large as North Africa, but a consensus on the broad patterns is crucial. Other questions pertain interpretation of sparse and discontinuous existing records, like defining the extent of large lakes in the Sahara (Quade et al., 2018). And even more unknowns arise when considering earlier times to study hominin evolution (Scerri et al., 2018), or future times to anticipate potential effects of climate change (Tierney et al., 2020b).

Clarifying details may emerge from looking at previous AHPs. Drake et al. (2022) stress the need for considering older AHPs when interpreting palaeolake data in the Sahara. Indeed, the Holocene AHP was only the youngest iteration of a phenomenon that occurred repeatedly and left multiple tracks (e.g. Geyh & Thiedig, 2008). But it is challenging to establish a continuous chronology of environmental change, covering pre-Holocene AHPs, based on existing continental sedimentary records, which are scarce and severely fragmented. For instance, Drake et al. (2011) group distant humidity dates into a single long pre-Holocene AHP around the previous interglacial (ca. 125 ka), yet it is possible the dates indicate multiple shorter AHPs.

Paucity in continental sources, as well as dating uncertainties, can be partly balanced with marine records, which are often highly resolved and indirectly linked to changes on land. Blome et al. (2012) and Drake et al. (2013) compile land and ocean records for the Middle and Upper Pleistocene (ca. 350 ka to 30 ka). They report likely time ranges of sustained humidity in North Africa roughly centred about 125 ka

(most certain), 105 ka and 80 ka. Widespread aridity probably resumed around 70 ka and prevailed until the Holocene AHP. Such three humid events may represent the closest predecessors to the Holocene AHP.

The timing of potential pre-Holocene AHPs coincides nearly with peak tropical insolation phases. This was also observed in marine stratigraphy by Rossignol-Strick (1983), who noted sapropel bands appeared in sediment cores only when summer solar radiation peaked at the tropics. Sapropels form in anoxic conditions, when deep waters stagnate due to poor overturning circulation (Rossignol-Strick et al., 1982). Increased rainfall over North African watersheds (like during an AHP) would lead to stronger river discharge offshore (e.g. Nile to Mediterranean) enough to disturb deep-water formation and promote sapropel formation. Thus, marine sediment cores not only contain biogeochemical gradients linked to wind activity, but also such sapropels tracking drainage in nearby water basins (Rohling et al., 2015).

A data compilation by Larrasoaña et al. (2013) showed that sapropels in marine cores track well North African climate variability, in line with the few existing terrestrial sources. Based on Mediterranean sapropels of the last 8 Myr, they report 230 potential past AHPs. Such figure might be even larger according to finely resolved geochemical analyses of the sediments, which can detect more subtle humidity signals (Grant et al., 2022). Moreover, the age of humidity fluctuations in the Sahara seems to be closer to 11 Ma (Crocker et al., 2022). In spite of the total count, the problem remains in estimating environmental conditions of such ancient AHPs.

Inferring pre-Holocene climatic conditions from the geological record is not straightforward. Various possible spatial arrangements of biogeographical and hydrological components could produce the signals recorded in the marine sediments. Difficult as well is to generalize over large areas the evidence of sparsely distributed continental sources. Nevertheless, using the more established Holocene AHP as a starting guide, Drake et al. (2011) and Larrasoaña et al. (2013) estimated the landscape of the previous-interglacial AHP (ca. 125 ka). A necessary assumption in Larrasoaña et al. (2013) is persistence of a broad zonal pattern of bioclimatic zones, interrupted by topographic constraints. The reconstruction shows a much stronger AHP, with larger precipitation estimates and almost no desert cover in the Sahara. Although the extent of the changes may be uncertain (Scerri et al., 2014), an updated version in Larrasoaña (2021) seems to agree with current findings.

Future field work and laboratory analyses may uncover further details about Holocene, previous-interglacial or past AHPs alike. Filling gaps in the geological record would help outline more accurately the extent of the changes in North African climate variability, as well as prevent regional biases in continent-wide assessments. What follows

is to also understand the forces behind AHP dynamics, which drive the climate changes of recorded humid–arid fluctuations. Why would a previous-interglacial AHP be stronger than a Holocene one? In the following section some of the main known mechanisms are discussed.

1.3 CLIMATE CHANGE DRIVERS IN NORTH AFRICA

The late Quaternary was a time of large-amplitude climate variability, in response to natural rhythms of Earth's planetary motion (Broecker et al., 1968; Hays et al., 1976). Astronomical variations in the timing of the seasons, axial tilt and orbit eccentricity modulated patterns of incoming solar radiation, effectively redistributing the solar input and forcing the climate system to change (Berger, 1988). Parts of the climate system then responded complexly across millennia, leading to adjustments in, for example, global temperature, ice sheets, carbon cycle and monsoon systems (Past Interglacials Working Group of PAGES, 2016; Cheng et al., 2022). In addition, long-lasting climatic effects could propagate globally and, due to diverse inertial times, superimpose the astronomically forced changes in some places.

In North Africa the immediate response to insolation emerged the major driver of past climate change and AHPs (Rossignol-Strick, 1983; Pokras & Mix, 1985; Prell & Kutzbach, 1987). Regional insolation was mainly controlled by Earth's precession (Pokras & Mix, 1987; Larrasoaña et al., 2003); a cycle in the Earth–Sun distance which defines seasons orbital position and length (Berger et al., 1992). At times when boreal summer solstice happened near the perihelion, increased summer solar heating intensified inter-hemispheric and land–ocean thermodynamic contrasts, thereby strengthening tropical circulation, monsoon winds and poleward moisture transport (Wang et al., 2014). Such precessional effects involved local and remote contributions, and were further tuned by coeval cycles in obliquity (Earth's axial tilt) and eccentricity (Tuenter et al., 2003, 2005).

Orbital forcing is perhaps a necessary but not sufficient condition to develop AHPs (Claussen et al., 2017). Based on the geological record, additional controls seem to set an insolation threshold that would explain the irregular spacing in humidity signals (Rossignol-Strick, 1983; Lourens et al., 2001). Moreover, the threshold seems to change over time, according to proxy records that show some insolation peaks at times triggering potential AHPs but not always (Grant et al., 2022). In models as well, orbital forcing alone failed to induce the magnitude of changes in geological records (e.g. Jolly et al., 1998). That suggests a nonlinear response to this forcing, as seen elsewhere in a complex climate system (Westerhold et al., 2020).

Several self-reinforcing mechanisms could amplify orbitally induced variations in North Africa. As rain-bearing systems intensified and

penetrated further north during AHPs, vegetation spread widely, and wet soils darkened, lowering surface albedo while increasing transpiration and surface roughness, which combined to promote convection, rainfall and more vegetation growth (Brovkin et al., 1998; Levis et al., 2004; Foley et al., 2003; Jungandreas et al., 2023). Similarly, water accumulation in wetlands and lakes could change surface energy and moisture fluxes to reinforce rainfall and water storage (Coe & Bonan, 1997; Specht et al., 2022). A reduced load of atmospheric dust was also shown to increase precipitation, which then expands soil-stabilising vegetation cover and further curtails dust emissions (Pausata et al., 2016). Furthermore, changes in low-level winds during AHPs also interact with nearby seas, via changes in upwelling mixing that maintain sea surface temperature (SST) gradients which favour monsoon precipitation (Kutzbach & Liu, 1997; Liu et al., 2004; Zhao et al., 2005). Such interactions likely accelerated and magnified any orbitally paced changes.

Besides orbital forcing and regional feedbacks, it is important to consider glacial variability and large-scale climate (Nicholson & Flohn, 1980; deMenocal et al., 1993; Chiang & Friedman, 2012). Changes in global ice cover, sea level and atmospheric greenhouse gases (GHGs) are fairly well characterized for the late Quaternary (Abe-Ouchi et al., 2013). Cryosphere, global carbon cycle and general circulations (atmosphere and ocean) are climate subsystems whose planetary impact probably acted as additional forcing on North African climate (Weber & Tuenter, 2011). The roughly 100-kyr cycle of glaciations is considerably slower than the roughly 20-kyr precessional cycle linked to AHPs (Cheng et al., 2022). A slowly adjusting global context would affect the local immediate response to insolation around the Sahara.

Continental ice sheets probably influenced the position of atmospheric flows important for North African rainfall (Collins et al., 2017; Wagner et al., 2019). When boreal ice cover melted into the North Atlantic, cold freshwater could disturb ocean temperature and circulation profiles, eventually preventing a northward displacement of tropical atmospheric circulation, thus weakening monsoon systems (Tjallingii et al., 2008; Marzin et al., 2013). GHGs and temperature directly influence the global water vapour distribution in the atmosphere, which affects moisture supply everywhere (Claussen et al., 2003; D'Agostino et al., 2019). Moreover, CO_2 in the atmosphere also has a direct influence on biomass production and ecosystem composition (O'Mara et al., 2022). And other complex long-range interactions are possible, like Walker Circulation variability inducing zonal gradients across Africa (Boos & Korty, 2016; Kaboth-Bahr et al., 2021).

In brief, even though the orbital forcing stands out as the pacemaker of the late Quaternary, many other climate processes should be relevant as well to understand the development of past AHPs. It is important to clarify how the externally driven changes propagate across

scales to periodically ameliorate the climate of North Africa. Isolating the individual or collective influence of some of these factors can be done through climate modelling. In the following section some past applications and current challenges of AHP modelling are discussed.

1.4 MODELLING SAHARA GREENING

AHPs were often featured in palaeoclimate simulations (Claussen et al., 2017). Their continental scale and drastic humidity swings made AHPs some of the most prominent climate changes of the late Quaternary. Accordingly, enough evidence existed to establish long ago North African palaeoclimate as a useful reference for evaluating numerical models (COHMAP Members, 1988). Especially the last greening of the Sahara around the mid-Holocene (ca. 6 ka) has been regularly used as a standard in model inter-comparison projects (Braconnot et al., 2007, 2012; Harrison et al., 2015; Brierley et al., 2020). While documentation of the geological record grew, climate models also improved (Haywood et al., 2019), and along the way integrated analyses enabled consensus on key aspects of AHP theory (Pausata et al., 2020). Nevertheless, well-known quantitative mismatches have limited model–data reconciliation for decades (Tierney et al., 2017b; Brierley et al., 2020).

Early (equilibrium) atmosphere-only simulations already detected the crucial effects of orbital forcing on monsoon intensification during AHPs (Kutzbach, 1981; Kutzbach & Otto-Bliesner, 1982; Kutzbach & Street-Perrott, 1985). Glacial variability (atmospheric boundary conditions and CO_2) was also shown to amplify slightly seasonal cycles (Kutzbach & Guetter, 1986; Prell & Kutzbach, 1987). Such effects were enough for simulations to align with broad trends in existing records at the time. However, as climate models and palaeoenvironmental analyses became more sophisticated, and broadened their spatial and temporal coverage, it became increasingly difficult to reconcile all evidence at regional scales (Webb III & Kutzbach, 1998). In North Africa, model–data comparisons for the mid-Holocene showed that AHP simulations fell short of rainfall intensity and desert reduction estimates (Jolly et al., 1998; Joussaume et al., 1999). Models failed to deliver enough rainfall (about 500 mm yr^{-1}) deep in the Sahara (north of 23°N) to sustain the biome types and lakes indicated by the data.

After interactive coupling of various Earth system components, amplifying feedback mechanisms emerged that reduced the model–data gap (Kutzbach et al., 1996; Texier et al., 1997; Claussen & Gayler, 1997; Coe & Bonan, 1997; Kutzbach & Liu, 1997; Broström et al., 1998; Braconnot et al., 1999). Feedbacks included coupled atmosphere–ocean interactions with land–sea surface properties like SST, sea ice, marine upwelling, vegetation cover, lakes, wetlands and soil moisture. Individually such interactions could push northward a few degrees

the southern limit of the Sahara (today straddling 18°N) or could double precipitation changes relative to the preindustrial era. Despite progress, some results were model-dependent and following studies would find competing effects between some of the interactions (Levis et al., 2004; Notaro et al., 2008). Above all, simulations still could not bring much additional rainfall past 23°N (Braconnot et al., 2007). It seemed feedback interactions could be missing or weakly represented in the models (Kutzbach et al., 2001).

The strength of the feedbacks came especially into focus when simulations, together with proxy records, suggested that the climate–vegetation coupling was strong enough to induce abrupt changes during AHPs (Claussen et al., 1999b; deMenocal et al., 2000). Abrupt meaning (also throughout this thesis) considerably faster change than prescribed by the orbital pacing. However, similar models did not have such strong coupling (Renssen et al., 2003; Liu et al., 2006), and other proxies indicated that an abrupt change probably was not a continent-wide coherent event, but rather a more localized response (Kröpelin et al., 2008; Brovkin & Claussen, 2008). The debate on abruptness underscored the potential of positive feedbacks, as well as the need for sub-regional scale analyses of AHPs.

What followed in terms of AHPs modelling could be broadly categorized in two groups: (1) studies with a deeper-past (glacial cycles) coarse-grained perspective on forcing–feedback relationships; and (2) studies of closer-past (last 10 kyr) fine-grained exploration of misrepresented or new feedbacks. The first group relied mostly on simplified or coarse-resolution climate models for long transient (or ensemble) global simulations, with realistic combinations of orbital and glacial forcings (e.g. Tuenter et al., 2003, 2005; Tjallingii et al., 2008; Timm et al., 2010; Weber & Tuenter, 2011; Kutzbach et al., 2020; Menviel et al., 2021; Blanchet et al., 2021). Such studies refined understanding on orbital forcing and its relation to known feedbacks and variations in large-scale circulation, GHGs and cryosphere.

The second group instead used comprehensive models and finer resolutions (mainly in equilibrium simulations) to spatially and seasonally resolve features of Holocene global climate, in search of missing AHP connections (e.g. Vamborg et al., 2011; Marzin et al., 2013; Perez-Sanz et al., 2014; Rachmayani et al., 2015; Pausata et al., 2016; Gaetani et al., 2017; Hopcroft et al., 2017; Groner et al., 2018). In some cases new model parts were developed (latent new feedbacks). Findings included relevant effects from sub-canopy albedo, glacial meltwater, competing feedbacks, dust emissions, soil texture and plant diversity. Still, modelling advances were insufficient thus far to bridge model–data gaps (Brierley et al., 2020). New developments of dynamic components or kilometre-scale models may improve performance and reduce AHP uncertainty (Specht et al., 2022; Jungandreas et al., 2021).

Besides misrepresentation of climate components, alternative explanations may have been overlooked. Much of the focus on AHPs is centred around the monsoon summer season, but it is possible extra-monsoonal processes hold important clues. Dallmeyer et al. (2020) find a good agreement with proxy records for the end of the last AHP, after considering spatial and temporal complexity at sub-regional scale across North Africa. Cheddadi et al. (2021) likewise stress the importance of including winter rainfall in AHP studies. Furthermore, because models and reference data sets have improved over the years, a continuous re-assessment of land surface boundary conditions is important (Krinner et al., 2012; Chandan & Peltier, 2020). Another possibility is "palaeoclimate tuning" of climate models which traditionally have used only present-day conditions during calibration stages (Hopcroft & Valdes, 2021).

Promising as well is a greater focus on pre-Holocene AHPs. The Holocene alone may be insufficient to solve all AHP unknowns (Braconnot et al., 2019). Placing the most familiar AHP into context with earlier events could highlight patterns and signal novel understanding. Moreover, an increasing number of long (marine) geological records are available as reference for the last few glacial cycles (Weldeab et al., 2007; Tjallingii et al., 2008; Ehrmann et al., 2017; Tierney et al., 2017a; Skonieczny et al., 2019; Ehrmann & Schmiedl, 2021; Blanchet et al., 2021). Times like the last interglacial (ca. 125 ka) are included in standardized climate modelling experiments (Masson-Delmotte et al., 2013; Otto-Bliesner et al., 2017); known for stronger-than-Holocene orbital forcing and proportionally stronger AHP (Larrasoaña et al., 2013). A data synthesis for this time (Scussolini et al., 2019) and model intercomparisons (Scussolini et al., 2020; Otto-Bliesner et al., 2021) indicate model–data agreement in the sign of changes in North Africa, but due to a highly sparse proxy network and large inter-model spread, considerable uncertainty clouds magnitude and extent of the changes.

The main focus of this thesis is on modelling several AHPs of the late Quaternary. Holocene and pre-Holocene AHPs constitute a larger sample size that may reveal patterns that help understand underlying physics and modelling issues. A common theme through this modelling work is an explicit association of the simulated response with some of the key forcing factors involved. The wider climate variability of studying multiple AHPs may reveal new forcing–response relationships. The following section presents specific research questions.

1.5 RESEARCH QUESTIONS

Previous sections explained the motivation and the broad scientific context underpinning this work. The main goal is to take advantage of existing climate models to expand AHP theory towards more ancient times that include a diverse set of humid responses. Partly in response

to the improved representation of ancient AHPs in the geological record. It means this thesis considers a wider interval of interest than many preceding modelling studies about AHPs. Because of this longer time window, special attention is paid to changes in background climate, which on longer timescales (than AHPs) is also experiencing glacial-cycle changes. Orbitally induced changes in Earth's radiation budget superimpose slow changes in atmospheric GHGs and high-latitude ice sheets to modulate the amplitude of the AHP responses. Consequently, the first research question is about isolating the effects of the various large-scale climate drivers involved:

> What were the contributions (weights) of orbital parameters, GHGs and ice sheets to AHP dynamics across glacial cycles of the late Quaternary?

This question focuses on the aggregate regional AHP response, meaning contributions are measured in average amounts of "greening" each forcing factor could influence. For simplicity only the three most conspicuous forcing factors are considered: (1) orbital parameters, (2) GHGs and (3) ice sheets. It is assumed that the regional North African climate had little influence on such large-scale climate variables, thus they all acted as forcing the AHP responses. Previous work has found the orbital parameters to set the predominant forcing (as described in sections above), yet a systematic separation of individual and synergistic effects of forcing factors is missing.

Climatic forcing also likely had a large influence on the patterned response of AHPs. The magnitude of the changes should have reflected in the spatial features that could form during the humid climates. For instance, the maximum extent of vegetation cover encroachment deep in the Sahara, or length of river networks and size of lakes. However, the spatial extent of AHPs remains poorly constrained, especially for pre-Holocene AHPs. Therefore, a second research question in this dissertation is:

> What spatial climate patterns developed during the AHPs of the last glacial cycle, and did these patterns scale proportionally to climatic forcing?

This problem may be larger than a single modelling study or dissertation. Not only there is a severe lack of continental data older than the Holocene, but also it is still a technical challenge to set up simulations for glacial cycles at enough spatial resolution. Nevertheless, this thesis profits from earlier advances in model development that have recently made it possible to consider a spatially detailed full glacial cycle simulation. Taking advantage of available suitable climate model and input data for such a task, this thesis aims at estimating climatic patterns of AHPs across this long interval by performing one such long experiment. Modelled patterns would at least be consistent with

the conservation laws in climate models, and a partial assessment could be based on the few proxy information available, even if biased towards the Holocene AHP. This research could actually generalize or extrapolate some of the best estimated features of the Holocene AHP to much earlier humid climate episodes. Related to the first research question, it will also be possible in this case to study the connection between climatic forcing and the AHP patterns (potential scaling with forcing). It is conceivable the various forcing factors could influence the patterning in some preferred ways. The next few chapters summarize the methods and outcome of the work developed to address these two research questions.

2 FORCING CONTRIBUTION TO SAHARA GREENING

In a first part this thesis is about separating contributions of known forcing factors to AHP development. Advances in climate modelling and documentation of the geological record now provide a better platform to investigate a wider array of AHPs. However, with a wider time horizon comes the challenge of quantifying the effects of combinations of forcing mechanisms that can reinforce or oppose at different moments the humidity changes. Previous modelling studies already described first-order effects on AHPs of several forcing factors, like Earth's orbital parameters (e.g. Tuenter et al., 2003), GHGs (e.g. Claussen et al., 2003) and ice sheets (e.g. Marzin et al., 2013). Briefly, such factors modulate atmospheric thermodynamics that determine the amount of moisture that arrives inland deep in the Sahara. A few modelling experiments extending several glacial cycles usually found the orbital forcing to stand out as the predominant control on humidity (Weber & Tuenter, 2011; Kutzbach et al., 2020; Blanchet et al., 2021). Still, no systematic approach had so far quantified individual and synergistic contributions of these forcing factors. How much of an AHP response amplitude can be attributed to each forcing? Are there necessary synergies that enhance or dampen the response intensity?

Addressing such questions requires a specific experiment design that can disentangle the contributions to an expected outcome. Such outcome is part of the North African climate evolution since 190 ka, which according to marine proxies should include five AHPs of varying magnitudes and rates of change (Ehrmann et al., 2017). For the simulations CLIMBER-2 is used, a climate model of intermediate complexity with very coarse spatial resolution (Petoukhov et al., 2000; Ganopolski et al., 2001). Realistic values are set in a control simulation for (1) orbital parameters (Berger, 1978), (2) GHGs and (3) ice sheets (both from Ganopolski & Calov, 2011). Isolating forcing contributions is done with an ensemble of additional simulations that follow a factor separation analysis with three factors (Stein & Alpert, 1993). Such an approach leads to several interesting findings that are described and published in a refereed journal (see Appendix A). The remainder of this chapter provides a summary of those findings.

2.1 PAST AFRICAN HUMID PERIODS

A control simulation produces five AHPs (vegetation peaks), in agreement with geological records (Fig. 2.1). For simplicity a single marine proxy record is shown, which is related to palaeo-rainfall intensity

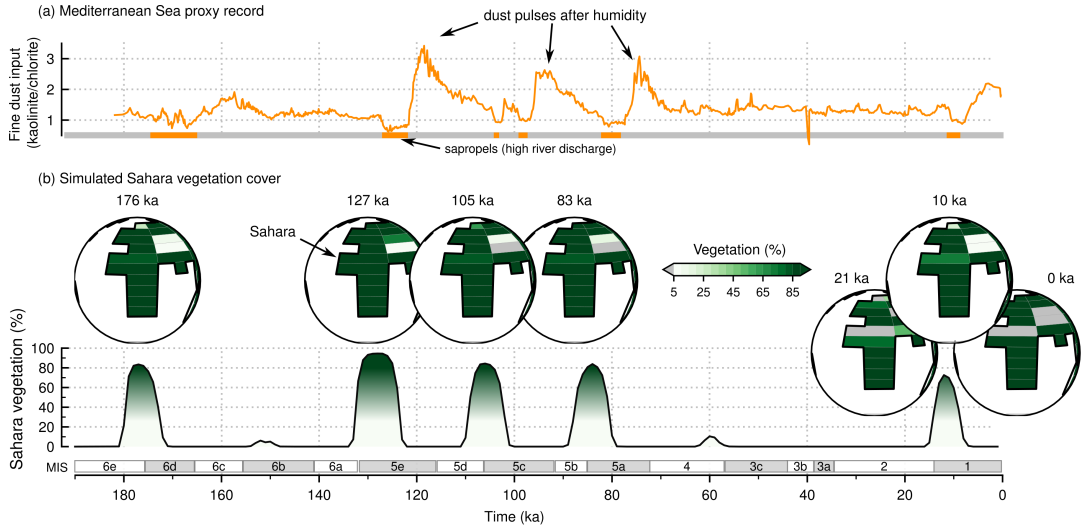

Figure 2.1: Data–model comparison for North African climate since 190 ka: (a) marine proxy record SL71 from the Eastern Mediterranean Sea (Ehrmann et al., 2017). It shows fine dust fluxes, according to a ratio of kaolinite and chlorite minerals. Sapropel bands are highlighted and signal high river discharge offshore during high-rainfall (humid) periods. A sapropel doublet near 100 ka should be a single event (Grant et al., 2016). (b) average vegetation response in the control simulation with CLIMBER-2. Interesting time slices are included as maps. Marine isotope stages (MIS).

over North African watersheds (Ehrmann et al., 2017). While an AHP was active, weathering probably accumulated more kaolinite in freshwater bodies. Only after an AHP terminated, desiccated water tracks became kaolinite sources for the Mediterranean Sea (dust pulses in Fig. 2.1a). Model and proxy show similar trends in magnitude, with the strongest Saharan greening occurring ca. 176 ka, 127 ka, 105 ka and 83 ka. They disagree, however, in the strength of the Holocene AHP (ca. 10 ka) with respect to other AHPs. This could be related to the core-to-shore distance of the marine sediments, which sets the strength of some of the regional signals (Ehrmann & Schmiedl, 2021).

The sapropel (bands rich in organic matter) sequence in the marine core also aligns well with vegetation peaks in the model. The comparison in Fig. 2.1 is only qualitative, since the climate model is neither simulating dust fluxes nor sapropel formation. The case of extreme aridity during the Last Glacial Maximum (LGM; ca. 21 ka) also seems well represented in the simulation. Moreover, model output compares as well with additional proxies offshore near East and West Africa (Tierney et al., 2017a; Skonieczny et al., 2019). Results support previous evidence that the model simulates well North African palaeoclimate on such long timescales (e.g. Tjallingii et al., 2008).

A realistic representation of AHPs invites further analysis of the control simulation. Of particular interest is the relationship of simulated

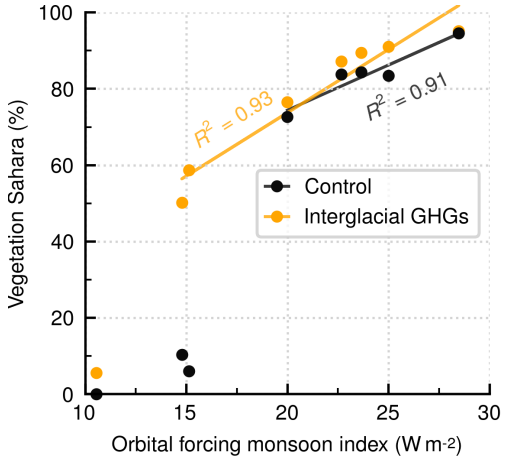

Figure 2.2: Correlation of Saharan vegetation fraction and orbital forcing monsoon index for the control simulation and another simulation with increased (interglacial) GHGs levels. Point values are at peak monsoon index times. Solid lines are ordinary least squares regressions only for simulated AHPs (higher than 50 % vegetation) with shown coefficients of determination (R^2).

AHPs with respective forcing values. A simple correlation analysis reveals the model response during AHPs is strongly positively correlated with the orbital forcing monsoon index defined by Rossignol-Strick (1983). Not only in magnitude but also in rate of change. The orbital forcing monsoon index measures an insolation gradient between the northern tropic (∼23.4°N) and the equator, and therefore has direct link with the precession cycle of the low latitudes.

For vegetation cover in the Sahara the control simulation shows a critical threshold for AHP onset that seems a function of such monsoon index (Fig. 2.2). Below a monsoon index critical value, located between 15 W m^{-2} to 20 W m^{-2}, the vegetation response would be insufficient to trigger an effective precipitation–vegetation feedback leading into an AHP. The amplifying feedback interaction is possible via changes in surface albedo, aerodynamic roughness and evapotranspiration. The critical value range for greening in the simulation aligns closely with the 19.8 W m^{-2} monsoon index threshold that Rossignol-Strick (1983) found for sapropel appearance in Mediterranean sediment cores. No previous modelling study had linked the sapropel record insolation threshold with simulated Saharan greening.

Figure 2.2 also includes another simulation that has increased GHGs levels. In that case atmospheric GHGs are fixed at interglacial values (similar to preindustrial) throughout the simulation. The simulation is part of the factor separation analysis presented in the next section. In Fig. 2.2 it seems that higher GHGs lower the threshold for AHP vegetation development some 5 W m^{-2} (to somewhere below 15 W m^{-2}). Considering that the difference in GHGs radiative forcing between simulations is on average about 2 W m^{-2}, this implies that the sensitivity

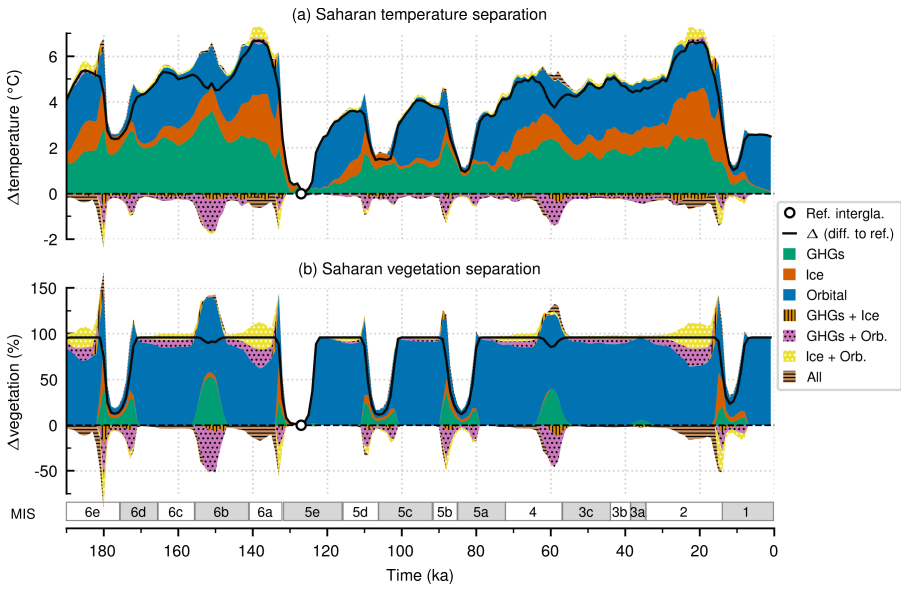

Figure 2.3: Forcing separation analysis for Saharan (a) temperature and (b) vegetation fraction from a last-interglacial perspective. The analysis reference is climate ca. 127 ka and the solid black line shows forcing induced changes relative to the control simulation (note zero changes at already-last-interglacial reference). Colour shades then show diverse forcing contributions to obtain at other times (in complementary simulations) a response equal to the 127-ka reference. Marine isotope stages (MIS).

of the threshold to GHGs levels is close to -2.5. Consequently, prior knowledge of the monsoon index (i.e. orbital parameters) and GHGs should be almost sufficient to predict AHPs in model CLIMBER-2.

2.2 FORCING FACTORS SEPARATION ANALYSIS

According to the previous section, at least two forcing conditions are key for the magnitude of Sahara greening in a simulation (orbital parameters and GHGs). Additional experiments are required to partition what each forcing alone and together with the others (synergies) contributes to the greening amplitude. The complementary (to the control) simulations follow the Stein and Alpert (1993) method of factor separation analysis for three factors: (1) orbital parameters, (2) GHGs and (3) ice sheets. In the method a specific target is selected that becomes the reference state about which deviations are caused by sequentially involved factors.

Figure 2.3 shows the separation for Saharan temperature and vegetation fraction from a warm interglacial perspective, which means the selected reference is climate near 127 ka. Shown are the changes with respect to the control simulation that are caused by the forcing factors, highlighting with colour shading their individual and synergistic contributions. Temperature and vegetation are included as two

contrasting cases. For temperature all three forcing factors seem to contribute only proportionally to their changes (to see this compare to changes in the forcing with respect to 127 ka in Appendix A). For vegetation cover, however, there is clearly a dominance of the orbital parameters (bluer shading), with secondary input from GHGs (greener shading). Synergistic contributions are also more noticeable in the vegetation fraction changes, for the synergies with the orbital forcing (pink and yellow hues). It is worth mentioning in the vegetation case that a fraction is a bounded quantity (range 0 % to 100 %), therefore synergies must be analysed carefully, since some of them will show up only as a mathematical constraint (cannot "green" the Sahara more than 100 %). The synergies with the orbital forcing (GHGs and orbital, and ice sheets and orbital) seem robust positive contributions, as seen for precipitation (see Appendix A). If they appear negative sometimes in Fig. 2.3b is only because the other predominant factors already induced maximum greening.

On average, the orbital forcing alone accounts for 80 % of the vegetation changes in the Sahara that led to the highly-vegetated state around 127 ka (see Fig. 2.1b). Only the remaining 20 % of vegetation change is influenced by GHGs and ice sheets, contributing either individually near 6 % and 2 %, respectively, or collectively via synergies roughly 12 %. Results agree with previous studies that also found GHGs and ice sheets to be secondary influences (Kutzbach et al., 2020; Blanchet et al., 2021), however, this is the first complete separation analysis quantifying orbital dominance and revealing synergies.

2.3 FUTURE AFRICAN HUMID PERIODS

These findings bear interesting consequences for future long-term climate change in North Africa. When will the next AHP occur? Based on the analysis of past AHPs in previous sections, the next AHP should happen when the critical threshold in monsoon index is crossed again. This happens next around 66 kyr AP (after present), when the orbital forcing monsoon index approaches 16.5 $W\,m^{-2}$. It would take this long mainly because the Earth stays in a low-eccentricity orbit still for a long time (main period about 400 kyr), which maintains a relatively small amplitude in the precession changes that lead to AHPs. However, as revealed also in the palaeoclimate simulations the insolation threshold is sensitive to levels of GHGs. Therefore, occurrence of the next AHP should also be susceptible to future changes in atmospheric GHGs.

Figure 2.4 shows predicted future Saharan greening in the next 100 kyr AP, according to different scenarios of CO_2 emissions from Archer and Brovkin (2008). If preindustrial levels of GHGs are fixed during this time (i.e. constant zero GHG emissions), then the next simulated AHP occurs in some 66 kyr AP, as dictated by the orbital forcing monsoon index. Conversely, under extreme emission scenar-

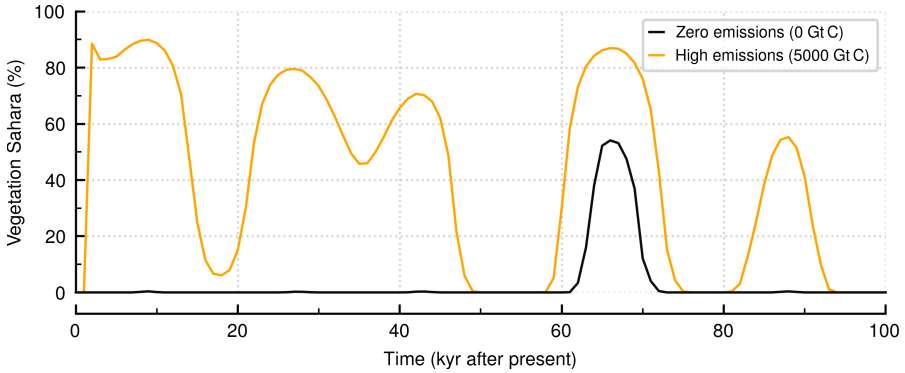

Figure 2.4: Simulated future climate change in Saharan vegetation fraction for two different CO_2 emission scenarios.

ios (about 5000 Gt C) the next simulated AHP develops within some 9 kyr AP. Moreover, multiple potential future AHPs take place. Such GHGs-enabled AHPs would most likely not resemble their glacial-cycle predecessors, since thermodynamic effects of increased GHGs affect AHPs differently than the long-term dynamic adjustments to the orbital parameters (Claussen et al., 2003; D'Agostino et al., 2019).

2.4 SYNOPSIS

The first contribution of this thesis used a climate model of intermediate complexity with fast computing turnaround time to investigate past and future climate change in North Africa. The coarse spatial resolution of the model restricts this assessment to the continental scale, where magnitude of the AHP response appears strongly correlated to the orbital forcing. This study discovered a critical insolation threshold in the model that controls climate–vegetation dynamics evolving into the AHPs of the late Quaternary. There is a striking resemblance between this threshold in the model and the threshold detected by Rossignol-Strick (1983) for appearance of sapropels in marine sediments. The simulated threshold appears clearly sensitive to GHGs levels. This means that even though the dominance of the orbital forcing for Saharan greening is clear (also confirmed here in a separation analysis) secondary effects of GHGs seem to crucially set the minimum for the AHP-inducing insolation threshold. This has important implications for an approaching future with smaller-amplitude orbital changes and potentially large GHGs emissions. Further details about this study are presented in a published research article that is also added as an Appendix A. In the next chapter some of the forcing–AHP relationships found in this study are investigated with a more comprehensive model and at higher spatial resolution.

3 NORTH AFRICAN PALAEOVEGETATION PATTERNS

The previous chapter considered only average changes aggregated over the largest spatial scale (continental averages). What follows is to try to understand how those changes distributed spatially at smaller (sub-regional) scales to form AHP patterns. As a second contribution this thesis focuses on spatial climate patterns of late Quaternary AHPs. North Africa is a large region and defining the total extent of the natural land cover changes during AHPs is difficult. Climate change frequently transformed much of the land, preventing extensive preservation of the geological record (Drake et al., 2018). Although existing terrestrial proxy records provide valuable insight into the changes, it is insufficient to assemble a complete picture of AHP landscapes without assumptions or perhaps overextending proxy local contexts. Even for the most recent AHP during the Holocene the proxies network contains only a few and scattered sites (Harrison & Bartlein, 2012). And uncertainty accumulates towards more ancient times. This study looks for broad patterns in simulated vegetation cover of North Africa. It aims at resolving spatial variability of regional land cover across glacial cycles. This is a necessary step to be able to outline the extent of environmental change during past AHPs.

An exceptionally long climate simulation is performed, using a comprehensive model and at enough spatial resolution to study sub-continental scale changes. The simulation takes roundabout two years to complete. Starting at 130 ka, the simulation covers the entire last glacial cycle, when, as seen in the previous chapters, probably four AHPs developed whose magnitude was largely set in proportion to the orbital forcing. The vegetation cover patterns of the four AHPs are studied and a common dominant mode of variability is used to investigate, similar to the first study, a relationship of the patterned vegetation response to the climatic forcing. The established forcing–response link is then used to estimate the vegetation cover over the last eight glacial cycles. Furthermore, future vegetation cover in North Africa is also simulated and included in the discussion. The findings of this study are part of a manuscript in preparation that is about ready for submission to a peer-review journal (see Appendix B). The next sections present the key findings thus far.

3.1 GLACIAL CYCLE VEGETATION PATTERNS

Global climate since 130 ka is simulated using the Max Planck Institute for Meteorology Earth System Model (MPI-ESM; Giorgetta et al.,

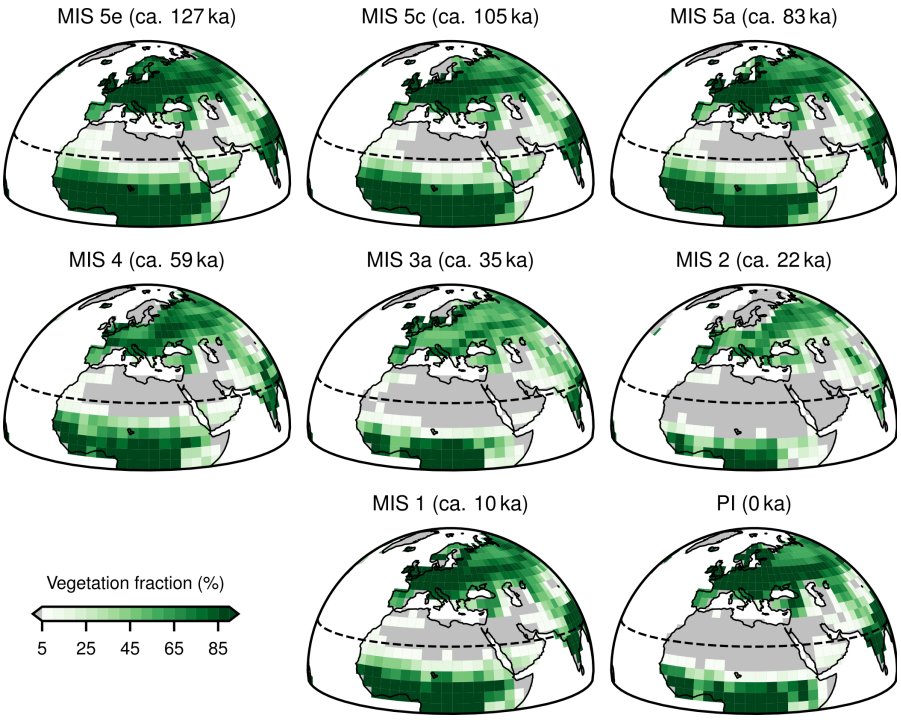

Figure 3.1: Simulated vegetation cover since 130 kyr. Shown are times of marked expansion and contraction of the Sahara; named after respective marine isotope stages (MIS). Northern tropic dashed.

2013) version 1.2 (Mauritsen et al., 2019) in the T31GR30 configuration (Mikolajewicz et al., 2018), which has a coarse resolution of about 3.75° horizontal grid spacing. The model includes dynamic components for the atmosphere, ocean, land surface and vegetation cover, which interact via fluxes of energy, momentum and water. Focusing on land cover, the model computes vegetation as fractions of predefined vegetation classes (plant functional types) that compete for space within grid cells according to (climate-dependent) net primary productivity (NPP). Bare land is the fraction where there is glacier cover (cold desert) or sustained near-zero values of NPP (hot desert). In the experiment climatic forcing is set according to orbital parameters from Berger (1978), atmospheric concentrations of GHGs from Köhler et al. (2017), and ice sheets from the GLAC-1D data set (Tarasov & Peltier, 2002; Tarasov et al., 2012, 2014; Briggs et al., 2014; Abe-Ouchi et al., 2013).

Figure 3.1 shows total vegetation cover fraction in part of the Northern Hemisphere, where large amplitude changes can be seen happening in North Africa, with desert cover (shown as vegetation fraction below 5 %) shrinking and expanding through isotopic stages. AHPs are the times when vegetation coverage increases northward, closely approaching the northern tropic (in the west it crosses it). Also, when there is a general intensification of vegetation fraction along all latitudinal bands. It happens clearly at MIS 5e, MIS 5c, MIS 5a and the Holocene (MIS 1). MIS 4 also appears somewhat green (it is close to

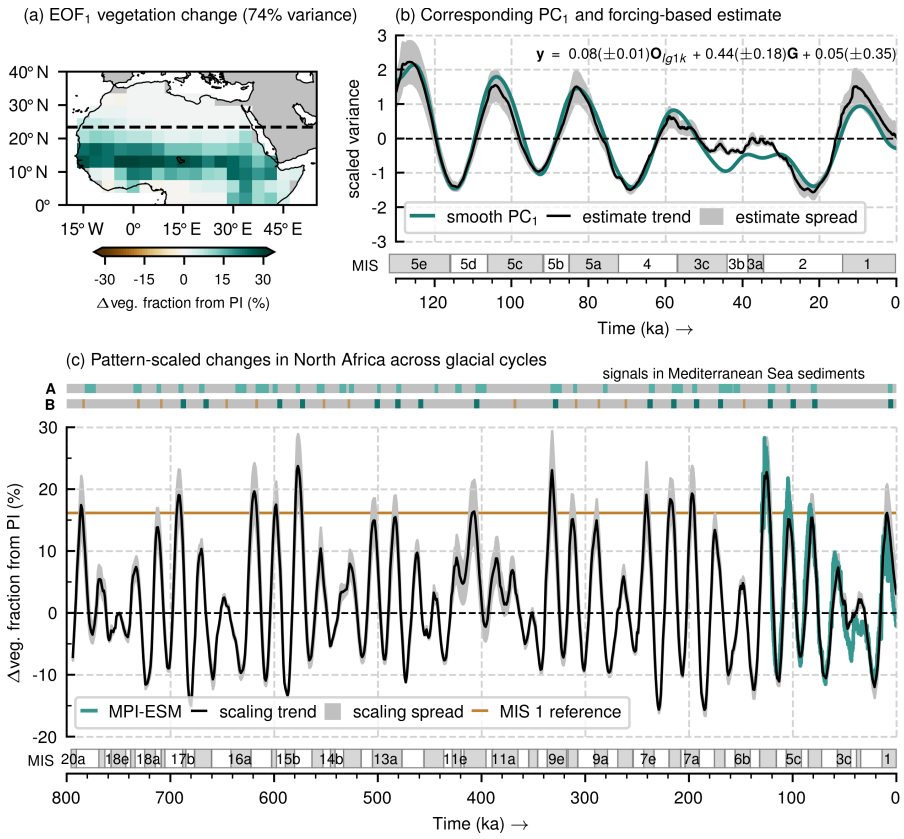

Figure 3.2: Empirical orthogonal functions (EOFs) analysis and pattern scaling of vegetation cover anomalies from preindustrial (PI) era: (a) leading mode of variability and (b) respective principal component (PC) time series (smoothed with low-pass filter); and (c) scaling-based estimates of vegetation changes of eight glacial cycles. In (b) a linear model approximates PC_1, using the monsoon index lagged 1 kyr (O_{lg1k}) and GHGs radiative forcing (G). In (c) humidity signals from Mediterranean marine sediments are: A, inferred AHP bands from sediments geochemistry (Grant et al., 2022), and B, composite sapropel record with clear (dark wide bands) and unclear (faint slim bands) sapropels (Emeis et al., 2000). In (c) a horizontal line shows the Holocene AHP baseline.

its insolation local maximum), but the pattern is not as clear (intense shading is discontinuous along the Guinea Coast) and lacks proxy evidence to support it. Found AHP vegetation patterns generalize to more ancient times some estimated features from the Holocene (Dallmeyer et al., 2020; Hopcroft & Valdes, 2021). A mostly northwest–southeast front of northward vegetation development is also seen in the ancient AHPs simulated in Armstrong et al. (2023).

3.2 PATTERN SCALING WITH CLIMATIC FORCING

Inspired by results of the first study, this analysis also looks for connections to the climatic forcing. Now that a patterned vegetation response

has been simulated, it is interesting to investigate to what extent the changes can be estimated according to forcing values. A simple relationship is established with a pattern scaling approach. Key for this is to find a coherent pattern of variability that can be assumed invariant (at least for recent glacial cycles) and scalable with the forcing. Such pattern is obtained via an analysis of empirical orthogonal functions (EOF), using vegetation cover anomalies from preindustrial era. The EOF analysis is only for grid cells inside North Africa (avoid noise from neighbouring regions). A resulting leading mode of variability, shown in Fig. 3.2a, is used for the pattern scaling. It explains about 74 % of the variance of vegetation cover anomalies.

Projecting the vegetation anomalies over EOF_1 produces a respective principal component time series which is shown smoothed (low-pass filter) in Fig. 3.2b. A direct link to climatic forcing is obtained with ordinary least squares curve fitting of forcing time series with PC_1. Figure 3.2b also shows the linear model, where a lagged orbital component is used after having noticed such lag between peak insolation and maximum average vegetation coverage. In the linear model it was found that it was possible to use any of the GHGs or ice sheets data, since they evolve similarly through glaciations. The regression parameters are obtained using a sliding window (two precession cycles long, about 42 kyr) along the time series, thereby yielding some statistical spread. Thus, using only the EOF_1 pattern and forcing values, much of the vegetation cover patterns over North Africa can be recovered.

The error of the pattern scaling with respect to the simulated fields is on average about ± 10 % vegetation cover change. Although it can be a large error for some places that perhaps see little change, it approximates generally well the simulated vegetation patterns. However, one important caveat is that because vegetation cover is a grid cell fraction with bounds 0 % to 100 %, it is possible the pattern scaling estimates changes (relative to preindustrial era) that exceed possible amounts of desertification or greening. Likewise, it is possible that such linear scaling only works because the model has a "desert bias" that prevents strong (non-linear) amplification of the greening response.

Despite such caveats, results make it possible to estimate vegetation changes since 800 ka as shown in Fig. 3.2c. This long interval has reliable forcing data available. Orbital forcing is computed according to Berger (1978), while GHGs come from Antarctic ice cores data (Petit et al., 1999; EPICA Community Members, 2004) as compiled by Ganopolski and Calov (2011). Taking the Holocene AHP as a reference in Fig. 3.2c it is possible to count 20 AHPs during this time. Many of the potential AHPs agree with data from Mediterranean marine sediments (Emeis et al., 2000; Grant et al., 2022). This number is also in line with the data synthesis of Larrasoaña et al. (2013) and the recent (discontinuous) simulations by Armstrong et al. (2023).

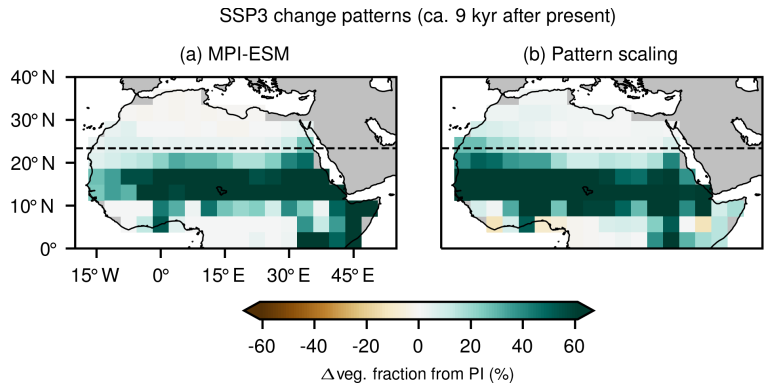

Figure 3.3: Estimates of future vegetation (ca. 9 kyr after present) coverage change under Shared Socioeconomic Pathway Three (SSP3) scenario: (a) simulated changes and (b) pattern scaling changes.

3.3 FUTURE VEGETATION COVER

The first study showed that under future scenarios of strong GHGs forcing, a next Saharan greening would take place around 9 kyr after present. Using the model in this second study it is possible to estimate the vegetation pattern that such an AHP would have. The future 10 kyr are simulated assuming the ice sheets stay at preindustrial levels, and that CO_2 emissions follow Shared Socioeconomic Pathway (SSP) scenarios of the Intergovernmental Panel on Climate Change (IPCC). The scenario CO_2 concentrations come from previous applications of reduced complexity carbon-cycle (Meinshausen et al., 2020) and climate (Brovkin et al., 2012) models.

Figure 3.3a shows the vegetation cover change from preindustrial era under a strong SSP scenario (SSP3), which assumes a global warming of about 7 K after the earth system adjusts to the GHGs radiative forcing. Unlike patterns from past AHPs, there is a clear zonal gradient favouring central and eastern North Africa. The footprint of the West African Monsoon is almost absent. However, the most intense changes remain within the 10°–20°N band. Figure 3.3b shows what the pattern scaling method predicts for this time. In this case the prediction is not close to what the dynamically resolved pattern shows. A pattern scaling that is based on past AHPs, when the orbital forcing was the main driver of change, fails to predict vegetation patterns of future GHGs-enabled AHPs. Such results agree with differences in dynamic and thermodynamic climate adjustments to the various forcing factors (Claussen et al., 2003; D'Agostino et al., 2019).

3.4 SYNOPSIS

The second part of this thesis estimated the vegetation cover in North Africa across glacial cycles and the future. A climate model produced

vegetation coverage for the last glacial cycle, which covers the last four AHPs. Vegetation patterns during ancient AHPs were analysed in relation to the more established Holocene AHP. Furthermore, the model output was decomposed in spatio-temporal patterns to establish an explicit pattern-forcing relationship that enables estimation of vegetation cover during preceding glacial cycles until 800 ka. Limitations of the estimates are discussed. In addition, patterns of future land cover change are also simulated to understand how they change as GHGs become the dominant climate driver. Further details about this study are presented in the manuscript in Appendix B. The next chapter offers a general overview of what was accomplished with the two studies included in this thesis and how this research contributes to answering relevant research questions.

4

SUMMARY AND CONCLUSIONS

Overall this dissertation advances current understanding of large-scale climate changes that happened in North Africa over the course of the last glacial cycles. For this, exceptionally long climate simulations were run, following a careful experiment design that enabled a fine-grained view on the various influences from climatic forcing on North African humidity and natural vegetation cover. Analyses of the past were always combined with complementary simulations of the future (also performed as part of this work), whose contrasting results were always useful to highlight interesting AHP features. Besides simulations, across this work constant attention is paid to available data sources from the geological record, which provided necessary reference points to avoid some of the pitfalls of complexity and high dimensionality in climate modelling. Following is a summary of the key findings that give answers to the two research questions in the introduction.

4.1 QUANTIFYING FORCING INFLUENCE ON AHP DYNAMICS

Past research identified basic climate forcing factors that most likely affected onset, development and termination of AHPs during the late Quaternary. Idealized modelling experiments successfully isolated and highlighted the role of relevant processes that would become implemented in the models in an attempt to understand and perhaps replicate signals in the geological record. However, technical and proxy limitations favoured for a long time the study of only the last AHP, when there is a narrow range of climatic forcing variability (in orbital timescales). Therefore, the effect of the various forcing factors involved could have been underrepresented within this range. Today, climate models and proxy records offer the possibility of investigating a wider range of AHP responses along glacial cycles, and a question that arises is stated in the introduction of this thesis:

> What were the contributions (weights) of orbital parameters, GHGs and ice sheets to AHP dynamics across glacial cycles of the late Quaternary?

To answer this question the first part of this thesis used a climate model to isolate forcing effects through multiple experiments. The glacial cycles provided a larger sampling space of forcing variability across several AHPs, which could be used to quantify individual and joint effects of the most important (forcing) contributors to the humidity changes. Main findings are:

- Orbital forcing alone sets about 60 % (80 %) of the AHP precipitation (vegetation cover) changes.
- GHGs and ice sheets influence at most 20 % of the AHP changes, but mainly through synergies with the orbital forcing.
- Simulated AHPs in a climate model can be predicted according to a critical threshold in the orbital forcing monsoon index between $15\,W\,m^{-2}$ to $20\,W\,m^{-2}$, in striking resemblance to an apparent insolation threshold in the geological record.
- The critical threshold is sensitive to levels of GHGs, lowering it about $2.5\,W\,m^{-2}$ per $1\,W\,m^{-2}$ change in GHGs radiative forcing.
- Both AHP magnitude and rate of change are strongly positively correlated to the orbital forcing.
- AHP onset vegetation growth rates are usually faster than termination vegetation decline rates, related to rates of global ice volume change.

These are all novel insights made possible by an ensemble of 21 simulations of transient global climate for since 190 ka. Together they can explain why some AHPs were stronger and faster than others, and why they did not occur at all under some circumstances. In the case of this thesis they answer the research question, although as with any modelling study, some results are susceptible to being strictly model dependent. Literature review and examination of the geological record seem to indicate that they at least agree with reported general trends.

4.2 GLACIAL-CYCLE VEGETATION COVER IN NORTH AFRICA

Forcing control on AHP intensity (from the first study) should also be determinant for AHP climate patterns in space. Despite other important local factors like topography or soil nutrients, the spatial changes during AHPs were probably different according to differences in global climate forcing factors. There is still uncertainty about the extension of AHP changes even for the most recent (Holocene) episode, yet there is the possibility of finding spatial patterns in climate models that are consistent with current basic physical understanding. The research question is:

> What spatial climate patterns developed during the AHPs of the last glacial cycle, and did these patterns scale proportionally to climatic forcing?

A second study in this thesis approached this question by performing a long climate simulation with a comprehensive model and a total runtime close to two years. Main findings are:

- Four simulated AHPs with distinct vegetation patterns, in proportion to forcing strength.
- Vegetation patterns agree with available information and generalize reported features for the Holocene event. For instance, a northwest–southeast frontal development of the vegetation northward migration across North Africa.
- The model has a "desert bias" that implies results are probably an underestimation. This means it is possible strong non-linear responses are missing.
- A dominant mode of simulated vegetation cover variability has the strongest changes enclosed within 10°–20°N.
- It is possible to use a simple forcing-based pattern scaling as a diagnostic tool to make quick rough estimates of the vegetation coverage in North Africa.
- The pattern scaling predicts 20 potential past AHPs since 800 ka.

These points provide new insight about some previously unseen patterns that await a more thorough evaluation as other similar simulations are performed or more of the geological record is uncovered. Moreover, the explicit forcing–pattern scaling relationship could have useful theoretical applications, as it bypasses the computational expense of comprehensive climate models.

4.3 CONCLUSIONS

Across the work presented in this thesis is a theoretical approach supported by well-established climate models. It tackled the general question of understanding glacial-cycle scale climate variability of North Africa. AHPs were some of the largest-scale examples of regional climate and land cover change, thus a rigorous description is scientifically relevant to make sense of a fragmented geological record and also learn about long-term climate–land surface interactions. Palaeoclimate modelling of this kind helps unveil the full range of climate states that were and are possible, plausible and pertinent for anticipating future climate change.

Altogether scientific contributions in this thesis illuminated several aspects of the evolution of AHPs along glacial cycles. The dominant role of the orbital forcing set magnitude and rate of change of past AHP development, possibly including threshold dynamics. GHGs and ice sheets were only of secondary importance in comparison, yet they have potential to act to remove insolation requirements for AHP onset. This has especially important consequences for situations when the earth follows an orbit with low eccentricity, when AHP orbital forcing becomes weakest. For instance, during the next some 100 kyr.

Also, part of this work was a description of AHP spatial development for the late Quaternary. More intense climatic forcing led to greater vegetation invasion into the Sahara. From the equator, the pattern of northward migration of vegetation remained mainly zonal until about the northern tropic, where a deeper push only happened along the west coast. This means it was possible a northeastern region in the Sahara remained bare for the entire glacial cycle. Such simulated patterned responses were found to be predictable to a considerable extent using a forcing-based pattern scaling. The scaling highlights the possibility for a large-scale underlying pattern that, in spite local factors, responds always similarly in proportion to the forcing.

Another common thread in this thesis is contrasting the past with the future. The overall lesson shows up that past AHPs should not resemble the future ones. In terms of orbital requirements the next broad Saharan greening would have arrived naturally some 66 kyr into the future. However, GHGs under strong emission scenarios could induce notable changes in Saharan humidity as soon as 9 kyr after present. Spatial development of such a GHGs-enabled AHP would not resemble its orbitally controlled predecessors, as the signature northward push near the west is not necessarily where the largest greening would occur.

Much of what was found throughout this research is supported on documented parts of the geological record. Likewise, on related previous applications of climate models. However, it is important to acknowledge the limits of single-model climate studies. In this case two models of different complexity were used to study the same research topic, but they approached the research questions from different angles, in direct relation with their large differences in computing requirements. It will be important to compare these findings with future proxy data and results from other modelling groups as they appear in the literature.

These findings also invite interesting follow-up questions. For instance, what mechanisms explain the potential synergies between forcing factors that contribute to AHP intensity? Also, what AHP patterns would develop in a model without such “desert bias”? What determines the shape of the dominant pattern of variability underpinning the pattern scaling method? How far into the past can these findings stretch before seen patterns also break?

APPENDIX

A

EFFECTS OF ORBITAL FORCING, GREENHOUSE GASES AND ICE SHEETS ON SAHARAN GREENING IN PAST AND FUTURE MULTI-MILLENNIA

The study in this appendix was published* as:

Duque-Villegas, M., Claussen, M., Brovkin, V., & Kleinen, T. (2022). Effects of orbital forcing, greenhouse gases and ice sheets on Saharan greening in past and future multi-millennia. *Climate of the Past*, *18*(8), 1897–1914. DOI: 10.5194/cp-18-1897-2022.

**It appeared as a highlight paper in the journal.*

AUTHOR CONTRIBUTIONS

MDV, MC and VB planned the research idea. MDV performed model experiments, led the formal analysis and drafted the manuscript. MC supervised and steered progress. VB and TK contributed to experiment design and provided model code and input data. All authors participated in the analysis of results and manuscript composition.

Effects of orbital forcing, greenhouse gases and ice sheets on Saharan greening in past and future multi-millennia

Mateo Duque-Villegas[1,2], Martin Claussen[1,3], Victor Brovkin[1], and Thomas Kleinen[1]

Received: 7 Mar 2022 – Accepted: 17 Jul 2022 – Pubslished: 22 Aug 2022

[1] Max Planck Institute for Meteorology, Hamburg, Germany

[2] International Max Planck Research School on Earth System Modelling, Hamburg, Germany

[3] Center for Earth System Research and Sustainability (CEN), Universität Hamburg, Hamburg, Germany

ABSTRACT

Climate archives reveal alternating arid and humid conditions in North Africa during the last several million years. Most likely the dry phases resembled current hyper-arid landscapes, whereas the wet phases known as African Humid Periods (AHPs) sustained much more surface water and greater vegetated areas that "greened" large parts of the Sahara region. Previous analyses of sediment cores from the Mediterranean Sea showed the last five AHPs differed in strength, duration and rate of change. To understand the causes of such differences we perform transient simulations of the past 190 000 years with Earth system model of intermediate complexity CLIMBER-2. We analyse amplitude and rate of change of the modelled AHPs responses to changes in orbital parameters, greenhouse gases (GHGs) and ice sheets. In agreement with estimates from Mediterranean Sea sapropels, we find the model predicts a threshold in orbital forcing for Sahara greening and occurrence of AHPs. Maximum rates of change in simulated vegetation extent at AHP onset and termination correlate strongly with the rate of change of the orbital forcing. As suggested by available data for the Holocene AHP, the onset of modelled AHPs happens usually faster than termination. A factor separation analysis confirms the dominant role of the orbital forcing in driving the amplitude of precipitation and vegetation extent for past AHPs. Forcing due to changes in GHGs and ice sheets is only of secondary importance, with a small contribution from synergies with the orbital forcing. Via the factor separation we detect that the threshold in orbital forcing for AHP onset varies with GHGs levels. To explore the implication of our finding from the palaeoclimate simulations for the AHPs that might occur in a greenhouse gas-induced warmer climate, we extend the palaeoclimate simulations into the future. For the next 100 000 years the variations in orbital forcing will be smaller than during the last hundred millennia, and the insolation threshold for the onset of late Quaternary AHPs will not be crossed. However, with higher GHGs concentrations the predicted threshold drops considerably. Thereby, the occurrence of AHPs in upcoming millennia appears to crucially depend on future concentrations of GHGs.

A.1 INTRODUCTION

Extensive evidence from geological records indicates that the landscape across North Africa changed repeatedly back and forth from wet to dry conditions during the late Quaternary (Larrasoaña et al., 2013; Grant et al., 2017). Wet phases or African Humid Periods (AHPs) were intervals with increased rainfall, abundant lakes and rivers, as well as extended vegetation cover that "greened" large parts of the Sahara (deMenocal et al., 2000). Environmental shifts occurred at mil-

lennial timescale, primarily in response to variations in the Earth's orbit, which altered the seasonal radiation budget and led to distinct regional circulation patterns and atmospheric moisture transports (Kutzbach, 1981). This link between orbital configuration and climate of North Africa is noticeable in the proxy data (e.g., Lourens et al., 2001) and supported by computer simulations (e.g., Tuenter et al., 2003). Orbitally induced changes in regional circulation were amplified by several feedback processes related mainly to surface properties such as sea temperature and land cover (Claussen et al., 2017; Pausata et al., 2020). Despite current knowledge about these key mechanisms, inconsistencies between proxy data and simulations suggest there are still gaps in understanding of AHP dynamics (Braconnot et al., 2012).

Much of what is known about AHPs stems out of the study of the last event during the Holocene epoch (Tierney et al., 2017b). The relatively vast amount of available proxy data that cover this epoch has allowed for extensive data analyses (e.g., Bartlein et al., 2011; Lézine et al., 2011; Shanahan et al., 2015) and numerical simulations of its AHP (e.g., Thompson et al., 2019; Chandan & Peltier, 2020; Dallmeyer et al., 2020; Cheddadi et al., 2021; Hopcroft & Valdes, 2021; Jungandreas et al., 2021). Yet the latest sediment records from the Mediterranean Sea have highlighted the diversity in intensity of earlier AHPs (Blanchet et al., 2021; Ehrmann & Schmiedl, 2021), reaching as far back in time as Marine Isotope Stage (MIS) 6 about 190 000 years ago (190 ka). The motivation behind this study lies in understanding the causes behind the different intensities. Although regional climate likely responded in a similar way for all previous AHPs, paced by orbital variations described in current theory (Claussen et al., 2017), an additional complication emerges from the added effects of simultaneous changes in greenhouse gases (GHGs) and ice sheets extent. The last two factors should act as additional forcing on the AHP response, considering that North African climate responds to changes in both of them (Claussen et al., 2003; Marzin et al., 2013), and assuming the region in turn has a negligibly small effect on these global climate drivers. Therefore we examine the changes in orbital, GHGs and ice sheets forcings in order to understand how the past five AHPs differed.

Previous modelling studies investigated the AHP response under these forcings separately, through sensitivity experiments that showed individually their first-order effects. For instance, Tuenter et al. (2003) described the consequences of changes in orbital parameters, while Claussen et al. (2003) focused on GHGs and Marzin et al. (2013) on the ice sheets. However, considering separately each forcing prevents simulation of synergistic or joint effects amongst them, and therefore a direct comparison of their individual impact on AHP response is limited. The transient experiments in Weber and Tuenter (2011), Kutzbach et al. (2020) and Blanchet et al. (2021) included all three forcing factors and showed the minor role the forcing from GHGs

and ice sheets plays in setting the strength of AHPs. Nonetheless, these studies focused more on the simulated response of North Africa (and how it compares with proxies) than on the evolution or absolute values of the forcings. The novelty of this work lies in our attention to the multiple forcings involved, since we look at their rates of change, threshold values and correlations, and we present the first factor separation analyses for these forcings in North Africa. Additionally we use future estimates of these forcings to simulate potential future AHP responses and assess how far our lessons from past regional climate change can take us into the future.

Our main goal is to investigate how much each forcing mechanism, by itself and in synergy with the others, contributes to the different AHPs intensities seen in proxy records. We use model CLIMBER-2 (Petoukhov et al., 2000; Ganopolski et al., 2001) of intermediate complexity (Claussen et al., 2002), to study the climate response of North Africa to changes in orbital parameters, GHGs radiative forcing and extent of ice sheets. We run an ensemble of transient global climate simulations for the last 190 millennia (190 kyr) and study the dynamics of the previous five AHPs. Thus we can compare our simulation results with the proxy data by Ehrmann and Schmiedl (2021), at least qualitatively. Using the factor separation method of Stein and Alpert (1993) we quantify individual and synergistic contributions of every forcing to the magnitude of an AHP. Our findings from the past humid periods are also useful when we extend experiments for a 100 kyr into the future and assess potential consequences of changes in GHGs in relation to development of future AHPs.

A.2 METHODS

A.2.1 *Model description*

CLIMBER-2 incorporates a 2.5 dimensional statistical–dynamical atmosphere model of coarse horizontal resolution of about 10° latitude and 51° longitude, and a parameterised vertical structure assuming universal profiles of temperature, humidity and meridional circulation (Petoukhov et al., 2000). The atmosphere component is coupled to a zonally averaged and multi-basin dynamic ocean model based on that of Stocker et al. (1992), with meridional resolution of 2.5° latitude and 20 vertical levels. Connected to these components the model also includes a one layer thermodynamic sea ice model with horizontal ice transport (Ganopolski & Rahmstorf, 2001), the three-dimensional polythermal ice sheet model SICOPOLIS (Greve, 1997), the dynamic global vegetation model VECODE (Brovkin et al., 1997), a dynamic global carbon cycle model with land and ocean biogeochemistry (Brovkin et al., 2002, 2007; Ganopolski & Brovkin, 2017), and modules for aeolian dust effects (Bauer & Ganopolski, 2010, 2014).

The model representation of the atmosphere–vegetation coupling is particularly important for this study. In CLIMBER-2 the interaction between these components occurs every year. Annual growing degree days and precipitation are used to compute equilibrium vegetation cover based on the approach by Brovkin et al. (1997). In turn, the vegetation-related variables modify surface albedo, aerodynamic roughness length and evapotranspiration, which affect energy and moisture fluxes between land and atmosphere components, similarly as in Dickinson et al. (1993). Vegetation cover is computed as fractional amounts of two plant functional types: trees and grasses. Non-vegetated areas can include fractions of desert or glacier cover types. Details about atmosphere–vegetation coupling in CLIMBER-2 and parameter values are given in Brovkin et al. (2002).

The model has a low computational cost that enables simulations over long timescales, when multiple components of the climate system can interact. Despite its coarse spatial resolution and simplifications the model captures well past climate changes (Claussen et al., 1999a), as well as the aggregated large–scale features of modern climate (Ganopolski et al., 1998). Its response to changes in boundary conditions and climate forcings is comparable to that of more comprehensive models (Ganopolski et al., 2001), and it successfully simulates glacial–interglacial cycles (Ganopolski et al., 2010; Ganopolski & Brovkin, 2017). In fact, CLIMBER-2 is currently the only geographically explicit model which can be used for an ensemble of simulations of glacial–interglacial cycles. For the specific case of North Africa CLIMBER-2 has already been used to study its climate on multi-millennia timescales with a favourable performance (e.g., Claussen et al., 1999b, 2003; Tuenter et al., 2005; Tjallingii et al., 2008).

A.2.2 *Experiments of past AHPs*

We simulate the coupled atmosphere, ocean, sea ice, land surface and vegetation dynamics for the past 190 kyr. The polythermal ice sheets model and global carbon cycle model components are not employed since we prescribe ice sheets extent and atmospheric GHGs levels using available data. Simulations start from an equilibrium state attained after a 5 kyr simulation that maintained parameters set at 190 ka values. We perform 15 transient simulations prescribing possible combinations of climate forcing factors: GHGs levels, ice sheets extent and orbital parameters. Forcings are prescribed either with a transient series from past evidence or with a single reference value as shown in Fig. A.1. Reference values are taken from the transient series close to the Eemian interglacial state at about 125 ka and close to the Last Glacial Maximum (LGM) at about 21 ka. The GHGs radiative forcing change from preindustrial (PI) conditions in Fig. A.1a comes from Ganopolski and Calov (2011) and it considers variations in gases:

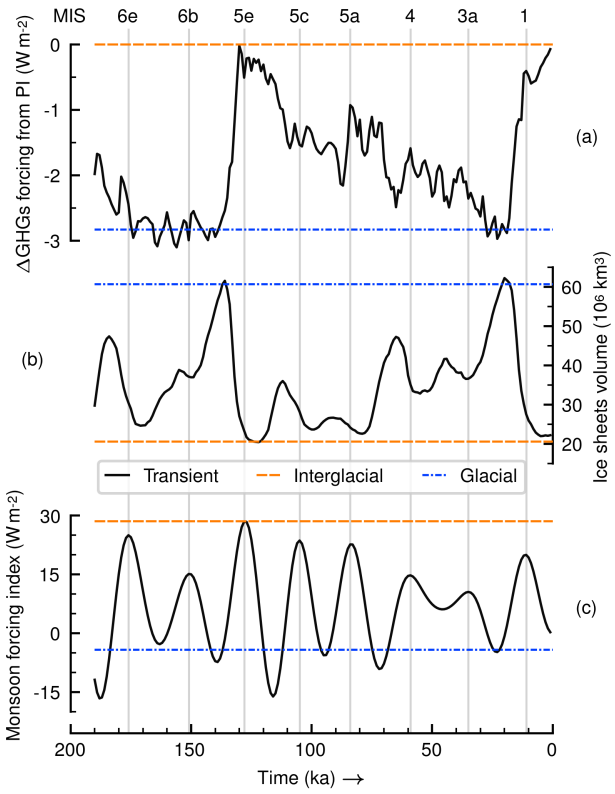

Figure A.1: Prescribed forcing parameters in simulations: (a) GHGs radiative forcing change (Δ) from preindustrial (PI), (b) ice sheets global ice volume and (c) orbital forcing via the monsoon forcing index. Transient series come from Antarctic ice cores, modelled ice sheets data and orbital theory, respectively. Horizontal lines are cases when forcings are fixed to interglacial or glacial reference values. Vertical lines indicate maxima in the monsoon forcing index and are labelled using MIS names on top (see Appendix A.A1 about notation).

CO_2, CH_4 and N_2O, that are in line with Antarctic ice cores (Petit et al., 1999; EPICA Community Members, 2004). Ice sheets data are model output from a simulation also in Ganopolski and Calov (2011) which agrees with sea level changes in Waelbroeck et al. (2002) and the reconstructions of Peltier (1994). Ice sheets are represented by a spatially distributed transient series varying mostly in the Northern Hemisphere, even though we show only the global cumulative ice volume (Fig. A.1b). Earth's orbital parameters (precession, obliquity and eccentricity) vary according to Berger (1978). We show their secular variations using the monsoon forcing index defined by Rossignol-Strick (1983), which measures an insolation gradient in the tropics relevant to monsoon systems and AHPs (Fig. A.1c). In the text and in Fig. A.1 we label peaks in the monsoon forcing index using MIS names to ease location of time slices when AHPs usually occur. Details

Table A.1: Experiments and forcing settings. Entries in "Field" column indicate how a climatic variable taken from an experiment is used in the factor separation method (see Appendix A.B1 with equations). Transient series are those in Fig. A.1. The future set is not part of the separation method. 0 ka is present-day and kyr AP is millennia after present-day.

Name	Time	Field	Description	GHGs radiative forcing change from PI ($W\,m^{-2}$)	Ice sheets volume ($10^6\,km^3$)	Monsoon forcing index ($W\,m^{-2}$)
E0	190 ka–0 ka	f_o	Control experiment.	Transient	Transient	Transient
EI1	190 ka–0 ka	$f_{I,\,GHG}$	Interglacial separation set.	0.0	Transient	Transient
EI2		$f_{I,\,Ice}$		Transient	20.5	Transient
EI3		$f_{I,\,Orbital}$		Transient	Transient	28.5
EI4		$f_{I,\,GHG\,+\,Ice}$		0.0	20.5	Transient
EI5		$f_{I,\,GHG\,+\,Orbital}$		0.0	Transient	28.5
EI6		$f_{I,\,Ice\,+\,Orbital}$		Transient	20.5	28.5
EI7		$f_{I,\,GHG\,+\,Ice\,+\,Orbital}$		0.0	20.5	28.5
EG1	190 ka–0 ka	$f_{G,\,GHG}$	Glacial separation set.	−2.8	Transient	Transient
EG2		$f_{G,\,Ice}$		Transient	60.7	Transient
EG3		$f_{G,\,Orbital}$		Transient	Transient	−4.2
EG4		$f_{G,\,GHG\,+\,Ice}$		−2.8	60.7	Transient
EG5		$f_{G,\,GHG\,+\,Orbital}$		−2.8	Transient	−4.2
EG6		$f_{G,\,Ice\,+\,Orbital}$		Transient	60.7	−4.2
EG7		$f_{G,\,GHG\,+\,Ice\,+\,Orbital}$		−2.8	60.7	−4.2
F0	0 ka–100 kyr AP	–	Future set.	0 Gt C scenario	22.2	Berger (1978)
F1		–		1000 Gt C scenario	22.2	Berger (1978)
F2		–		2000 Gt C scenario	22.2	Berger (1978)
F3		–		3000 Gt C scenario	22.2	Berger (1978)
F4		–		4000 Gt C scenario	22.2	Berger (1978)
F5		–		5000 Gt C scenario	22.2	Berger (1978)

about forcings, computation of the monsoon forcing index and MIS nomenclature are given in Appendix A.A1.

Experiments of past AHPs and their forcing setup combinations follow the factor separation method of Stein and Alpert (1993) for three factors: (1) GHGs radiative forcing changes from PI, (2) ice sheets extent and (3) orbital parameters. Using this method it is possible to estimate individual (also called "pure") and synergistic contributions of the forcing factors to a simulation outcome (or predicted climatic field). The method assumes all contributions are additive and can be separated subtracting fields of a set of sensitivity simulations. To implement the method a specific simulation target must be chosen in order to calculate deviations from a baseline or control state (i.e., the factor separation depends on the target or point of view). We are interested in knowing how much the forcings contribute to the simulation of AHPs. We choose two simulation targets with opposing global climates and AHP situations: the Eemian interglacial around 125 ka (i.e., warm global climate) with a strong AHP and the LGM around 21 ka (i.e., cold global climate) with no AHP. Experiments and forcings combinations are shown in Table A.1. Only in the control experiment E0 all forcings vary realistically as in the transient series obtained from past data (see Fig. A.1). For the rest of experiments we have two sets of simulations using the interglacial or glacial reference values shown in Table A.1, with all possible "fixed-or-transient" combinations in

each set. For instance, simulation EI4 has both GHGs forcing change and ice sheets fixed at the interglacial reference values for the entire 190 kyr run (i.e., they are kept constant at interglacial levels). Likewise for EG4 but instead the fixed values are the glacial levels. Experiments EI7 and EG7 have the three forcings fixed at their respective reference points. Details and equations of the separation analyses are given in Appendix A.B1.

A.2.3 *Experiments of future AHPs*

The low computational cost of the model and information available about future changes in the forcings enable us to also look into potential future climate change in North Africa. We are also interested in knowing how much our findings from the past can inform the future. Additional simulations start from present-day conditions in the control experiment E0 and cover the next 100 millennia after present (kyr AP). Projections of GHGs radiative forcing changes from PI are based on the CO_2 emissions scenarios of Archer and Brovkin (2008), which estimate possible cumulative amounts of carbon to be released to the atmosphere in units of gigatonnes of carbon (Gt C). The emission estimates take into account both data from the reports of the Intergovernmental Panel on Climate Change (IPCC) and the size of available coal deposits to designate "moderate" or "large" amounts. Six experiments include a scenario of null emissions since preindustrial conditions (0 Gt C), a "moderate" emissions scenario with a release of 1000 Gt C, a "large" emissions scenario with a release of 5000 Gt C, and the intermediate cases of 2000, 3000 and 4000 Gt C. In these scenarios 90 % of the emissions are assumed to occur within the first few centuries of simulation, meaning there is an early peak of atmospheric concentration of CO_2 that subsequently decays to an equilibrium value (higher than preindustrial). These experiments are also shown in Table A.1. For these simulations we ignore the radiative forcing effect of other GHGs. The orbital forcing is considered to continue changing following Berger (1978). We keep the ice sheets fixed at the preindustrial setting, neglecting the effects of a potential complete deglaciation or a new glacial inception. The latter is justified since a large ice sheet should not emerge within the next 100 kyr AP, even for the moderate emissions scenario (Ganopolski et al., 2016).

A.3 RESULTS

We study century-mean values of model output for near-surface air temperature, daily precipitation and fractional vegetation coverage in the Sahara region. In the model the Sahara is a single grid box spanning approximately 20°–30°N and 15°W–50°E. We present astronomical seasons averages of summer (June-July-August) and win-

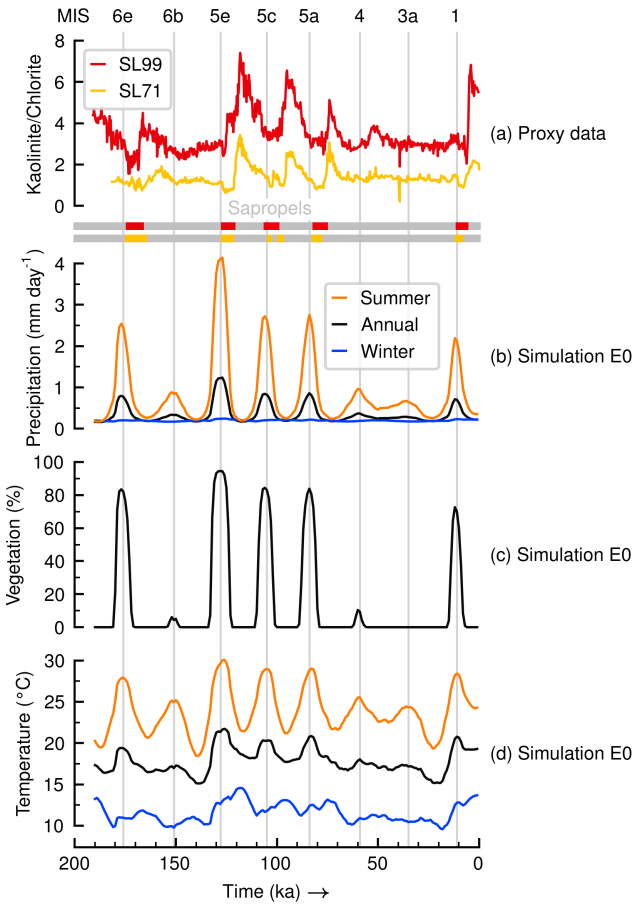

Figure A.2: Comparison of (a) proxy data with (b, c, d) results from control simulation E0 in the Sahara grid box: annual and seasonal means of (b) precipitation, (c) vegetation cover fraction and (d) near-surface temperature. Proxy data are ratios of clay minerals and sapropel layers from sediment cores SL71 and SL99 from the Eastern Mediterranean Sea described in Ehrmann and Schmiedl (2021). Vertical lines indicate maxima in the monsoon forcing index and are labelled using MIS names on top.

ter (December-January-February) for temperature and precipitation, which are resolved daily in the model, whereas for vegetation cover fraction only annual mean values can be reported.

A.3.1 *Simulation of past AHPs*

Results of the control simulation E0 are shown in Fig. A.2, alongside proxy data from sediment cores SL71 and SL99 from the Eastern Mediterranean Sea (Ehrmann & Schmiedl, 2021). The proxies in Fig. A.2a show pulses in the ratios of fine-grained minerals (kaolinite and chlorite), found always following a sapropel layer in the sediments. The sapropel doublet during MIS 5c for core SL71 corresponds to a single event in spite of the interruption in the sediments, which

could be explained by postdepositional redox reactions (Grant et al., 2016). The sapropel layers indicate past instances of AHPs, when enhanced riverine discharge suppressed seabed oxygenation in the Mediterranean Sea, while the amplitudes of the dust pulses reveal the strength of the hydrological cycle during their preceding AHPs, since the minerals production depends on rainfall intensity (weathering). In Fig. A.2a the dust pulses lag the sapropel layers because aeolian dust transport from water bodies across (most likely) North Africa can only occur once arid conditions are re-established after an AHP. The comparison between the proxy data and our simulations can only be qualitative in nature, since we do not model either dust transport into the Mediterranean Sea nor sapropel formation. It is remarkable, however, that the control simulation E0 (Fig. A.2b–d) shows large peaks close in time with the sapropel layers in the proxies. Also both in simulation E0 and the proxies the strongest signals happen during MIS 5e. The simulation E0 is in closer agreement with the data from core SL71, where the pulses after MIS 5c and 5a have similar magnitude. Comparison with other proxy data from marine cores off the coasts of West Africa (Skonieczny et al., 2019) and East Africa (Tierney et al., 2017a), likewise reveals agreement in timing and in magnitude of the E0 simulation with the proxies (not shown).

In Fig. A.2 simulation E0 shows that peak values of precipitation, vegetation cover fraction and temperature in the Sahara region coincide with peaks in the monsoon forcing index during the past 190 kyr. The peak values are summarised in Table A.2. In the case of precipitation (Fig. A.2b) and temperature (Fig. A.2d) this is most conspicuous in the summer seasonal means, with large peaks similarly as evident as those in the vegetation cover fraction (Fig. A.2c). The strongest peak values occur during the last two interglacial periods at stages MIS 5e and 1, as well as during stages MIS 6e, 5c and 5a. Only these five MIS periods have a vegetation cover fraction above 70 %. The vegetation peaks happen during warmer periods when annual mean daily precipitation is greater than $0.7\,\mathrm{mm\,d^{-1}}$. This could accumulate to more than $250\,\mathrm{mm\,yr^{-1}}$, well above the minimum limit estimated to support perennial grasslands and savanna biome types in North Africa (Larrasoaña et al., 2013). Although this precipitation value is low compared to estimates from proxy data (Braconnot et al., 2012), any amount over $200\,\mathrm{mm\,yr^{-1}}$ is still distinctly greater than present-day values across the region (Bartlein et al., 2011), and is within the variability range of more sophisticated climate models for the last AHP during the Holocene (e.g., Harrison et al., 2015; Pausata et al., 2016; Dallmeyer et al., 2020). Therefore we consider these peak times to be simulated past AHPs with CLIMBER-2. The oldest one at MIS 6e was also found by Tuenter et al. (2005), and those at MIS 5c, 5a and 1, agree with the results of Tjallingii et al. (2008). Measuring from the moment the modelled vegetation starts growing until the moment it

Table A.2: Forcing values and results in the Sahara grid box of seasonal and annual mean values in control experiment E0, taken near maxima of the monsoon forcing index. Sapropel layers are those in Fig. A.2a. Values in parentheses are winter and summer means, in that order.

		Forcing values			Simulated response in Sahara			
MIS	Time (ka)	GHGs forcing change ($W\,m^{-2}$)	Ice sheets volume ($10^6\,km^3$)	Monsoon forcing index ($W\,m^{-2}$)	Temperature (°C)	Precipitation ($mm\,d^{-1}$)	Vegetation (%)	Sapropel layer
6e	176	−2.4	30.5	25.0	19.4 (11.0, 27.9)	0.8 (0.2, 2.5)	83.5	Yes
6b	151	−3.0	37.1	15.1	17.3 (10.1, 25.2)	0.3 (0.2, 0.9)	6.1	No
5e	128	−0.5	23.3	28.5	21.6 (13.0, 30.0)	1.2 (0.2, 4.1)	94.5	Yes
5c	105	−1.5	28.2	23.6	20.3 (12.0, 29.0)	0.8 (0.2, 2.7)	84.4	Yes
5a	84	−0.9	24.1	22.7	20.8 (12.5, 29.0)	0.9 (0.2, 2.8)	83.8	Yes
4	59	−1.6	35.1	14.8	18.0 (10.9, 25.6)	0.4 (0.2, 1.0)	10.4	No
3a	35	−2.4	36.6	10.5	17.3 (10.6, 24.4)	0.3 (0.2, 0.7)	0.0	No
1	11	−0.4	27.5	20.0	20.8 (12.8, 28.4)	0.7 (0.2, 2.2)	72.6	Yes

vanishes (Fig. A.2c), the AHPs last on average 10.8 kyr, with the one at MIS 5e being the longest (12 kyr) and the one at MIS 1 the shortest (9 kyr).

A.3.2 *Correlation of forcings and AHPs*

A first approximation to study the effects of the forcings on the modelled AHP response follows a simple linear regression analysis. With the values from Table A.2 we plot paired combinations of forcings and response variables in phase diagrams and fit regression lines with the ordinary least-squares method and use the statistic R^2 and the p-value of the F-statistic as goodness-of-fit estimates. The forcings are included in the regression analysis (besides the modelled response) because even though we know that GHGs levels and ice sheets are not independent from the orbital forcing, we do not know exactly how they relate to each other during AHPs. We also recognise that GHGs and ice sheets are global features while the monsoon forcing index is a regional insolation gradient. We find there is a strong correlation ($R^2 = 0.75$, p-value $= 0.006$) between the average ice sheets volume and the monsoon forcing index peaks, with the highest monsoon forcing index values having the least ice volume. In contrast, we see a weak correlation ($R^2 = 0.27$, p-value $= 0.19$) between the GHGs radiative forcing and the monsoon forcing index peaks.

The modelled response correlates strongly with the monsoon forcing index during its peak times, as shown in Fig. A.3. For precipitation (Fig. A.3a) we observe a positive linear relationship for summer seasonal ($R^2 = 0.93$, p-value $= 0.0001$) and annual ($R^2 = 0.92$, p-value $= 0.0001$) means, therefore higher monsoon forcing index values yield higher precipitation in the Sahara grid box. Winter precipitation being almost a flat line shows this modelled variable in the Sahara does not depend on the monsoon forcing index. In the case

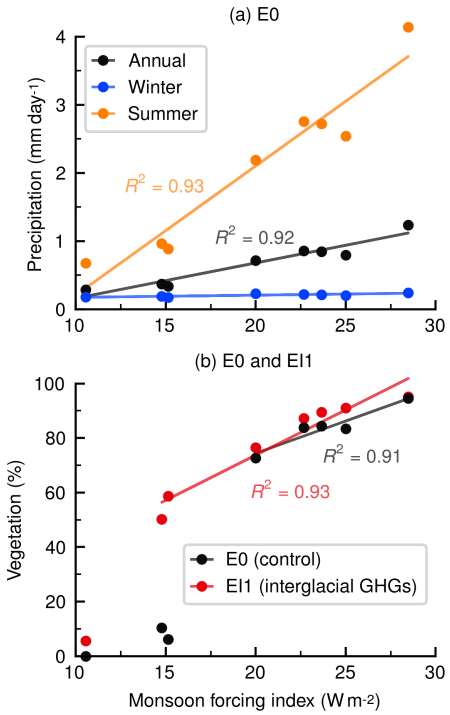

Figure A.3: Correlation of the monsoon forcing index with the simulated response in the Sahara grid box in control simulation E0 for mean values of (a) precipitation and (b) vegetation cover fraction during peak times of the monsoon forcing index. Values of E0 are the same from Table A.2. In (b) we also include the modelled vegetation from experiment EI1 with fixed interglacial GHGs.

of vegetation (Fig. A.3b) we see non-linear behaviour with an abrupt large jump from low (about 10 %) to high (about 70 %) vegetation coverage within a small range of variation of the monsoon forcing index from around 15 to 20 $\mathrm{W\,m^{-2}}$. In fact, for vegetation cover the change-point analysis of Killick et al. (2012) finds a change-point (i.e., a significant jump in the linear regression) between values of the monsoon forcing index of 15 $\mathrm{W\,m^{-2}}$ and 20 $\mathrm{W\,m^{-2}}$. When applied to the correlation of precipitation with the monsoon forcing index, the change-point analysis does not find a jump in the linear regression at the same level of significance as for vegetation cover. Vegetation cover values occurring past the threshold range have a strong correlation ($R^2 = 0.91$, p-value $= 0.012$) with the monsoon forcing index.

We also include in Fig. A.3b the vegetation response of sensitivity simulation EI1 (with interglacial GHGs forcing) because it shows that the insolation threshold might be sensitive to the GHGs forcing. With interglacial GHGs radiative forcing (experiment EI1) the threshold decreases below 15 $\mathrm{W\,m^{-2}}$ and the correlation past this threshold between vegetation cover and the monsoon forcing index is still strong ($R^2 = 0.93$, p-value $= 0.0005$). Looking also at the GHGs radiative forcing values in Table A.2 for MIS 6b and 4 (the points close to

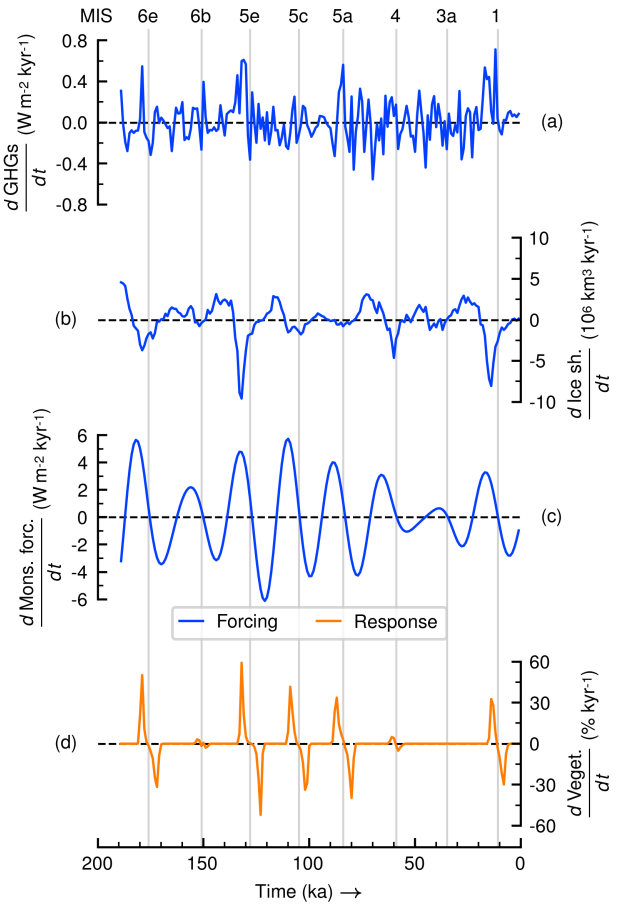

Figure A.4: Rates of change of forcings and modelled response in control experiment E0: (a) GHGs radiative forcing change from PI, (b) global ice sheets volume, (c) monsoon forcing index and (d) simulated vegetation cover fraction in the Sahara grid box. Vertical lines show maxima of monsoon forcing index and are labelled using MIS names on top.

15 W m^{-2} in Fig. A.3), we find that there is an average increase of about 2 W m^{-2} in the GHGs forcing in simulation EI1 relative to the control simulation E0. Hence we tentatively suggest that an increase in GHGs forcing of some 2 W m^{-2} is associated with a decrease in the threshold of the monsoon forcing index by some 5 W m^{-2}. This implies a sensitivity of the threshold in monsoon forcing index to a change in GHGs forcing of around -2.5.

Existence of such threshold behaviour suggests that changes in the model should happen at a fast rate. Already in Fig. A.2c we see that vegetation growth and decline phases occur rapidly. To look into the rates of change more carefully we plot in Fig. A.4 the temporal derivatives of the forcings and the simulated vegetation fraction in the Sahara in the control experiment E0. This figure shows how the non-linear dynamics of the vegetation response does not follow smoothly the speeds of change in any of the forcings. However, vegetation

growth and decline phases are coherent with times of increasing and decreasing rates of the monsoon forcing index, respectively. In fact, we also find a strong correlation ($R^2 = 0.96$, p-value < 0.0001) between peak speeds of change of the monsoon forcing index and peak growth and decline rates of the vegetation response. The fastest vegetation growth rate occurs during MIS 5e ($59.2\,\%\,\mathrm{kyr}^{-1}$), when a peak in the increasing rate of the monsoon forcing index coincides with a relatively strong increase in the speed of change of the GHGs radiative forcing and the strongest decline rate in the ice sheets volume. Figure A.4d shows that usually the vegetation growth phases, during AHP onset, occur at faster rates than the decline phases during AHP terminations, which is most conspicuous during MIS 6e (onset at $50.1\,\%\,\mathrm{kyr}^{-1}$ versus termination at $-31.6\,\%\,\mathrm{kyr}^{-1}$). Only during MIS 5a this is not the case (onset at $33.7\,\%\,\mathrm{kyr}^{-1}$ versus termination at $-39.7\,\%\,\mathrm{kyr}^{-1}$), when ice sheets do not wane at a strong pace. In average, during AHPs the vegetation growth phase lasts about 5.2 kyr, while the vegetation decline about 6.2 kyr.

A.3.3 *Factor separation analyses*

We suspect that differences in intensity amongst AHPs should be mainly determined by differences in the state of GHGs, ice sheets and orbital configuration at the time they occur. However, we do not know how much each of the forcings is affecting the AHPs intensities. To look into this we perform simulations according to the factor separation method of Stein and Alpert (1993) and implement its equations (see Appendix A.B1) using the model output for annual means of temperature, precipitation and vegetation fraction in the Sahara region. Because the separation method depends on the chosen simulation target we carry out two analyses: one of them isolates the contributions of the forcing factors to attain an Eemian-like strong AHP response (i.e., interglacial perspective), while another one does it for an LGM-like non-AHP response (i.e., glacial perspective).

Both target responses for the two separation analyses are represented in simulations EI7 and EG7. Simulation EI7 from the interglacial perspective has all three forcing factors fixed at interglacial conditions (using the Eemian as reference). In this simulation, annual mean Saharan temperature stays for all times at 21.8 °C, precipitation at $1.3\,\mathrm{mm\,d}^{-1}$ and vegetation cover fraction at 95.8 %. These values resemble those around the Eemian peak (about 125 ka) in the control simulation E0 (see Fig. A.2). Simulation EG7 from the glacial perspective has forcings fixed at glacial conditions (using LGM as reference). In this simulation, annual mean Saharan temperature remains for all times at 15.2 °C, precipitation at $0.2\,\mathrm{mm\,d}^{-1}$ and vegetation cover fraction at 0.0 %. These values resemble those around the LGM (about 21 ka) in the control simulation E0 (see Fig. A.2). Therefore,

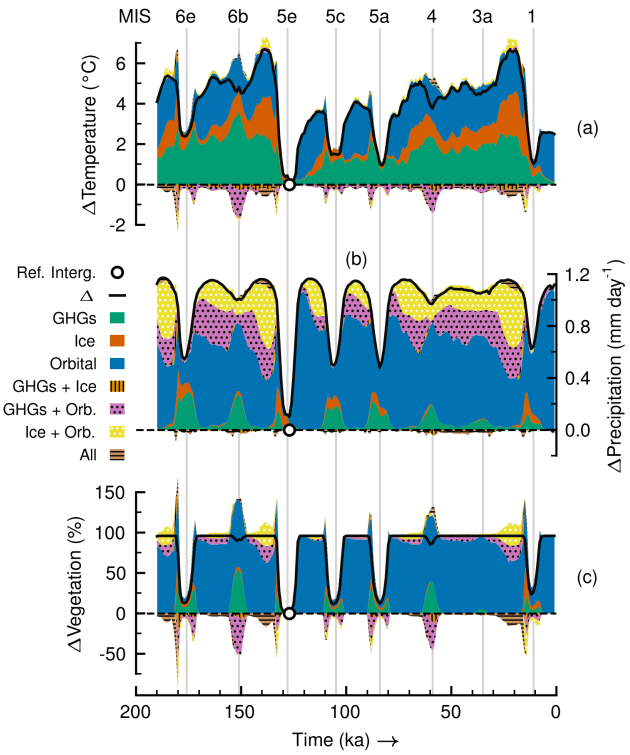

Figure A.5: Factor separation analysis in the Sahara grid box from interglacial perspective for annual means of (a) near-surface temperature, (b) precipitation and (c) vegetation cover fraction. Colours indicate contributions from individual forcings and related synergies to the total deviation in EI7 (Eemian-like AHP) from the control experiment (Δ = EI7 − E0). Synergies are shown also with hatching. A marker shows the location of the reference interglacial state, where the difference between EI7 and E0 is minimum. Vertical lines indicate maxima of the monsoon forcing index and are labelled using MIS names on top.

the interglacial perspective experiment EI7 keeps a permanent strong Eemian-like AHP for the entire simulation, whereas the glacial EG7 keeps none. Through the factor separation method we then estimate how much each of the forcings is contributing at all times to the differences between the control experiment E0 and targets EI7 (strong AHP) and EG7 (no AHP).

Results of the separation analysis from the interglacial perspective are shown in Fig. A.5 for AHP temperature, precipitation and vegetation cover fraction. With the forcing factors fixed at interglacial levels, the modelled response in EI7 (Eemian-like AHP) deviates always positively from the control experiment E0 for the three climatic variables. This is as expected since the resulting values of EI7 in the previous paragraph are higher than those in the control E0 at all times (only Eemian in E0 is close to EI7). The slight offset between E0 and EI7 at MIS 5e occurs because the combination of prescribed forcings in

EI7 all happen closely around MIS 5e, but not exactly at the same time during the control experiment E0. The relevant outcome of the separation method lies in the colours (and hatching) in Fig. A.5, which show how the forcings contribute to the EI7 − E0 difference. For AHP temperature (Fig. A.5a) the individual contribution of each forcing is directly proportional to the change in the forcing. To see this it is necessary to compare differences between the control forcing values in the transient series in Fig. A.1 and the interglacial reference level in that same figure. For instance, at stage MIS 6b the largest contribution to temperature change comes from the GHGs radiative forcing change (Fig. A.5a), since that is the forcing with the largest difference between the transient series and the interglacial horizontal line (see also Fig. A.1a). For the AHP temperature response the synergistic effects are small in comparison to the individual contributions. Averaging the contributions to AHP temperature for the whole time series in Fig. A.5a yields that GHGs add about 1.6 °C (41.1 % of change from E0), ice sheets 0.8 °C (19.9 % of change from E0) and the orbital forcing 1.8 °C (45.9 % of change from E0). The synergy between GHGs and the orbital forcing is small but is the synergy with the largest effect adding in average about −0.2 °C (−4.9 % of change from E0).

The AHP precipitation case in the separation analysis is different to the temperature one. Figure A.5b shows that the AHP precipitation response largely depends on the orbital forcing (substantial blue colour). Not only the individual contribution of this forcing is the largest for all times, but also its synergies with the other two forcings have relatively large effects. The individual contribution of the GHGs radiative forcing to changes in AHP precipitation is small. The individual effects of ice sheets on AHP precipitation are negligible as well. No synergistic effects seem to exist between the ice sheets forcing and the GHGs radiative forcing. Averaging the contributions to AHP precipitation for the whole time series in Fig. A.5b we obtain that GHGs add about 0.1 mm d^{-1} (6.7 % of change from E0), ice sheets close to 0.0 mm d^{-1} (2.2 % of change from E0) and the orbital forcing about 0.6 mm d^{-1} (59.3 % of change from E0). Both synergies of the orbital forcing with GHGs and ice sheets round up each one to 0.2 mm d^{-1} (each about 15 % of change from E0). This means the effects of the orbital forcing and these two synergies with GHGs and ice sheets amount to about 90.9 % of the change from E0.

AHP vegetation results in Fig. A.5c are similar to the AHP precipitation case, although the individual effect of the orbital forcing is much more conspicuous (predominant blue colour). The negative synergistic effects seen in the vegetation changes should be an artefact of the separation analysis method because vegetation is a bounded quantity. Consider, for example, the time around 150 ka during MIS 6b, when the Sahara is much greener, close to a 100 % vegetation cover, in simulation EI7 than in simulation E0 (Fig. A.5c). The individual contribution

of orbital forcing (blue colour) would make some 90 % of the Sahara green, and the GHGs forcing (green colour) some 50 %. If both forcings are active, then the pure contributions cannot be superposed (do not add linearly), because the Sahara cannot be more than 100 % covered with vegetation. Therefore, the synergy between these forcings (pink colour and dot hatching) has to be negative. Average contributions to AHP vegetation for the whole series in Fig. A.5c are about 5.8 % from GHGs (6.4 % of change from E0), 2.2 % from ice sheets (2.4 % of change from E0) and 72.6 % from the orbital forcing (79.5 % of change from E0). The synergy (when positive) between GHGs and orbital forcing adds in average about 4.0 % (4.4 % of change from E0) while the synergy (when positive) between ice sheets and orbital forcing about 5.3 % (5.8 % of change from E0). The orbital forcing and all of its synergies account for about 90.4 % of vegetation change from E0.

From the glacial perspective in the additional separation analysis we do not find anything significantly new, hence details are to be found in Appendix A.C1. Figure A.C1.1 shows that in this case the deviations in EG7 from the control E0 are always negative for the three climatic variables and the effects of the ice sheets changes are larger than those of the GHGs. Nonetheless, the same behaviour for temperature is observed, with changes being proportional to the changes in the forcings. This analysis demonstrates that it is the relatively low maxima in orbital forcing that result in the absence of AHP conditions at MIS 6b, 4 and 3a – rather than the low GHGs radiative forcing or the large ice sheets. From this perspective synergies are more difficult to assess because of the lower bounds in precipitation ($0\,\mathrm{mm\,d^{-1}}$) and vegetation cover fraction (0 %).

A.3.4 *AHPs in scenarios of future climate change*

When computing the monsoon forcing index for the next 100 kyr AP (millennia after present) we see that the onset threshold range of past AHPs (15–20 $\mathrm{W\,m^{-2}}$ in the model) will not be crossed within the next some 60 kyr (Fig. A.6a). The amplitude in the monsoon forcing index (proxy for orbital forcing) is much smaller than that of past times (see Fig. A.1) due to low eccentricity in the Earth's orbit. Only for the time around 66 kyr AP the monsoon forcing index approaches the onset threshold range. From the sensitivity simulation EI1 in which the GHGs radiative forcing change is set to interglacial level, we find that an increase in GHGs forcing by some $2\,\mathrm{W\,m^{-2}}$ can lower the threshold in the monsoon forcing index by some $5\,\mathrm{W\,m^{-2}}$ (Fig. A.3b). Hence we expect that in a climate with much stronger GHGs forcing and much warmer global temperatures (Fig. A.6b and c) the threshold might decrease even further. The simulations F0–5 corroborate the lesson learnt from the study of the past; Fig. A.6d shows AHP responses for monsoon forcing indices below $10\,\mathrm{W\,m^{-2}}$.

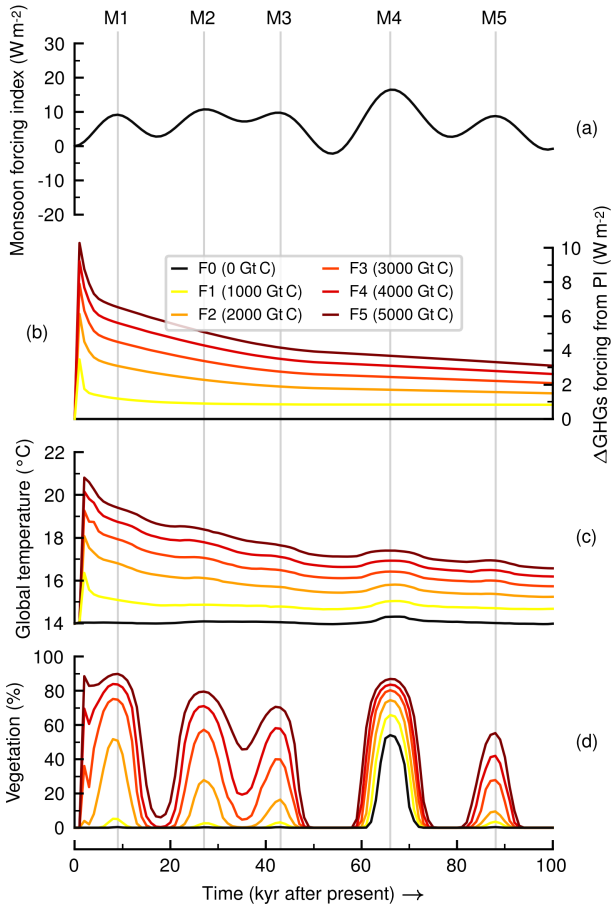

Figure A.6: AHPs in future climate change scenarios for the next 100 kyr AP: (a) computed monsoon forcing index, (b) scenarios of GHGs radiative forcing changes from PI, (c) simulated global near-surface temperature and (d) modelled vegetation fraction in the Sahara grid box. Vertical lines indicate future peaks in the monsoon forcing index. Total cumulative emissions of carbon are shown in parentheses in the legend.

The modelled vegetation response in Fig. A.6d shows the potential effects of increased GHGs radiative forcing for climate in the Sahara. The no-emissions scenario F0 (0 Gt C) predicts that no AHP should occur before the next 60 kyr AP. For this scenario only at 66 kyr AP (named peak M4) the threshold range of the monsoon forcing index is crossed slightly at 16.5 W m^{-2}, and we see a vegetation response of about 54.1 %. However, for the "moderate" emissions scenario F1 (1000 Gt C) we see already that additional vegetation responses begin to occur at earlier monsoon forcing index peaks. These are still quite small responses, since the average change in GHGs radiative forcing stays close to 1 W m^{-2} for this scenario, and according to our estimate from the past simulations, this means the threshold range only decreases 2.5 W m^{-2} from its original position at 15–20 W m^{-2}, thus it remains higher than most peaks in the monsoon forcing index in Fig.

A.6a. Such mild responses are amplified as the GHGs radiative forcing increases with the other scenarios. For instance, for the "large" emissions scenario F5 (5000 Gt C) the vegetation cover response at 9 kyr AP (peak M1) with monsoon forcing index of only 9.2 $W m^{-2}$ is already at about 89.9 %, which is higher than that of the strongest monsoon forcing index peak M4 for any scenario. In this case the average GHGs forcing change is close to 6 $W m^{-2}$, which according to our calculations should lower the threshold range in the monsoon forcing index to about 2–7 $W m^{-2}$ (lowered 13 $W m^{-2}$), and this would explain why with only 9.2 $W m^{-2}$ of monsoon forcing index we see such a strong response. Therefore we see that the effect of the large GHGs radiative forcing in the early 60 kyr AP of simulation is compensating for the low monsoon forcing index values during this time. Nonetheless, this effect is only seen at the monsoon forcing index peaks, therefore the orbital forcing is still the triggering mechanism for the AHP response.

A.4 DISCUSSION

Our aim is to quantify the effects of multiple forcings on the simulated vegetation cover in the Sahara region during AHPs. To this end we use CLIMBER-2, a climate system model of intermediate complexity. CLIMBER-2 runs at a coarse resolution with three grid cells representing North Africa: Sahara, Sahel and tropical North Africa. CLIMBER-2 is a statistical–dynamical model in which the effect of weather on climate is parameterised. Hence CLIMBER-2 does not reveal any variability at decadal timescales and shorter. This implies that CLIMBER-2 cannot be used to study the role of decadal internal variability on AHPs, which might play an important role during transition phases (e.g., Liu et al., 2006; Bathiany et al., 2012; Brierley et al., 2018). Despite these limitations, CLIMBER-2 has proven a useful tool in many studies of large-scale climate processes at time scales of centuries to millions of years, including the first transient simulations of abrupt vegetation changes in Africa (e.g., Claussen et al., 1999b, 2003).

We begin by re-assessing the ability of CLIMBER-2 to simulate past occurrences of AHPs during glacial–interglacial cycles. Our results broadly agree with previous efforts which also found the model's performance adequate (e.g., Tuenter et al., 2005; Tjallingii et al., 2008). Magnitude and timing of the simulated AHPs compare favourably not only with the proxy data in Tierney et al. (2017a), Skonieczny et al. (2019) and Ehrmann and Schmiedl (2021), but also with the data and simulations of Blanchet et al. (2021) and Kutzbach et al. (2020). Although comparison between simulations is limited due to large differences in spatial resolution, one difference that might be discussed is the magnitude of the simulated Holocene AHP. In the case of Blanchet et al. (2021) the AHP during the Holocene is stronger than those at MIS 5c and 5a. Our simulations show the opposite, in

agreement with the simulations in Kutzbach et al. (2020). To reconcile this we can look at the sediment records from the Mediterranean Sea discussed in Ehrmann and Schmiedl (2021) and say that simulations of Saharan climate in CLIMBER-2 evolve like the proxy data from semi-distal sites off the North African coastline, whereas those in Blanchet et al. (2021) resemble the data from proximal sites. Spatial heterogeneity of the changes during AHPs hinders model consistency with all proxy data. Nevertheless our simulations show a reasonable representation of the evolution of the climate in the Sahara during the last 190 kyr and this enables us to study the effects of forcing from GHGs, ice sheets and orbital parameters.

Analysis of our control simulation reveals that the AHP response in CLIMBER-2 is strongly correlated with the variations of the monsoon forcing index (proxy for orbital forcing based on a gradient in tropical insolation). This correlation was also found in the proxy data of Rossignol-Strick (1983) and Ehrmann et al. (2017). We find that there is a critical value of the monsoon forcing index that must be crossed to simulate Saharan greenings with the model. Past this threshold vegetation and precipitation feed back through biogeophysical changes (see Section A.2.1) and the climatic response in Sahara is amplified, resulting in an AHP (Brovkin et al., 1998; Claussen et al., 1999b). The amplification effect of the vegetation is clearly shown for this model in the sensitivity experiments of Claussen et al. (2003). Such non-linear responses from monsoon regions are also seen in proxy data (e.g., Rossignol-Strick, 1983; Ziegler et al., 2010). The threshold value we find lies somewhere between 15 and 20 $W\,m^{-2}$, thus we refer to it rather as a threshold range. Depending on the strength of additional factors (such as GHGs or ice sheets) the critical value could be closer to the lower or the upper boundary of this range. Below 15 $W\,m^{-2}$ until about 10 $W\,m^{-2}$ the model simulates only a weak vegetation response that cannot develop into an AHP, probably because within this range the amplifying feedback between vegetation and precipitation is not yet effective. Rossignol-Strick (1983) found that the threshold for occurrence of sapropel layers in sediment cores from the Mediterranean Sea (an indication of past AHPs) is about 19.8 $W\,m^{-2}$ (41 Langley d^{-1}). How close this value is from the estimate from CLIMBER-2 is useful as additional validation for the model, even though we simulate Saharan greening and not sapropel formation.

From the control simulation we also find that the maximum onset and termination speeds of the AHP vegetation response correlate well with the speed of change in the monsoon forcing index. However, for the fastest rates of vegetation change to occur it is also important that the trends of change in the ice sheets and the GHGs radiative forcing are favourable. For instance, at AHP onset during MIS 5e (fastest vegetation growth rate) the three forcing factors are synchronised with increasing monsoon forcing index, strong reduction of ice sheets and

an increasing rate of warming from GHGs radiative forcing change. Synchronisation of the forcings may also explain why we find that vegetation growth speeds during AHP onsets are generally faster than those of vegetation decline during AHP terminations. Such difference between onset and termination speeds was also suggested for the Holocene AHP in Shanahan et al. (2015). Because of a lag in the ice sheets rate of change with respect to the orbital forcing change, and because of the rather erratic rate of change in the GHGs, the three forcing factors are not usually coherent during AHPs terminations, resulting in slower vegetation rates of change (than those during AHP onsets). The only AHP termination that has faster vegetation changes than its onset occurs in stage MIS 5a, when a strong increase in ice sheets happens closely after the monsoon forcing index negative peak rate of change. In Lézine et al. (2011) the role of groundwater is described to explain why there is a rapid climate response during AHP onset and a subsequent slower more gradual AHP termination (with aquifers providing base flow). However, the model's hydrology does not include this feature and we focus only on the speeds of the forcings and their synchronisation.

We complement the study of the control simulation with a factor separation analysis. Its outcome confirms the dominant role of the orbital forcing in setting the amplitude of the modelled precipitation and vegetation responses of past AHPs. This was already described, for instance, in Tuenter et al. (2003), Kutzbach et al. (2020) and Blanchet et al. (2021). In particular, a factor analysis in Blanchet et al. (2021) showed that the individual roles of the GHGs radiative forcing and the global ice volume are of secondary importance for the strength of simulated AHPs. What we do with the factor separation method is quantitative estimates of said dominance or secondary importance of these forcings. From our results, when we add together the individual contributions from GHGs and ice sheets to the AHP precipitation or vegetation coverage responses, we find they amount to less than 20 % of the change induced by the orbital forcing alone. In fact, according to the simulations the orbital forcing alone (without effects from GHGs and ice sheets) should account for about 60 % (80 %) of changes in the AHP precipitation (vegetation cover) during the last 190 kyr. If its synergies are included, then the orbital forcing is responsible for more than 90 % of precipitation and vegetation changes. The factor separation also shows that GHGs and ice sheets have a larger impact on precipitation (and vegetation extent) when in synergy with the orbital forcing than individually. For near-surface temperature, in contrast, all the three forcing factors have a large effect individually and the synergies are all small in comparison.

But besides the dominance of the orbital forcing, the experiments of the factor separation method also reveal that the GHGs forcing has important consequences for the existence of the threshold behaviour in

the Sahara greening in the model. Our results suggest that an increase in GHGs radiative forcing of some $1\,W\,m^{-2}$ can lower the threshold in the monsoon forcing index by some $2.5\,W\,m^{-2}$. We explain this reduction by the fact that both, GHGs and orbital forcings, tend to amplify precipitation and greening. Hence, with higher GHGs levels the system responds earlier to a smaller orbital forcing. This has been demonstrated by, for instance, sensitivity experiments in Claussen et al. (2003) using also CLIMBER-2. They show how CO_2 and orbital forcings affect dynamic and thermodynamic contributions to Saharan precipitation. D'Agostino et al. (2019) also looked into these contributions in experiments of the Coupled Model Intercomparison Project phase 5 and arrived at a similar result. To understand how GHGs radiative forcing changes can alter the threshold in orbital forcing we look at the precipitation–vegetation feedback mechanism in the model (Claussen et al., 1999b). There is a minimum of Saharan vegetation (or precipitation) after which the precipitation–vegetation feedback sets in. With dynamic (circulation) effects alone, caused mainly by the changes in orbital parameters, the minimum triggering value of vegetation (or precipitation) is only reached when the monsoon forcing index is strong enough. However, when thermodynamical effects become stronger (increased GHGs, increased atmosphere warming, increased water vapour), the minimum value of vegetation (or precipitation) can be reached sooner or with a lower value of tropical insolation.

We take this lesson from the simulation of the past, about the relationship between GHGs and the threshold in orbital forcing, to evaluate the potential for future occurrences of humid periods. During the next 100 kyr AP the effects of changes in GHGs radiative forcing become larger while those of the orbital forcing become weaker. The future of the ice sheets is more uncertain, but a glacial inception is not likely to happen (Ganopolski et al., 2016) and if we ignore potential catastrophic consequences of a complete deglaciation, the impact of the ice sheets on AHPs should not change much from its current interglacial-like effect. The main finding is that the GHGs radiative forcing has an amplification effect on the simulated vegetation response that is large enough to overcome the limiting threshold for Sahara greening imposed by the orbital forcing. An alternative interpretation is that the GHGs forcing lowers the tropical insolation requirement for AHP onset. Here it is also important to mention that we are neglecting biogeochemical effects, since we prescribe GHGs levels, therefore potential effects of feedbacks between the carbon cycle and vegetation are being ignored. The AHP responses are still paced by precession variations but the increased atmospheric moisture (product of GHGs radiative warming) compensates for a weaker gradient in insolation (i.e., lower monsoon forcing index).

A.5 CONCLUSIONS

We have used the climate model of intermediate complexity CLIMBER-2 to assess the role on AHP strength of three climate forcing factors: (1) Earth's orbital parameters, (2) GHGs radiative forcing changes from preindustrial conditions and (3) ice sheets extent. Consistent with previous studies we find the model simulates reasonably well the evolution of past AHPs in terms of timing and magnitude. A newly discovered feature is the model contains the threshold behaviour of AHPs associated with the orbital forcing, previously found in proxy data. For the Saharan greening response during past AHPs, the simulated threshold in the monsoon forcing index lies within the range 15–20 $\mathrm{W\,m^{-2}}$. Besides this critical threshold range, the monsoon forcing index also correlates well with the simulated precipitation and vegetation cover responses during AHPs, not only with their magnitudes, but also with their rates of change: higher monsoon forcing index values lead to larger and faster changes. We show also that for fast changes to occur it is important that the rates of change of the forcings are synchronised. In the experiments this happens most often during AHP onset than termination and therefore the onset vegetation rate of change is generally faster.

In addition to the results from a control experiment we include two complete factor separation analyses that make explicit the dominant role of the orbital forcing setting the strength of past AHPs. The individual effects of the GHGs and ice sheets put together cause less than 20 % of the change induced by the orbital forcing. The effects of GHGs and ice sheets are notably greater when in synergy with the orbital forcing than separately. When we add together the effects of the orbital forcing and its synergies it amounts to over 90 % of the change in the AHP precipitation and vegetation cover responses. Despite the dominance of the orbital forcing, when we extend the simulations to cover the next 100 kyr AP we see that increased GHGs radiative forcing indeed lowers the critical value of the monsoon forcing index that must be crossed to simulate Saharan greening and the subsequent AHP response.

These findings both support previous research and contribute new insights to our understanding of AHPs dynamics. In several cases we are able to extrapolate previous knowledge from the Holocene AHP to earlier humid periods. In general the results agree with the consensus on predominance of the orbital forcing and make explicit the minor role that additional forcing from GHGs and ice sheets played during previous AHPs. However, because we consider both past and future simulations of AHPs we are able to show that GHGs may be more important than previously thought. A key message from this work is that even though the orbital forcing is the leading factor setting intensity and timing of AHPs, the atmospheric levels of GHGs have

the potential to lower the insolation requirement for AHP onset. We estimate the effect of the GHGs on the orbital forcing as a reduction of roughly 2.5 $W\,m^{-2}$ in the monsoon forcing index threshold range per 1 $W\,m^{-2}$ change in the GHGs radiative forcing. Such an effect of GHGs in the past might have been hidden by the strength of the non-linear response to the orbital forcing, combined with a relatively narrow range of GHGs variability, yet it may be particularly important when considering future occurrences of AHPs under climate change scenarios.

CODE AND DATA AVAILABILITY

Model source code of CLIMBER-2 is available upon request to the authors. Data and post-processing Python scripts to reproduce the authors' work are archived by the Max Planck Institute for Meteorology and are accessible without any restrictions at http://hdl.handle.net/21.11116/0000-000A-1217-8. The Ehrmann and Schmiedl (2021) data in Fig. A.2 are available at https://doi.org/10.1594/PANGAEA.923491, last access: 13 May 2021. The Lisiecki and Raymo (2005) data shown in Fig. A.A1.1 are available at http://lorraine-lisiecki.com/LR04stack.txt, last access: 16 December 2020.

APPENDIX

A.A1 *Forcings, monsoon forcing index and MIS notation*

Experiments with CLIMBER-2 differ only in the input data concerning the GHGs radiative forcing changes from preindustrial conditions, the extent of ice sheets and the orbital parameters (precession, obliquity and eccentricity). The GHGs radiative forcing input series agrees with data from Antarctic ice cores (Petit et al., 1999; EPICA Community Members, 2004). It is described in Ganopolski et al. (2010) as an equivalent CO_2 concentration (C_e) that includes variations of CO_2, CH_4 and N_2O. The total GHGs radiative forcing change from preindustrial (ΔRF) is computed as

$$\Delta RF = 5.35 \ln \frac{C_e}{C_0}, \tag{A.1}$$

where C_0 is set to 280 ppm. The reference values for glacial and interglacial conditions are about 165 ppm and 280 ppm of equivalent CO_2 respectively, which translate using Eq. A.1 into the radiative forcing values summarised in Table A.1.

In the case of ice sheets, Fig. A.1 shows only a global cumulative sum. For our simulations the input for the model is a gridded time series that is itself model output from an earlier simulation by Ganopolski and Calov (2011), who ran CLIMBER-2 model employing the ice sheets

Table A.A1.1: Orbital parameters in CLIMBER-2 simulations and their respective monsoon forcing index value.

Forcing type	Longitude of perihelion − 180°	Obliquity	Eccentricity	Monsoon forcing index
Transient	Berger (1978)	Berger (1978)	Berger (1978)	Berger (1978)
Interglacial–like	261.271°	24.124°	0.039	28.5
Glacial–like	97.771°	22.787°	0.019	−4.2

model component SICOPOLIS (Greve, 1997). The ice sheets evolution is in agreement with the sea level changes data from Waelbroeck et al. (2002) and the ice sheets maps of Peltier (1994). The reference values in this case are actually maps taken from the gridded series during the Eemian around 124 ka and the LGM around 21 ka. Their global cumulative ice volumes are those seen in Table A.1. Sea level change corresponding to the Eemian ice sheets map is −0.21 m, while that of the LGM is −106.44 m.

CLIMBER-2 by default computes the orbital parameters using the formulae of Berger (1978). In the experiments with fixed orbital forcing, we switch off the module for the Berger (1978) computation, and fix the values of precession (setting the angle from vernal equinox to perihelion), obliquity and eccentricity to those calculated for the Eemian and LGM periods. These values are shown in Table A.A1.1. To summarise them into a single value we use the monsoon forcing index defined by Rossignol-Strick (1983). To compute the index it is necessary first to compute the cumulative insolation during the Northern Hemisphere caloric summer season defined by Milankovitch (1941). We do this using the daily insolation values computed with the Berger (1978) theory (to obtain astronomical seasons) and the equations presented in Vernekar (1972). The caloric summer insolation is obtained for latitudes at the North Tropic near 23.45°N (I_T) and at the Equator (I_E) and then the monsoon forcing index (MI) at millennia before the present-day time slice t is

$$MI^t = 2I_T^t - I_E^t. \tag{A.2}$$

Figure A.1 shows in fact the variations in the monsoon forcing index from the 1950 Common Era (CE) reference value of about 482 W m^{-2} (around 995 Langley d^{-1}). Because AHPs occur usually at peak times of this index, it is convenient for the discussion to be able to identify every monsoon forcing index maximum. Therefore, to label them we use the Marine Isotope Stage (MIS) name that occurred at the time of the monsoon forcing index maximum. This is also useful because MIS names give hints about the state of the climate system at the time. In spite of there not being consensus in some of the names, here we make use of the notation scheme put forth by Railsback et al. (2015). Figure A.A1.1 shows the monsoon forcing index in the control experiment and the Lisiecki and Raymo (2005) dataset used by Railsback et al. (2015). In Fig. A.A1.1 a thin bar with coloured boxes

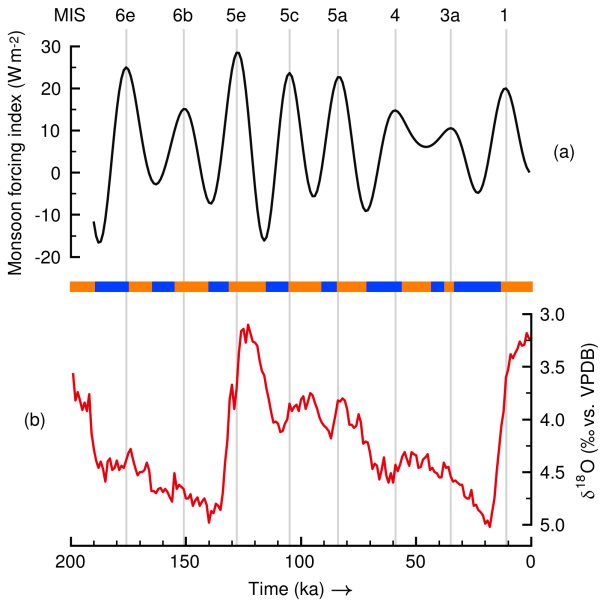

Figure A.A1.1: Notation for peaks of (a) monsoon forcing index uses MIS labels on top, following the scheme in Railsback et al. (2015), who used the (b) Lisiecki and Raymo (2005) marine isotope stack data to label the time slices shown in a bar with different colours. The isotope data are with respect to the standard Vienna Peedee Belemnite (VPDB). Vertical lines indicate the monsoon forcing index peaks.

shows the different periods they identified. Vertical lines then help us choosing the names for each monsoon forcing index peak.

A.B1 *Equations of separation analyses*

We perform experiments following the separation method of Stein and Alpert (1993). In this case it is done for three factors: (1) GHGs radiative forcing changes from PI, (2) global ice sheets volume and (3) orbital parameters. Consequently 2^3 simulations are needed for one separation analysis. The technique uses deviations of a simulation target with respect to a baseline or control state (experiment E0). We choose two different simulation targets: (1) global interglacial conditions with a strong AHP, and (2) global glacial conditions with no AHPs. The targets correspond to simulations EI7 and EG7 respectively. Therefore we do two separation analysis for AHPs: one from an

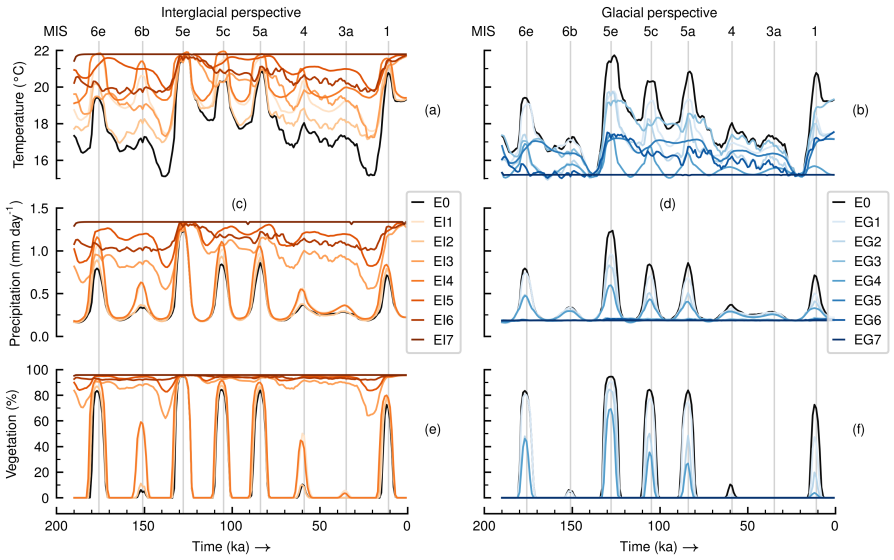

Figure A.A1.2: Results of annual means of (a, b) near-surface temperature, (c, d) precipitation and (e, f) vegetation cover fraction in the Sahara grid box for all simulations involved in the separation analyses from interglacial and glacial perspectives. Vertical lines indicate monsoon forcing index maxima and are labelled using MIS names on top.

interglacial perspective and another from a glacial one. The equations for the separation analysis from the interglacial perspective are

$$\hat{f}_0 = f_0, \tag{A.3}$$

$$\hat{f}_{\mathrm{I,\,GHG}} = f_{\mathrm{I,\,GHG}} - f_0, \tag{A.4}$$

$$\hat{f}_{\mathrm{I,\,Ice}} = f_{\mathrm{I,\,Ice}} - f_0, \tag{A.5}$$

$$\hat{f}_{\mathrm{I,\,Orbital}} = f_{\mathrm{I,\,Orbital}} - f_0, \tag{A.6}$$

$$\hat{f}_{\mathrm{I,\,GHG\,+\,Ice}} = f_{\mathrm{I,\,GHG\,+\,Ice}} - (f_{\mathrm{I,\,GHG}} + f_{\mathrm{I,\,Ice}}) + f_0, \tag{A.7}$$

$$\hat{f}_{\mathrm{I,\,GHG\,+\,Orbital}} = f_{\mathrm{I,\,GHG\,+\,Orbital}} - (f_{\mathrm{I,\,GHG}} + f_{\mathrm{I,\,Orbital}}) + f_0, \tag{A.8}$$

$$\hat{f}_{\mathrm{I,\,Ice\,+\,Orbital}} = f_{\mathrm{I,\,Ice\,+\,Orbital}} - (f_{\mathrm{I,\,Ice}} + f_{\mathrm{I,\,Orbital}}) + f_0, \tag{A.9}$$

$$\begin{aligned}\hat{f}_{\mathrm{I,\,GHG\,+\,Ice\,+\,Orbital}} = f_{\mathrm{I,\,GHG\,+\,Ice\,+\,Orbital}} - (&f_{\mathrm{I,\,GHG\,+\,Ice}} \\ &+ f_{\mathrm{I,\,GHG\,+\,Orbital}} + f_{\mathrm{I,\,Ice\,+\,Orbital}}) \\ &+ (f_{\mathrm{I,\,GHG}} + f_{\mathrm{I,\,Ice}} \\ &+ f_{\mathrm{I,\,Orbital}}) - f_0,\end{aligned} \tag{A.10}$$

where letters with hats in the left-hand side are the estimated effects on the simulation outcome of each forcing factor alone, when having a single subscript, or together in synergy with others when multiple subscripts. The letters on the right-hand side (known as climatic fields) represent the model output for a variable taken from the set of experiments part of the analysis. Therefore what is shown in Fig. A.2 are the fields f_0 from simulation E0 for temperature, precipitation and vegetation cover. Likewise $f_{\mathrm{I,\,GHG\,+\,Ice\,+\,Orbital}}$ represents the variables

when taken from simulation EI7. All fields for these variables are shown in Fig. A.A1.2, including all the other simulations. For the separation analysis from the glacial perspective the equations are

$$\hat{f}_0 = f_0, \tag{A.11}$$

$$\hat{f}_{\text{G, GHG}} = f_{\text{G, GHG}} - f_0, \tag{A.12}$$

$$\hat{f}_{\text{G, Ice}} = f_{\text{G, Ice}} - f_0, \tag{A.13}$$

$$\hat{f}_{\text{G, Orbital}} = f_{\text{G, Orbital}} - f_0, \tag{A.14}$$

$$\hat{f}_{\text{G, GHG + Ice}} = f_{\text{G, GHG + Ice}} - (f_{\text{G, GHG}} + f_{\text{G, Ice}}) + f_0, \tag{A.15}$$

$$\hat{f}_{\text{G, GHG + Orbital}} = f_{\text{G, GHG + Orbital}} - (f_{\text{G, GHG}} + f_{\text{G, Orbital}}) + f_0, \tag{A.16}$$

$$\hat{f}_{\text{G, Ice + Orbital}} = f_{\text{G, Ice + Orbital}} - (f_{\text{G, Ice}} + f_{\text{G, Orbital}}) + f_0, \tag{A.17}$$

$$\begin{aligned} \hat{f}_{\text{G, GHG + Ice + Orbital}} = f_{\text{G, GHG + Ice + Orbital}} &- (f_{\text{G, GHG + Ice}} \\ &+ f_{\text{G, GHG + Orbital}} + f_{\text{G, Ice + Orbital}}) \\ &+ (f_{\text{G, GHG}} + f_{\text{G, Ice}} \\ &+ f_{\text{G, Orbital}}) - f_0, \end{aligned} \tag{A.18}$$

where now, for instance, there is $f_{\text{G, GHG + Ice + Orbital}}$ to represent the variables taken from simulation EG7. We do a total of 15 simulations (and not 16) for the two separation analyses because they share the same baseline state E0.

A.C1 *Glacial separation analysis*

The factor separation analysis from the glacial perspective is shown in Fig. A.C1.1. In this case deviations in EG7 from the control experiment E0 are negative. In simulation EG7 there is a permanent non-AHP state. Different to the interglacial case, the effect of the ice sheets is larger than that of the GHGs or the orbital forcing in some cases. Saharan temperature negative changes in Fig. A.C1.1a happen everywhere except during glaciations before the Eemian interglacial around 140 ka and the LGM. Average contributions to temperature change during the series at times close to peaks of monsoon forcing index in Fig. A.C1.1a (when changes are most visible) are $-1.0\,^{\circ}\text{C}$ from GHGs ($-25.8\,\%$ of change from E0), $-2.0\,^{\circ}\text{C}$ ($-49.4\,\%$ of change from E0) from ice sheets and $-1.5\,^{\circ}\text{C}$ from orbital forcing ($-38.6\,\%$ of change from E0). There is a rather small counteracting (positive) temperature change from the synergy between ice sheets and orbital forcing that amounts to about $0.5\,^{\circ}\text{C}$ ($13.1\,\%$ of change from E0).

Glacial precipitation (Fig. A.C1.1b) and vegetation cover (Fig. A.C1.1c) reductions only occur at peak times of the monsoon forcing index (where AHPs occur in control E0). For these two variables the deviations from the control experiment are bounded at $0\,\text{mm}\,\text{d}^{-1}$ and $0\,\%$. Due to these bounds the synergies are not reliable and they show in Fig. A.C1.1 as the symmetrical opposite shapes of their individual contributions for GHGs and ice sheets. Average contributions to

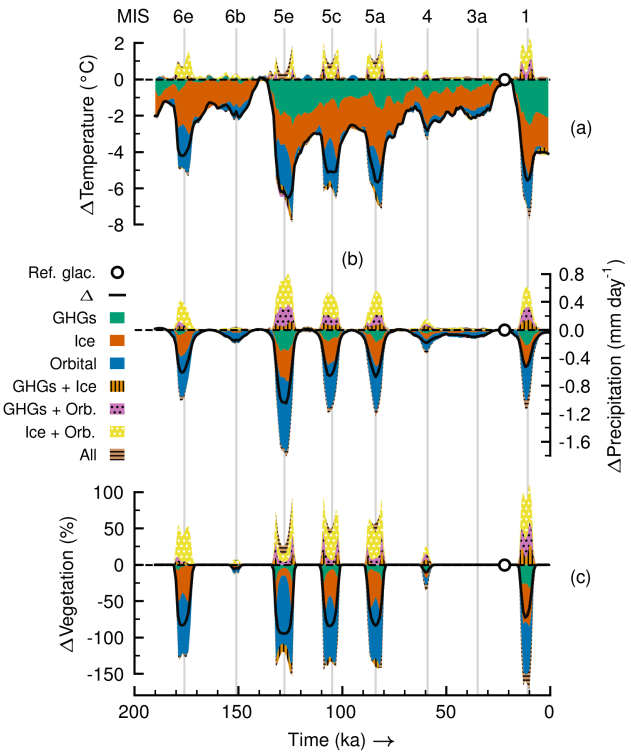

Figure A.C1.1: Factor separation analysis in the Sahara grid box from glacial perspective for annual means of (a) near-surface temperature, (b) precipitation and (c) vegetation cover fraction. Colours indicate contributions from individual forcings and related synergies to the total deviation in EG7 (glacial non-AHP) from the control experiment (Δ = EG7 − E0). Synergies are shown also with hatching. A marker shows the location of the reference glacial state, where the difference between EG7 and E0 is minimum. Vertical lines indicate monsoon forcing index maxima and are labelled using MIS names on top.

precipitation reductions near monsoon forcing index peaks in Fig. A.C1.1b (not the whole series) are about $-0.1\,\mathrm{mm\,d^{-1}}$ from GHGs ($-13.0\,\%$ of change from E0), $-0.2\,\mathrm{mm\,d^{-1}}$ from ice sheets ($-27.0\,\%$ of change from E0) and $-0.4\,\mathrm{mm\,d^{-1}}$ from orbital forcing ($-54.0\,\%$ of change from E0). For vegetation cover change near times of peak monsoon forcing index in Fig.A.C1.1c (not the whole series) contributions average about $-7.3\,\%$ from GHGs ($-8.3\,\%$ of change from E0), $-26.0\,\%$ from ice sheets ($-29.0\,\%$ of change from E0) and $-49.0\,\%$ from orbital forcing (55.0 % of change from E0). We reach a similar conclusion as from the interglacial perspective: contributions to temperature are proportional to the size of the change in the forcings, while for precipitation and temperature the orbital forcing changes are the main cause of change.

B

VEGETATION COVER CHANGES IN NORTH AFRICA SCALED WITH CLIMATIC FORCING ACROSS GLACIAL CYCLES

The study in this appendix is a manuscript about to be submitted:

Duque-Villegas, M., Claussen, M., Kleinen, T., Bader, J., & Reick, C. H. (2023). Vegetation cover changes in North Africa scaled with climatic forcing across glacial cycles. *In preparation*, 1–20.

AUTHOR CONTRIBUTIONS

MDV and MC planned the research idea. MDV and TK performed model experiments. MDV led the formal analysis and drafted the manuscript. MC supervised and steered progress. TK provided model code and input data. TK, JB and CHK contributed to experiment design and methodology. All authors participated in the analysis of results and manuscript composition.

Vegetation cover changes in North Africa scaled with climatic forcing across glacial cycles

Mateo Duque-Villegas[1,2], Martin Claussen[1,3], Thomas Kleinen[1], Jürgen Bader[1], and Christian H. Reick[1]

To be submitted

[1] Max Planck Institute for Meteorology, Hamburg, Germany

[2] International Max Planck Research School on Earth System Modelling, Hamburg, Germany

[3] Center for Earth System Research and Sustainability (CEN), Universität Hamburg, Hamburg, Germany

ABSTRACT

Over the last hundreds of thousands of years natural rhythms in Earth's astronomical motions triggered large-scale climate changes. In North Africa, orbitally induced changes were amplified by local feedback interactions, resulting in widespread amelioration of environmental conditions across the Sahara. African humid periods (AHPs) sustained river networks, vegetation, wildlife and prehistoric settlements. The mechanisms, extent and timing of the changes still cannot be completely outlined. Refining our understanding is key to explain regional geomorphology, hominin evolution and climate modelling theory. Most available information covers only the single most recent event, and it is possible that processes related to older climates are missing consideration. We simulate the last glacial cycle at coarse but affordable spatial resolution. The simulation produces four AHPs that are in broad agreement with available evidence. We find a common vegetation change pattern for AHPs that can be scaled linearly using orbital forcing and atmospheric levels of greenhouse gases (GHGs), in order to approximate vegetation cover over the last eight glacial cycles. Although the simple linear estimation can only account for about 70 % of the modelled vegetation variability, it helps to generalize some broad-scale spatial features that were well-established for the single best-known case of an AHP. Extending the climate simulation several millennia into the future reveals that such pattern scaling breaks when GHGs become the dominant climate change driver in North Africa.

B.1 INTRODUCTION

Broad swings in environmental conditions over North Africa have happened for at least the last 11 million years (Crocker et al., 2022). What is now the hyper-arid Sahara was formerly at times a much wetter region, adequate for sustaining perennial water bodies and vast expanses of vegetation cover (Gasse, 2000; deMenocal et al., 2000). Such times, known also as African humid periods (AHPs), were recorded as quasi-periodic intervals of moist conditions in regional geological archives (Grant et al., 2017, 2022). Establishment of humid climates came along with changes in the land surface that, via feedback loops, amplified Earth's orbital effects on incoming solar radiation (Claussen et al., 2017; Pausata et al., 2020). Extent, timing and causes of the changes are still being investigated, considering data limitations and persistent discrepancies between proxy records and climate simulations (Brierley et al., 2020; Yacoub et al., 2023).

Distinct humidity increases marked North African landscapes during the previous two interglacial stages (Larrasoaña et al., 2013). The interglacial during Marine Isotope Stage (MIS) 5e near 127 thousand years ago (henceforth ka) had probably the wettest AHP, as pointed

out by palaeolake shorelines and speleothems in northeastern Sahara (Gaven et al., 1981; Petit-Maire, 1996; Brook et al., 2002). However, only an incomplete AHP picture emerges from the few terrestrial proxies that stretch reliably to those times (Scussolini et al., 2019). In turn, the Holocene interglacial contained a relatively weaker AHP, roughly between 11.7 ka to 4.2 ka, but it is better represented in current proxies. Changes during the Holocene AHP can be estimated in terms of, for instance, past lake stands (Lézine et al., 2011), river flow (Drake et al., 2011), dust fluxes (McGee et al., 2013), vegetation cover (Hély et al., 2014) and rainfall (Shanahan et al., 2015). Field evidence alike, together with climate modelling, provided deep insight into basic mechanisms of AHP dynamics (Claussen et al., 2017; Holmes & Hoelzmann, 2017; Lézine, 2017; McGee & deMenocal, 2017; Shanahan, 2018). Nevertheless, interpretation of the two AHPs remains limited and even more uncertain is what developed outside these events.

Marine proxies from around North Africa reveal potential additional AHPs during the last few glacial cycles (e.g. Rossignol-Strick, 1983; Ehrmann & Schmiedl, 2021). Biogeochemical gradients in layered sediment cores can be interpreted as environmental changes over nearby land. The continuous orbital-scale resolution of stacks of marine sediments partially solves the need for records spanning deeper than the Holocene (Hoffmann et al., 2016; Drake et al., 2018). Compilations of ocean and land records suggest likely humid climates also around 105 ka and 80 ka (Blome et al., 2012; Drake et al., 2013). However, limitations in projecting marine proxy signals far inland, combined with scant terrestrial sources, narrows understanding about the spatial extent of such AHPs. A clear outline of AHP changes is crucial to explain, for instance, regional geomorphology (Drake et al., 2022), ecological corridors during hominin evolution (Scerri et al., 2018) and long-term climate–land surface interactions (Pausata et al., 2020).

Climate models offer an alternative to understand possible patterns of ancient AHPs. Early sensitivity experiments with an atmosphere-only model already coarsely simulated the four AHPs since 150 ka (Prell & Kutzbach, 1987). However, modelling long glacial cycles that include multiple AHPs requires a compromise between model complexity, simulation length and spatial resolution, which hinders the amount of detail that can be reproduced and evaluated. Studies that kept relatively complex models and higher spatial resolutions chose to either simulate discontinuous time slices (Singarayer & Burrough, 2015), or accelerate climate forcing rates (Kutzbach et al., 2008, 2020); in both cases reducing the effects of high-frequency variability. Other studies opted for intermediate complexity models and large grid spacings to focus mostly on temporal patterns of average changes of AHPs (e.g. Tuenter et al., 2003; Tjallingii et al., 2008; Menviel et al., 2021). Although simulations broadly agreed with proxy records, underes-

timation of Sahara shrinking during AHPs and associated rainfall increments is a consistent problem across models (Tierney et al., 2017b; Brierley et al., 2020). Unprecedented glacial-cycle long, transient, fully interactive climate simulations at enough spatial resolution may reveal the dominant AHP patterns underlying geological record networks or behind data–model mismatches.

We use a comprehensive climate model to perform a transient global climate simulation since 130 ka, at an affordable spatial resolution to see subcontinental changes in North Africa. The main goal is to find general trends in simulated climate patterns during AHPs of the last glacial cycle. We evaluate similarities amongst AHP responses and relate them explicitly with large-scale climate drivers: (1) Earth's orbital parameters, (2) atmospheric greenhouse gases (GHGs) radiative effects and (3) high-latitude ice sheets. These drivers are known to set multiple controls on localized rain-bringing mechanisms (Dallmeyer et al., 2020; Blanchet et al., 2021), which could lead to diverse arrangements of, for instance, vegetation cover. Assuming local environments always reacted similarly to climatic forcing, it is possible AHP patterns could be approximated according to given forcing values. We explore such a connection between the drivers and the patterns they induce during AHPs. In addition, we simulate and briefly assess potential future evolution of North African climate. In the following sections we describe the climate model, explain the experimental set-up, present results focused on North African vegetation cover during AHPs and discuss the possibility of forcing-based pattern scaling.

B.2 METHODS

B.2.1 *Model description*

We use the Max Planck Institute for Meteorology Earth System Model (MPI-ESM; Giorgetta et al., 2013) version 1.2 (Mauritsen et al., 2019). It couples dynamical components representing the general circulations of the atmosphere (ECHAM6.3; Stevens et al., 2013) and ocean (MPIOM1.6; Jungclaus et al., 2013), as well as changes in vegetation cover and the land surface (JSBACH3.2; Reick et al., 2013). The standard release of this model version participated in the Coupled Model Inter-comparison Project Phase Six (CMIP6; Eyring et al., 2016). Implementation of the coarse resolution set-up T31GR30 (about 3.75° horizontally) with 31 atmospheric and 40 oceanic levels enables long climate simulations at about maximum 700 simulated years per day (Mikolajewicz et al., 2018). Such long glacial-cycle simulations require updates during runtime of the land-sea mask, glacier mask and river routing, in line with reconstructions of ice sheet and sea level changes. This is done once every decade as described in Meccia and Mikolajewicz (2018) and Riddick et al. (2018). The specific model set-up is

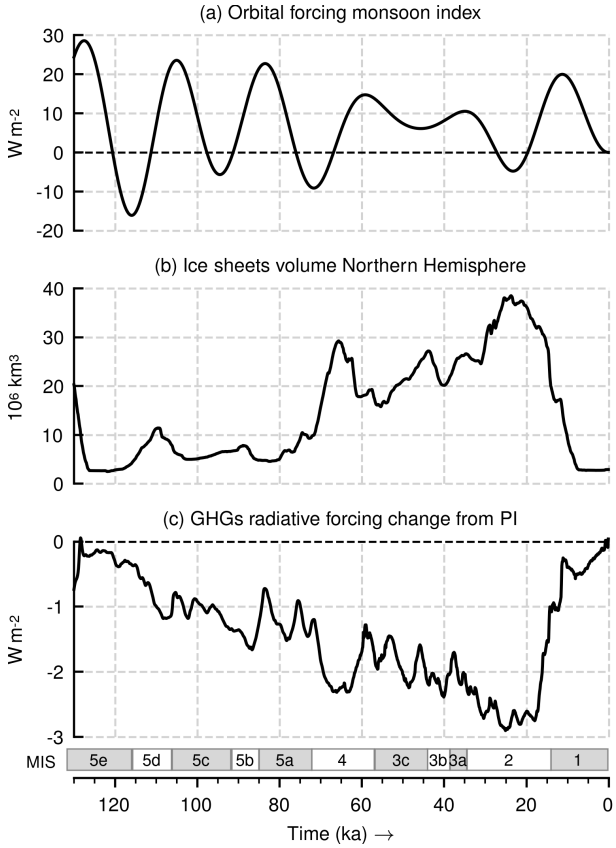

Figure B.1: Prescribed forcing of transient simulation since 130 ka until preindustrial (PI) era: (a) orbital forcing according to a monsoon forcing index, (b) Northern Hemisphere ice sheets volume and (c) radiative forcing from changing atmospheric GHGs. Showing marine isotope stages (MIS).

actively maintained and performs well within the range of current general circulation models (Kapsch et al., 2022).

How the model computes natural vegetation cover is particularly relevant for this study. An in-depth description is given in Reick et al. (2021), and a performance assessment for current climate is in Brovkin et al. (2013). Briefly, the model uses a "mosaic" approach where each land surface grid cell is tiled to be occupied by fractions of predefined plant functional types (PFTs). PFTs include 8 cover classes between woody (tropical and extra-tropical trees plus shrubs) and herbaceous (C3 and C4 grasses) vegetation with different turn-over timescales. When one vegetation type dies via natural causes (age) or via disturbances (fire or wind-throw), the "void" it leaves is filled (or "colonized") by growth of the most competitive PFT in terms of net primary productivity (NPP), which is a function of climate and atmospheric CO_2. Fractions of PFTs can only occupy the portion of a grid cell that is hospitable for growth, which is determined based on positive NPP over consecutive years. The distribution of inhospitable fractions across the globe corresponds to hot and cold

deserts. Vegetation cover in the model has immediate effects on the exchange processes between land surface and the atmosphere, which can subsequently alter climate patterns and feedback on vegetation (Brovkin et al., 2009). Soil formation is not simulated and seeds for all PFTs are assumed to be universally present.

B.2.2 *Experiments*

We simulate a transient Earth system response to prescribed forcing since 130 ka. Almost entirely as a single continuous run (120 ka to 0 ka), except for a short interval spliced a posteriori to extend analysis until 130 ka (see details about splicing in Appendix B.A1). Earth's orbital parameters are computed from Berger (1978). Atmospheric GHGs (CO_2, CH_4 and N_2O) from Köhler et al. (2017) are updated every 10 model years as decade means. Ice sheets from the GLAC-1D dataset (Tarasov & Peltier, 2002; Tarasov et al., 2012, 2014; Briggs et al., 2014; Abe-Ouchi et al., 2013) are prescribed also at decennial time steps, with corresponding adjustments in topography, bathymetry and river routing (Meccia & Mikolajewicz, 2018; Riddick et al., 2018). Figure B.1 shows set forcing according to the orbital forcing monsoon index, the Northern Hemisphere total volume of ice sheets and the GHGs radiative forcing change relative to the preindustrial era. The monsoon index of Rossignol-Strick (1983) is an insolation difference between the northern tropic and the equator during the Milankovitch (1941) caloric summer season. GHGs radiative forcing is based on an "equivalent-CO_2 concentration" as in Ganopolski et al. (2010). We ignore any anthropogenic land use and aerosols in the atmosphere remain at 1850 Common Era (CE) values (Kinne et al., 2013).

Additionally, we run two transient experiments past the preindustrial era, both 10 thousand years (henceforth kyr) into the future. In both the ice sheets remain unchanged at preindustrial conditions, while the orbital forcing continues to change according to Berger (1978). For GHGs we choose two alternative Shared Socioeconomic Pathway (SSP) scenarios from the Sixth Assessment Report (AR6) of the Intergovernmental Panel on Climate Change (IPCC): SSP1-1.9 and SSP3-7.0. The two scenarios are selected simply as contrasting cases of potential future GHGs dominance. The GHGs data for these scenarios come from Meinshausen et al. (2020) until the year 2500 CE, and onwards from previous modelling output of Brovkin et al. (2012), as described in Kleinen et al. (2021).

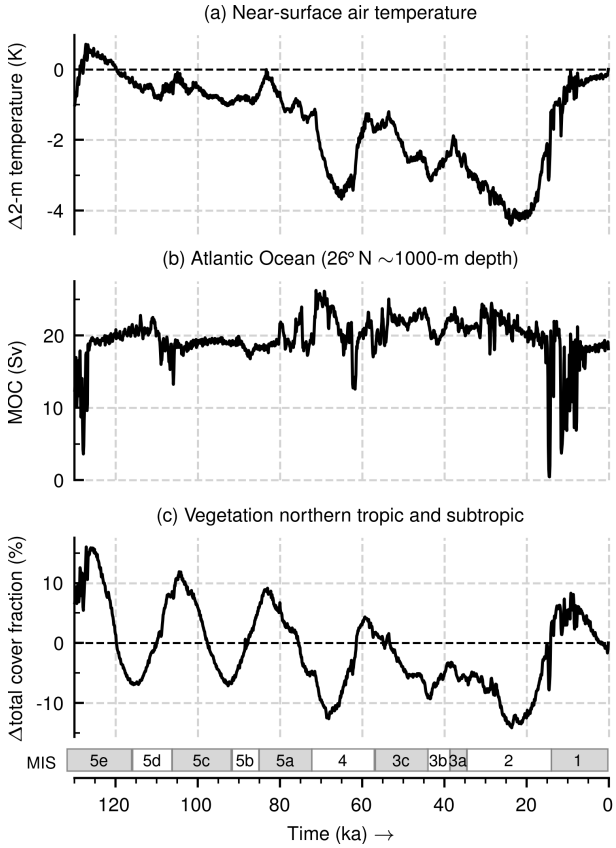

Figure B.2: Simulated Earth system response since 130 ka: centennial variability of (a) near-surface temperature change relative to preindustrial (PI) era, (b) meridional overturning circulation (MOC) in the Atlantic Ocean and (c) vegetation cover change from PI in the northern tropic and subtropic (0°–35°N).

B.3 RESULTS

B.3.1 *Earth system response*

Global climate is warmest during the MIS 5e interglacial near 127 ka (Fig. B.2a). About 0.7 K warmer than simulated preindustrial temperature, it matches proxies in the sign of change, but the amount of warming is underestimated (Turney & Jones, 2010) like in similar models (Lunt et al., 2013; Otto-Bliesner et al., 2021). Minimum average temperature occurs during the Last Glacial Maximum (LGM) around 24 ka with roughly 4.4 K less than during the preindustrial era, close to recent estimates ranging from 5 K to 7 K (Tierney et al., 2020a; Osman et al., 2021). Ocean dynamics maintains a meridional overturning circulation (MOC) in the Atlantic Ocean around 20 Sv (Fig. B.2b), including millennial-scale fluctuations related to freshwater input from river run-off as the ice sheets change. Strongest MOC variability occurs during late deglaciation phases around 130 ka to 128 ka and 15 ka to 9 ka. The last deglaciation includes especially strong meltwater pulses

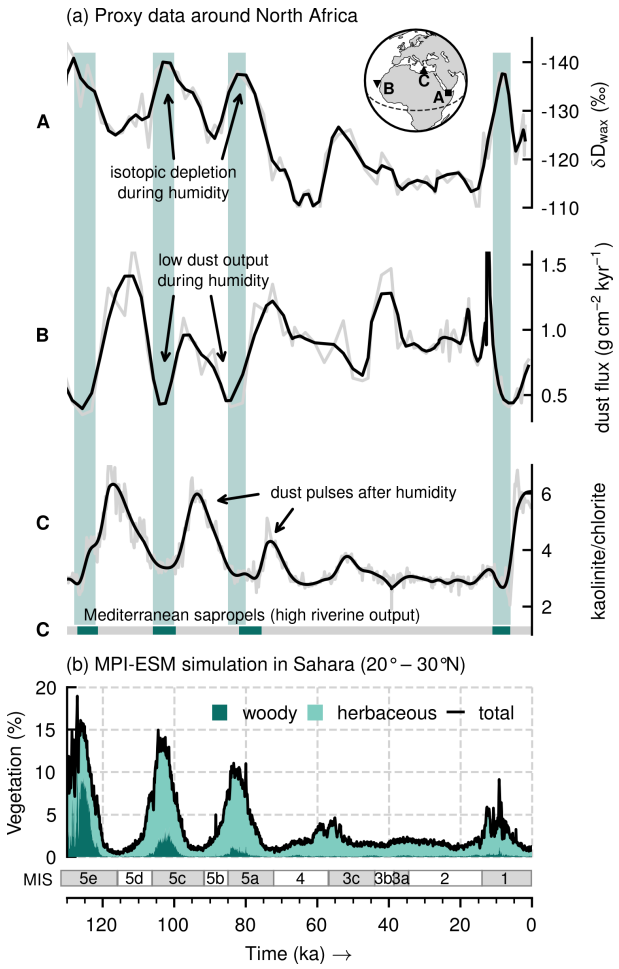

Figure B.3: North African climate since 130 ka as seen in (a) marine proxies offshore and (b) simulation results of average vegetation cover fractions (woody, herbaceous and total) in the Sahara (20°–30°N). Proxies are shown with (black) and without (grey) smoothing of a low-pass filter. A: deuterium ratio changes (δD) in terrestrial plant lipids (wax) in core RC9-166 near East Africa (Tierney et al., 2017a). B: ^{230}Th-normalized Saharan dust flux into the Atlantic Ocean according to core MD3-2705 near West Africa (Skonieczny et al., 2019). C: influx of fine-sized dust to the Eastern Mediterranean Sea according to the ratio of kaolinite and chlorite minerals in core SL99, together with its sapropel sequence (Ehrmann & Schmiedl, 2021). Proxy locations are shown in inset globe. Simulation as centennial variability. Vertical bars for approximate timings of past AHPs.

that nearly collapse the MOC several times (Kleinen et al., 2023). MOC changes appear also as drops in global temperature and northern regional vegetation cover (see Fig. B.2a and c). Changes in total vegetation cover in the northern tropic and subtropic (Fig. B.2c) follow the trend in temperature (see Fig. B.2a), with large superimposed oscillations in phase with the orbital forcing monsoon index (see Fig. B.1a).

B.3.2 *African humid periods*

Marine sediments off the coast of North Africa reveal four AHPs since 130 ka (Fig. B.3a). Briefly, AHPs appear in the proxies as times of pronounced depletion of deuterium ratios in East Africa (increased rainfall dilutes isotopic signal), reduced Saharan dust output to the Atlantic Ocean and Mediterranean Sea (increased soil-stabilising vegetation cover) and sapropel bands in Mediterranean sediments (increased river discharge stratifies seawater). In spite of large differences in location and methods amongst proxies, AHPs stand out rather consistently. Focusing on the kaolinite/chlorite proxy reveals details about the intensity of the AHPs, according to the amplitude of dust pulses which depends on the degree of (rain-fed) weathering that accumulates the kaolinite mineral in water bodies while an AHP is active (Ehrmann et al., 2017). The MIS 5e AHP (ca. 127 ka) stands out clearly as the strongest, while the estimated magnitude of other AHPs has been shown to vary with the core-to-shore distance (Ehrmann & Schmiedl, 2021).

The simulation appears well in phase with trends in the geological records (Fig. B.3b). It produces four such AHP-like changes in North African climate, as seen in the periodic peaks in total vegetation fraction in the Sahara (20°–30°N). Simulated AHPs appear also as times of herbaceous cover expansion and woody types invasion of the Sahara. The MIS 5e AHP is the strongest event with above 15 % Saharan vegetation cover, followed by two weaker AHPs during MIS 5c and 5a, both clearly over 10 % total vegetation fraction. The Holocene has the weakest AHP, barely approaching 10 % of vegetation in the Sahara, which also seems to be largely affected by MOC variability (see Fig. B.2). Strength of these AHPs is meant only relative to each other, since an overall Sahara greening below 20 % is still substantially less than previous estimates from intermediate complexity models (e.g. Menviel et al., 2021; **Duque-Villegas** et al., 2022), as well as less than estimates from the same model but implemented at higher spatial resolution (Dallmeyer et al., 2020). Explaining the mismatch between different complexity models is beyond the scope of this work, thus we focus on relative changes rather than absolute values.

The spatial extent of the AHP response is also key to assess its intensity. Figure B.4 shows mean vegetation cover fraction in North Africa during AHPs and deviations from the preindustrial era (also shown). AHP time slices are chosen around peak monsoon index values. Preindustrial conditions in the simulation seem to underestimate zonal patterns of vegetation, showing little vegetation near Lake Chad and an exaggerated Dahomey Gap dividing the Coast of Guinea that is much less conspicuous in higher resolution versions of the same climate model (Bathiany et al., 2014). During AHPs there is a continent-wide increment in vegetation, closely approaching the northern tropic

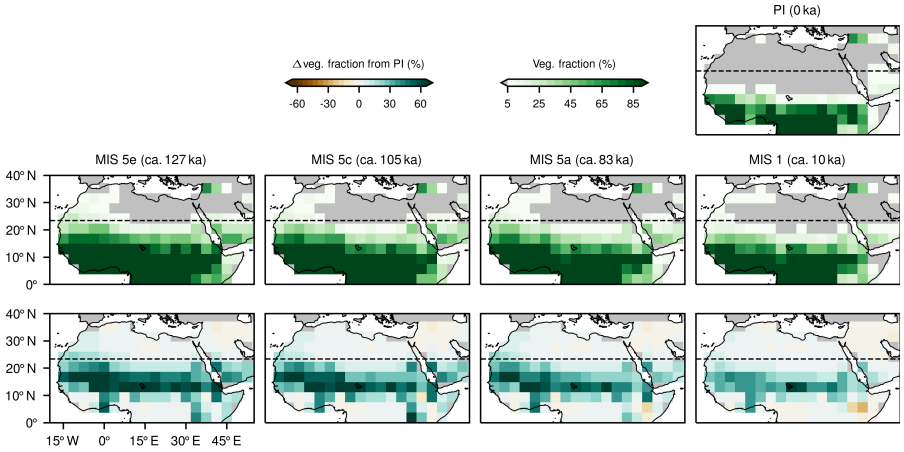

Figure B.4: AHP patterns of vegetation cover and change relative to preindustrial (PI) era. 2-kyr time slices for statistics are chosen close to orbital forcing monsoon index peaks (centre age noted in parentheses). A dashed line shows the northern tropic.

and effectively shrinking the Sahara. The largest changes occur within 10°–20°N, with over 30 % increases. The smallest changes seem to be cornered towards a northeastern region in the Sahara. Near the equator, in places where there is already close to 100 % vegetation cover under preindustrial forcing, there are also small or no changes during AHPs.

AHP patterns in Fig. B.4 seem to become weaker sequentially, starting with more intense changes during the MIS 5e AHP on the left, and progressing towards milder ones in the Holocene (MIS 1) on the right, with two intermediate cases in between. Most apparent is the fading of intense changes within the 10°–20°N band, as well as a less pronounced northward push along the west coast. Such step-wise (ignoring time gaps between AHPs) weakening of AHPs is also evident in the average vegetation fraction in the Sahara (see Fig. B.3b). Incremental change occurs in the same direction as the orbital forcing (compare Fig. B.1a), therefore suggesting the possibility of a linear scaling of baseline patterns with climatic forcing. In the following section we explore such linear relationship for vegetation cover.

B.3.3 *Spatio-temporal analysis*

AHPs seem quasi-periodic in response to natural rhythms in the Earth system. Possibly there are preferred modes (patterns) of AHP variability that regularly appeared in the past during AHP development. In such case it may be assumed that the broadest patterns would tend to scale proportionally to forcing conditions. We investigate this possibility of pattern scaling in simulated AHPs. To find a latent spatial pattern underlying AHP variability we perform an empirical orthogonal function (EOF) analysis (also known as principal components

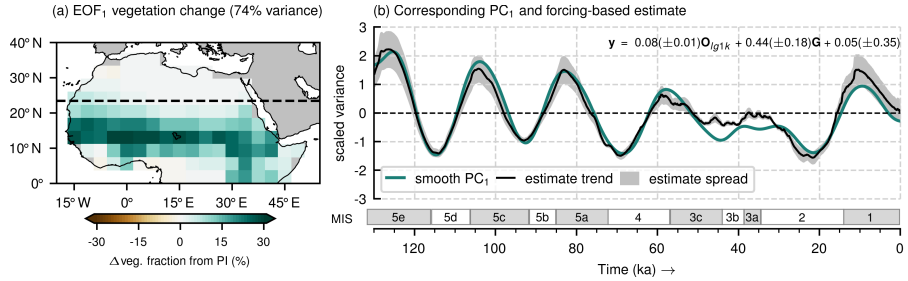

Figure B.5: EOF analysis of North African changes in vegetation fraction from preindustrial (PI) era: (a) leading variability mode (EOF_1) and (b) corresponding PC_1 time series, scaled to unit variance, shown after smoothing using a low-pass filter (polynomial degree three). In (b) there is also a forcing-based estimate for the smoothed PC_1 (trend and spread due to parameter uncertainty) with a linear regression model whose equation is shown. In the equation: O_{lg1k} is orbital forcing monsoon index lagged 1 kyr, and G stands for GHGs radiative forcing.

analysis). We construct a matrix with deviations from preindustrial of total vegetation cover fraction for all grid cells inside North Africa. This matrix is centred about its mean (remove trend) and used in a singular value decomposition to obtain its eigenvectors ordered according to explained variance. We keep only the first eigenvector (EOF_1) as it should be the largest variability pattern. Projecting the matrix onto the EOF_1 yields its principal component time series (PC_1).

Figure B.5 shows the results of the EOF analysis. The dominant pattern of variability (EOF_1) explains about 74 % of the variance in vegetation fraction changes (Fig. B.5a). It is a mostly zonally coherent pattern with an action centre largely inside 10°–20°N. Near eastern Africa the pattern adopts a more meridional structure, between 30°–45°E. According to corresponding PC_1 (smoothed in Fig. B.5b) this mode is related to uniform changes in vegetation fraction with respect to preindustrial conditions, which are positive and of great amplitude usually during warm interstadials (shaded MIS boxes). PC_1 also seems in phase with the orbital forcing monsoon index (compare Fig. B.1a). The phasing with the monsoon index is a good indicator of the possibility of estimating PC_1 as a function of climatic forcing. Figure B.5b shows also a linear model obtained with ordinary least squares fitting of the monsoon index (lagged 1 kyr) and GHGs radiative forcing. Similar results can also be obtained with global ice volume values instead of GHGs forcing (both evolve similarly). Fitting is done in different parts of the time series using a sliding (every 10 kyr) window of 42 kyr (about two precession cycles), which explains the uncertainty in the regression parameters. The lag in the monsoon index is implemented after noticing such short time difference between peak monsoon index values and peak average vegetation cover fraction in North Africa. Overall the linear model estimates a similar trend to the smoothed

PC_1, with some uncertainty in the parameters that leads to a rather narrow spread.

B.3.4 *Pattern scaling*

Results of the previous section are used to obtain forcing-based estimates of the vegetation changes (relative to preindustrial era) in North Africa. This is also known as pattern scaling, where an invariant spatial pattern is assumed to scale linearly with some forcing factor. The linear relationship to the climatic forcing is based on (ordinary least squares) curve fitting of the monsoon index (lagged 1 kyr) and GHGs radiative forcing to the PC_1 time series. Therefore, a generic name for this method is principal component emulator (Wilkinson, 2010), which has been used before also in palaeoclimate modelling contexts (e.g. Holden et al., 2019). Using EOF_1 and a forcing-based estimate of the temporal pattern (a "pseudo" PC_1) we can estimate to some extent the vegetation change patterns. Figure B.6a shows an assessment of the pattern scaling mean error during AHP time slices, taking the simulation as a reference (i.e. errors are scaled field minus simulated field). Only for the Holocene (MIS 1) it seems that the method gives a general overestimation, while for the other time slices results are mixed. Errors occur mostly around the centre of action of the EOF_1 (see Fig. B.5a), as expected since it is the most dynamical region. Considering the magnitude of some of the changes in Fig. B.4, root-mean-square errors (RMSE) below $\pm 10\,\%$ vegetation cover change in Fig. B.5a may be seen as acceptable. In the case of the temporal-pattern performance of the method, Fig. B.6b shows the scaling method trend follows closely the evolution of the average changes, with the extreme values often included in the scaling spread due to uncertain regression parameters.

B.3.5 *Late Quaternary AHPs*

The pattern scaling method opens an interesting possibility to quickly obtain a rough estimate of the vegetation fraction distribution in North Africa for other times for which reliable forcing data are available (and yet may lie outside of current modelling capabilities). Two main assumptions underlying this approach are that (1) the EOF_1 pattern captures the large-scale pattern of regional variability and (2) the forcing-based linear model effectively emulates the long-term time-dependence of variation at that scale and the climatic forcing. Although it may likely be biased towards a single glacial cycle, proxy data suggests the last glacial cycle could be representative of large-scale climate changes happening for at least the last eight glacial cycles (Lüthi et al., 2008). Therefore, it is plausible that the pattern scaling generalizes to multiple other cycles. We use this approach to estimate changes in North Africa since 800 ka using available forcing data.

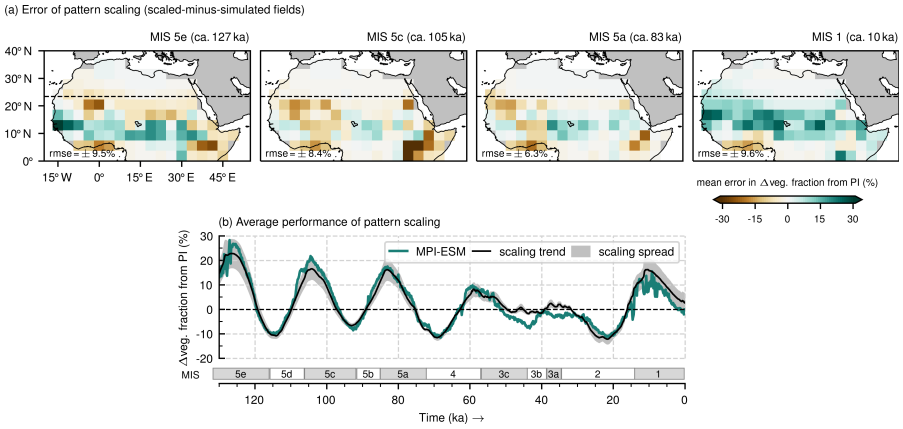

Figure B.6: Assessment of pattern scaling method for estimation of change in vegetation fraction from preindustrial (PI) era: (a) mean spatial errors during 2-kyr time slices around AHPs (centre age noted in parentheses); and (b) domain-wide average performance. This assessment uses the MPI-ESM simulated output as a reference (i.e. errors are scaled minus simulated patterns). In (a) the root-mean-square error (RMSE) is shown.

Orbital forcing monsoon index is computed for this interval based on the parameters of Berger (1978). GHGs radiative forcing is from Ganopolski and Calov (2011), who compiled data from Antarctic ice cores (Petit et al., 1999; EPICA Community Members, 2004).

Figure B.7a shows the last eight glacial cycles of average vegetation changes in North Africa according to pattern scaling and Antarctic ice cores data. As a guide, a reference line set at the Holocene (MIS 1) value can be used to guess potential ancient AHPs. According to this two other potential AHPs stand out and may have been similarly strong as the one during MIS 5e, the first one happening around 577 ka within MIS 15a, and another one near 330 ka within MIS 9e. Mediterranean records also clearly contain these two events (Emeis et al., 2000; Grant et al., 2022). Figures B.7b and c show the estimated changes from preindustrial and vegetation fraction pattern, respectively, during one of these other potential strong AHPs. It is only one example of the pattern scaling for out-of-sample AHPs. Based on the Holocene reference, and considering the spread in the estimates, this approach can identify 20 potential AHPs, most of them in agreement with signals in Mediterranean sediment cores. This is the same amount as calculated with many independent equilibrium simulations along this time range (Armstrong et al., 2023). A data synthesis by Larrasoaña et al. (2013) indicated a similar amount of 22 potential AHPs for this time interval. Refined geochemical analyses by Grant et al. (2022) read subtle humidity variations to estimate about 30 episodes of Saharan greening since 800 ka (see Fig. B.7a). However, some of the events could in fact be grouped into single cases of AHPs.

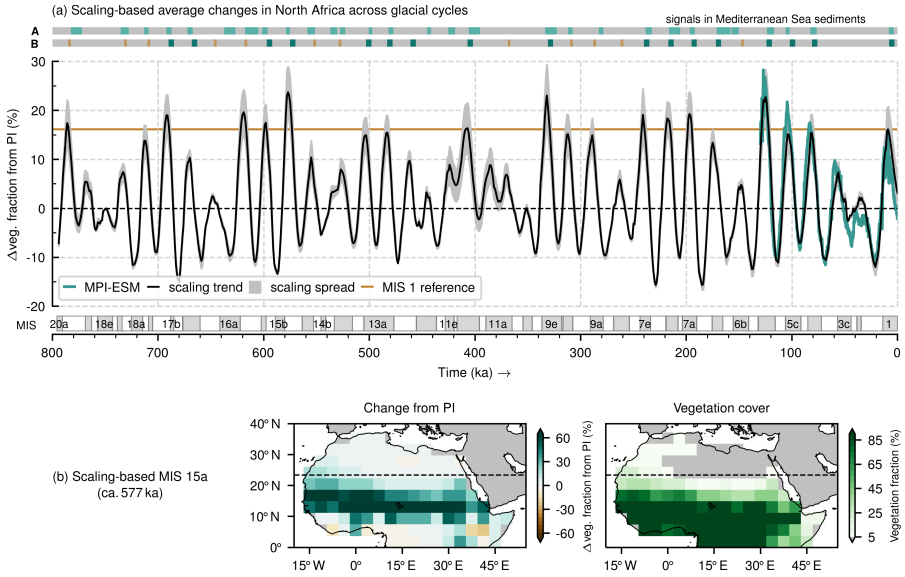

Figure B.7: Pattern scaling estimates of North African vegetation fraction changes since 800 ka: (a) average domain-wide changes from preindustrial (PI) era; (b) patterns during potential ancient AHP during MIS 15a (vegetation cover is after adding PI field). Two proxies are included that have a common origin in Mediterranean Sea sediments. A: inferred AHPs (colour bands) from bulk elements in sediments core ODP160-967 (Grant et al., 2022). B: composite sapropel record (cores ODP160-966/7), with wider and darker bands meaning clear signals, and otherwise bands meaning oxidized or unclear signals (Emeis et al., 2000). A straight line uses the Holocene (MIS 1) AHP peak as a reference to estimate the number of potential ancient AHPs according to the scaling method.

B.3.6 *Future AHPs*

Previous studies pointed out differences between orbitally dominated AHPs in the past and GHGs-modulated AHPs predicted for upcoming millennia (Claussen et al., 2003; D'Agostino et al., 2019; **Duque-Villegas** et al., 2022). For the next 100 kyr Earth keeps a low eccentricity orbit (a cycle of about 400-kyr), which should not trigger a new AHP until some 66 kyr in the future (**Duque-Villegas** et al., 2022). This is reflected in the small variation in the monsoon index in Fig. B.8a. Conversely, increasing emission rates of GHGs could increase planetary radiative forcing as shown in the scenarios in Fig. B.8b to enhance overall humidity. Scenarios have peak emissions in the near future and later maintain a constant positive forcing, leading to an average global warming of about 7 K (SSP3) and 1 K (SSP1). Figure B.8c shows simulated North African vegetation response to those scenarios. SSP3 seems to arrive at AHP conditions with a similar level as during MIS 5e (about 30 % average change from preindustrial), while SSP1 at about 10 % average vegetation change (which is smaller than during

the Holocene) does not resemble an AHP. Figure B.8d (left) shows that the simulated future change pattern of SSP3 does not resemble its AHP predecessors, missing the northward vegetation push along the west coast.

Figure B.8c also shows the average performance of the pattern scaling into future times. It overestimates predicted greening for both scenarios. This could be expected since the linear model for PC_1 is fitted in a narrower range of GHGs variability (and with almost entirely negative forcing values). Moreover, patterns in Fig. B.8d show how different the dynamically simulated pattern (left) looks from the scaling estimate (right). The strength of the GHGs radiative forcing breaks the pattern scaling based on past AHPs. The scaling based pattern is included in the figure rather as an example of the limitations of the scaling approach. Looking at the dynamically simulated vegetation changes for the SSP3 scenario (left in Fig. B.8d) it seems that after GHGs-induced warming the eastern parts of the domain see the largest positive changes. However, the control of the orbital parameters can still be interpreted from the fact that changes remain confined to the 10°–20°N band.

B.4 DISCUSSION

We present results of a fully coupled climate simulation for the last glacial cycle. The simulation may be one of a kind due to the model complexity, its length and the absence of any acceleration technique. Other studies with similar times of interest opted for atmosphere-only models (Prell & Kutzbach, 1987), lesser complexity models (Blanchet et al., 2021; Menviel et al., 2021; **Duque-Villegas** et al., 2022), ensembles of discontinuous equilibrium simulations (Singarayer & Burrough, 2015; Armstrong et al., 2023), or acceleration methods (Kutzbach et al., 2008, 2020). In this case the simulation includes a realistic representation of interactions across a broad spectrum of variability frequencies, which means disturbances can propagate across the globe to superimpose climatic forcing and local effects. However, for the same reason it is not possible to implement a highly resolved grid in this palaeoexperiment, which would enable a more refined comparison with the geological record and reconstructions.

We focus our analyses on vegetation cover in North Africa, where continental-scale climate changes produce four AHPs and northward greening into the Sahara. Simulated humidity changes align well with available terrestrial and marine proxies (Blome et al., 2012; Drake et al., 2013; Tierney et al., 2017a; Skonieczny et al., 2019; Ehrmann & Schmiedl, 2021), at least in terms of trends in deviations from preindustrial conditions. In absolute terms, we find the model underestimates the extent of vegetation already at preindustrial times, which for AHPs it means vegetation advancement into the Sahara is likewise underesti-

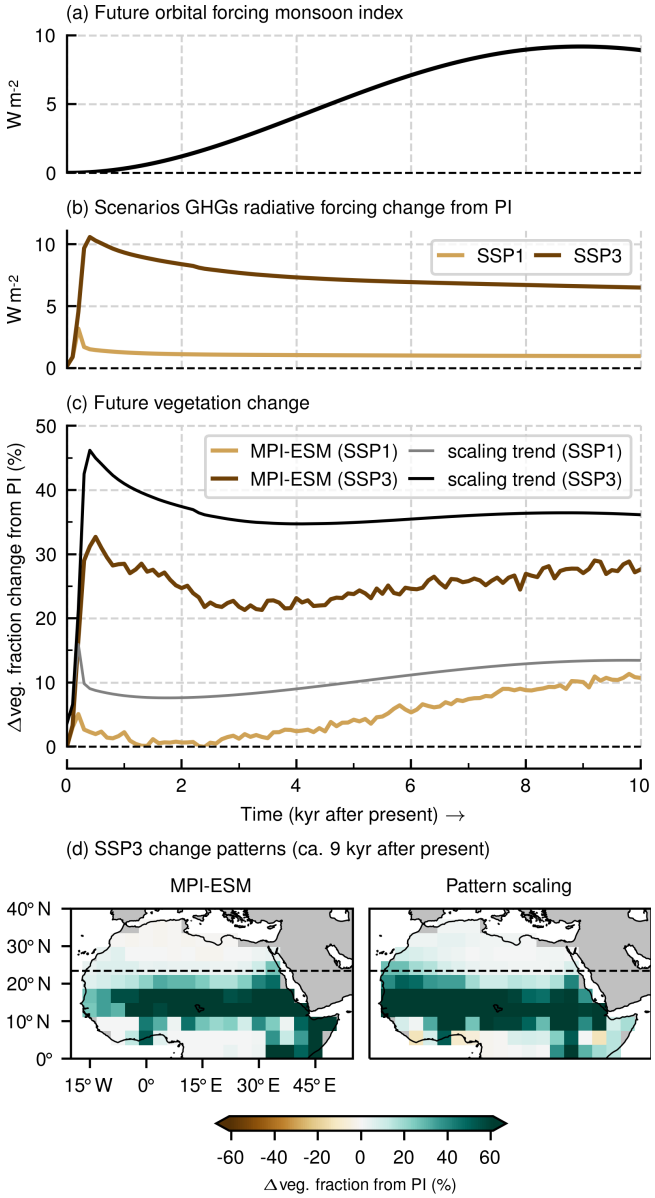

Figure B.8: Potential future climate change in North Africa: (a) orbital forcing monsoon index, (b) GHGs radiative forcing scenarios, (c) simulated and scaling-based average vegetation fraction change from preindustrial (PI) era, and (d) mean simulated (left) and scaling-based (right) vegetation fraction under scenario SSP3 near 9 kyr after PI. In (c) the scaling spread is not shown, but it is substantially large (for SSP3 about $\pm 11\,\%$ vegetation change), since the GHGs parameter has the most uncertainty in the linear model.

mated. Especially the Holocene AHP appears largely underestimated in the simulation because of the large MOC fluctuations in the Atlantic Ocean product of deglacial meltwater.

Despite magnitude problems, trends in the change patterns of the four simulated AHPs seem consistent with estimated features from

the Holocene humid event (Brierley et al., 2020; Dallmeyer et al., 2020). There is a northward progression of mostly zonal vegetation bands that extend east until about 40°E, with a slight northwest–southeast tilt related to further inland penetration of the West African Monsoon system. Such tilted AHP development pattern is also detected in the simulations and reconstructions of Armstrong et al. (2023). Moreover, it was shown that palaeo-conditioning or re-tuning a climate model to improve palaeomodelling results also led to a similar vegetation pattern during the Holocene (Hopcroft & Valdes, 2021). Specifically during interglacials (MIS 5e and Holocene) simulated AHP vegetation patterns generally agree with the reconstructions of Larrasoaña (2021), except perhaps that our results, in line with Armstrong et al. (2023), indicate the possibility of some desert cover remaining in a northeastern corner of the domain (due to the slight tilt), thereby breaking the zonal pattern of vegetation towards the north. Also, during MIS 5e vegetation changes align well with the precipitation changes in the model–data comparison of Scussolini et al. (2019). One pattern we do not find for interglacial AHPs is a green corridor in central Sahara (Menviel et al., 2021).

Agreement with reconstructions and models alike means the dominant pattern of variation we find for total vegetation cover fraction may be model-independent and perhaps a close representation of a large-scale structure underlying all changes happening in North Africa during the last glacial cycles. In such case the simple pattern scaling relationship established here could indeed approximate to some extent the land cover changes, following mainly forcing values of orbital parameters and GHGs levels. The pattern scaling could be useful to produce quick estimates of North African vegetation coverage, since simulating glacial cycles even at coarse resolution can take prohibiting long computing times. However, an important caveat about pattern scaling for vegetation fraction must be considered. Because this quantity is bounded (0 % to 100 %), it can happen that in some cases the scaling "overshoots" the estimation of the changes, since there is some maximum possible amount of change (from preindustrial era) leading to completely bare (0 %) or vegetated (100 %) grid cells. Overshooting could happen, for instance, under more intense forcing (than in the last glacial cycle), or in case there is a greater sensitivity to the forcing. This implies the linear scaling may work well for vegetation fraction in this study only because of a dry bias in the model that prevents simulation of stronger (non-linear) greening.

Another factor to be considered is the role of non-linear effects, which should be contained in the roughly 26 % variability that we discard after the EOF decomposition and do not include in the pattern scaling approach. Critical thresholds related to the climatic forcing may prevent the pattern scaling approach from correctly representing parts of the changes in the domain (Brovkin et al., 1998; Claussen et al.,

2003; **Duque-Villegas** et al., 2022), most likely near transition zones like around the southern fringe of the Sahara or where there is steep topography like towards East Africa. Those are the places that stand out when we assess the errors in the pattern scaling. Although it is possible that some of the other coherent modes of variance improve our estimates (i.e. reduce emulation minus simulation differences), we opt for the simplicity of capturing only the variance at the largest scales, at the cost of a mean error of about $\pm 10\,\%$ vegetation fraction change.

B.5 CONCLUSIONS

After simulating a realistic climate evolution for the last glacial cycle we produce new estimates of the vegetation cover patterns during the last four AHPs. A comparison with available data sources from the geological record and relevant modelling studies indicates that the estimated patterns capture well the continental-scale features in the evidence. Nevertheless, we identify a "desert bias" for this model version that frames our results rather as probable minimum estimates. We reduce the high-dimensionality in the variability of the vegetation cover changes in North Africa to a single dominant pattern that accounts for 74 % of the variations. When we scale this pattern according to climatic forcing we are able to replicate to an acceptable extent the simulated changes. Considering the high computational costs of running glacial cycle simulations, we think our approach could be used as a quick diagnostic tool for palaeovegetation cover in North Africa, which we demonstrate by estimating vegetation cover changes for the last eight glacial cycles with considerable success. Moreover, extension of our simulation several millennia into the future reveals how different AHPs form under strong GHGs forcing. Predicting future vegetation patterns should not be possible assuming a simple scaling of climatic forcing.

APPENDIX

B.A1 *Backwards extension of transient simulation*

The complete 130-kyr simulation is mostly a single experiment that was run continuously from 125 ka to 0 ka. This interval is planned for studies about global climate of the last glacial cycle. However, because for this study we are particularly interested in the regional climate of North Africa, we choose to complement this long experiment with another shorter, independent, and overlapping experiment that has an initial date slightly earlier, spanning from 134 ka to 120 ka. We could use this to extend the longer experiment backwards in time. The main reason is to include in our analysis the tropical insolation maximum

near 127 ka, which according to available evidence is an important time of extensive humidity over North Africa. We opt for such an extension due to the computational expense and long waiting time (around two years) that it would take to re-run an entirely new simulation. The overlap in the experiments is to measure their level of agreement near a merging point. They should not be drifting away from each other or at completely different states. We find the splicing together of both experiments to have only a small consequence, producing a low amplitude change that can be ignored for the study of the long-term climate signals we focus on for the study of AHPs. Figure B.A1.1 shows an example of the state evolution of both experiments for one grid cell in a highly variable region in the North Atlantic (Fig. B.A1.1a) and at the centre of our region of interest (Fig. B.A1.1b). The experiments are spliced together at 120 ka and the first 4 kyr are not included in the analysis. Consequently, we arrive at the full long simulation since 130 kyr.

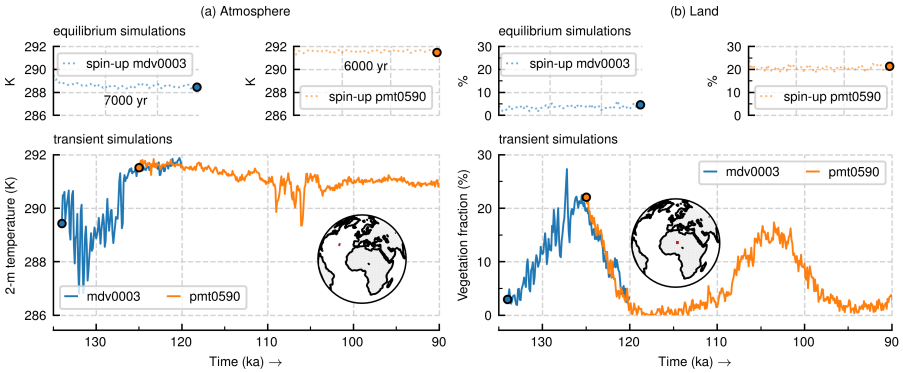

Figure B.A1.1: Extending the simulation backwards in time by merging overlapping experiments. Comparison of equilibrium and transient experiments for single grid cells (a) in the atmosphere of the North Atlantic (33.75°W 35.26°N) and (b) on land in North Africa (7.5°E 20.41°N). Experiment "mdv0003" spans between 134 ka to 120 ka, while experiment "pmt0590" from 125 ka to 0 ka. Here we zoom time on the interval close to the merging. Circle markers show the end state of the equilibrium experiments, which is the starting point of the transient experiments.

BIBLIOGRAPHY

Abe-Ouchi, A., Saito, F., Kawamura, K., Raymo, M. E., Okuno, J., Takahashi, K., & Blatter, H. (2013). Insolation-driven 100,000-year glacial cycles and hysteresis of ice-sheet volume. *Nature*, *500*(7461), 190–193. DOI: 10.1038/nature12374.

Archer, D., & Brovkin, V. (2008). The millennial atmospheric lifetime of anthropogenic CO_2. *Climatic Change*, *90*(3), 283–297. DOI: 10.1007/s10584-008-9413-1.

Armitage, S. J., Drake, N. A., Stokes, S., El-Hawat, A., Salem, M. J., White, K., Turner, P., & McLaren, S. J. (2007). Multiple phases of North African humidity recorded in lacustrine sediments from the Fazzan Basin, Libyan Sahara. *Quaternary Geochronology*, *2*(1-4), 181–186. DOI: 10.1016/j.quageo.2006.05.019.

Armstrong, E., Tallavaara, M., Hopcroft, P. O., & Valdes, P. J. (2023). North African humid periods over the past 800,000 years. *Nature Communications*, *14*(5549), 1–11. DOI: 10.1038/s41467-023-41219-4.

Bartlein, P. J., Harrison, S. P., Brewer, S., Connor, S., Davis, B. A. S., Gajewski, K., Guiot, J., Harrison-Prentice, T. I., Henderson, A., Peyron, O., Prentice, I. C., Scholze, M., Seppä, H., Shuman, B., Sugita, S., Thompson, R. S., Viau, A. E., Williams, J., & Wu, H. (2011). Pollen-based continental climate reconstructions at 6 and 21 ka: A global synthesis. *Climate Dynamics*, *37*(3), 775–802. DOI: 10.1007/s00382-010-0904-1.

Bathiany, S., Claussen, M., & Fraedrich, K. (2012). Implications of climate variability for the detection of multiple equilibria and for rapid transitions in the atmosphere-vegetation system. *Climate Dynamics*, *38*(9), 1775–1790. DOI: 10.1007/s00382-011-1037-x.

Bathiany, S., Claussen, M., & Brovkin, V. (2014). CO2-induced Sahel greening in three CMIP5 Earth System Models. *Journal of Climate*, *27*(18), 7163–7184. DOI: 10.1175/jcli-d-13-00528.1.

Bauer, E., & Ganopolski, A. (2010). Aeolian dust modeling over the past four glacial cycles with CLIMBER-2. *Global and Planetary Change*, *74*(2), 49–60. DOI: 10.1016/j.gloplacha.2010.07.009.

Bauer, E., & Ganopolski, A. (2014). Sensitivity simulations with direct shortwave radiative forcing by aeolian dust during glacial cycles. *Climate of the Past*, *10*, 1333–1348. DOI: 10.5194/cp-10-1333-2014.

Berger, A. (1978). Long-term variations of daily insolation and Quaternary climatic changes. *Journal of the Atmospheric Sciences*, *35*(12), 2362–2367. DOI: 10.1175/1520-0469(1978)035<2362:LTVODI>2.0.CO;2.

Berger, A. (1988). Milankovitch theory and climate. *Reviews of Geophysics*, *26*(4), 624–657. DOI: 10.1029/RG026i004p00624.

Berger, A., Loutre, M. F., & Laskar, J. (1992). Stability of the astronomical frequencies over the Earth's history for paleoclimate studies. *Science*, *255*(5044), 560–566. DOI: 10.1126/science.255.5044.560.

Blanchet, C. L., Osborne, A. H., Tjallingii, R., Ehrmann, W., Friedrich, T., Timmermann, A., Brückmann, W., & Frank, M. (2021). Drivers of river reactivation in North Africa during the last glacial cycle. *Nature Geoscience*, *14*, 97–103. DOI: 10.1038/s41561-020-00671-3.

Blome, M. W., Cohen, A. S., Tryon, C. A., Brooks, A. S., & Russell, J. (2012). The environmental context for the origins of modern human diversity: A synthesis of regional variability in African climate 150,000–30,000 years ago. *Journal of Human Evolution*, *62*(5), 563–592. DOI: 10.1016/j.jhevol.2012.01.011.

Boos, W. R., & Korty, R. L. (2016). Regional energy budget control of the intertropical convergence zone and application to mid-Holocene rainfall. *Nature Geoscience*, *9*(12), 892–897. DOI: 10.1038/ngeo2833.

Braconnot, P., Joussaume, S., Marti, O., & de Noblet, N. (1999). Synergistic feedbacks from ocean and vegetation on the African Monsoon response to Mid-Holocene insolation. *Geophysical Research Letters*, *26*(16), 2481–2484. DOI: 10.1029/1999gl006047.

Braconnot, P., Zhu, D., Marti, O., & Servonnat, J. (2019). Strengths and challenges for transient Mid-to Late Holocene simulations with dynamical vegetation. *Climate of the Past*, *15*(3), 997–1024. DOI: 10.5194/cp-15-997-2019.

Braconnot, P., Otto-Bliesner, B. L., Harrison, S. P., Joussaume, S., Peterchmitt, J.-Y., Abe-Ouchi, A., Crucifix, M., Driesschaert, E., Fichefet, T., Hewitt, C. D., Kageyama, M., Kitoh, A., Laîné, A., Loutre, M.-F., Marti, O., Merkel, U., Ramstein, G., Valdes, P., Weber, S. L., … Zhao, Y. (2007). Results of PMIP2 coupled simulations of the Mid-Holocene and Last Glacial Maximum – Part 1: Experiments and large-scale features. *Climate of the Past*, *3*(2), 261–277. DOI: 10.5194/cp-3-261-2007.

Braconnot, P., Harrison, S. P., Kageyama, M., Bartlein, P. J., Masson-Delmotte, V., Abe-Ouchi, A., Otto-Bliesner, B. L., & Zhao, Y. (2012). Evaluation of climate models using palaeoclimatic data. *Nature Climate Change*, *2*(6), 417–424. DOI: 10.1038/nclimate1456.

Brierley, C., Manning, K., & Maslin, M. (2018). Pastoralism may have delayed the end of the green Sahara. *Nature Communications*, *9*(1), 1–9. DOI: 10.1038/s41467-018-06321-y.

Brierley, C., Zhao, A., Harrison, S. P., Braconnot, P., Williams, C. J. R., Thornalley, D. J. R., Shi, X., Peterschmitt, J.-Y., Ohgaito, R., Kaufman, D. S., Kageyama, M., Hargreaves, J. C., Erb, M. P., Emile-Geay, J., D'Agostino, R., Chandan, D., Carré, M., Bartlein,

P. J., Zheng, W., ... Abe-Ouchi, A. (2020). Large-scale features and evaluation of the PMIP4-CMIP6 midHolocene simulations. *Climate of the Past*, *16*(5), 1847–1872. DOI: 10.5194/cp-16-1847-2020.

Briggs, R. D., Pollard, D., & Tarasov, L. (2014). A data-constrained large ensemble analysis of Antarctic evolution since the Eemian. *Quaternary Science Reviews*, *103*, 91–115. DOI: 10.1016/j.quascirev.2014.09.003.

Broecker, W. S., Thurber, D. L., Goddard, J., Ku, T.-l., Matthews, R. K., & Mesolella, K. J. (1968). Milankovitch hypothesis supported by precise dating of coral reefs and deep-sea sediments. *Science*, *159*(3812), 297–300. DOI: 10.1126/science.159.3812.297.

Brook, G. A., Embabi, N. S., Ashour, M. M., Edwards, R. L., Cheng, H., Cowart, J. B., & Dabous, A. A. (2002). Djara Cave in the Western Desert of Egypt: Morphology and evidence of Quaternary climatic change. *Cave and Karst Science*, *29*(2), 57–66.

Broström, A., Coe, M. T., Harrison, S. P., Gallimore, R., Kutzbach, J. E., Foley, J., Prentice, I. C., & Behling, P. (1998). Land surface feedbacks and palaeomonsoons in northern Africa. *Geophysical Research Letters*, *25*(19), 3615–3618. DOI: 10.1029/98GL02804.

Brovkin, V., Boysen, L., Raddatz, T., Gayler, V., Loew, A., & Claussen, M. (2013). Evaluation of vegetation cover and land-surface albedo in MPI-ESM CMIP5 simulations. *Journal of Advances in Modeling Earth Systems*, *5*(1), 48–57. DOI: 10.1029/2012MS000169.

Brovkin, V., & Claussen, M. (2008). Comment on "Climate-driven ecosystem succession in the Sahara: The past 6000 years". *Science*, *322*(5906), 1326–1326. DOI: 10.1126/science.1163381.

Brovkin, V., Claussen, M., Petoukhov, V., & Ganopolski, A. (1998). On the stability of the atmosphere-vegetation system in the Sahara/Sahel region. *Journal of Geophysical Research: Atmospheres*, *103*(D24), 31613–31624. DOI: 10.1029/1998jd200006.

Brovkin, V., Ganopolski, A., Archer, D., & Munhoven, G. (2012). Glacial CO_2 cycle as a succession of key physical and biogeochemical processes. *Climate of the Past*, *8*(1), 251–264. DOI: 10.5194/cp-8-251-2012.

Brovkin, V., Ganopolski, A., Archer, D., & Rahmstorf, S. (2007). Lowering of glacial atmospheric CO_2 in response to changes in oceanic circulation and marine biogeochemistry. *Paleoceanography*, *22*(4, PA4202), 1–14. DOI: 10.1029/2006pa001380.

Brovkin, V., Ganopolski, A., & Svirezhev, Y. (1997). A continuous climate-vegetation classification for use in climate-biosphere studies. *Ecological Modelling*, *101*(2-3), 251–261. DOI: 10.1016/s0304-3800(97)00049-5.

Brovkin, V., Raddatz, T., Reick, C. H., Claussen, M., & Gayler, V. (2009). Global biogeophysical interactions between forest and

climate. *Geophysical Research Letters*, *36*(7, L07405), 1–5. DOI: 10.1029/2009gl037543.

Brovkin, V., Bendtsen, J., Claussen, M., Ganopolski, A., Kubatzki, C., Petoukhov, V., & Andreev, A. (2002). Carbon cycle, vegetation, and climate dynamics in the Holocene: Experiments with the CLIMBER-2 model. *Global Biogeochemical Cycles*, *16*(4, 1139), 1–13. DOI: 10.1029/2001gb001662.

Causse, C., Ghaleb, B., Chkir, N., Zouari, K., Ouezdou, H. B., & Mamou, A. (2003). Humidity changes in southern Tunisia during the Late Pleistocene inferred from U–Th dating of mollusc shells. *Applied Geochemistry*, *18*(11), 1691–1703. DOI: 10.1016/s0883-2927(03)00043-x.

Chandan, D., & Peltier, W. R. (2020). African Humid Period precipitation sustained by robust vegetation, soil, and lake feedbacks. *Geophysical Research Letters*, *47*(e2020GL088728), 1–12. DOI: 10.1029/2020gl088728.

Chase, B. M., Boom, A., Carr, A. S., & Reimer, P. J. (2022). Climate variability along the margin of the southern African monsoon region at the end of the African Humid Period. *Quaternary Science Reviews*, *291*(107663), 1–11. DOI: 10.1016/j.quascirev.2022.107663.

Cheddadi, R., Carré, M., Nourelbait, M., François, L., Rhoujjati, A., Manay, R., Ochoa, D., & Schefuß, E. (2021). Early Holocene greening of the Sahara requires Mediterranean winter rainfall. *Proceedings of the National Academy of Sciences*, *118*(23, e2024898118), 1–7. DOI: 10.1073/pnas.2024898118.

Cheng, H., Li, H., Sha, L., Sinha, A., Shi, Z., Yin, Q., Lu, Z., Zhao, D., Cai, Y., Hu, Y., Hao, Q., Tian, J., Kathayat, G., Dong, X., Zhao, J., & Zhang, H. (2022). Milankovitch theory and monsoon. *The Innovation*, *3*(6), 100338. DOI: 10.1016/j.xinn.2022.100338.

Chiang, J. C. H., & Friedman, A. R. (2012). Extratropical cooling, interhemispheric thermal gradients, and tropical climate change. *Annual Review of Earth and Planetary Sciences*, *40*(1), 383–412. DOI: 10.1146/annurev-earth-042711-105545.

Claussen, M., Brovkin, V., Ganopolski, A., Kubatzki, C., & Petoukhov, V. (2003). Climate change in Northern Africa: The past is not the future. *Climatic Change*, *57*(1/2), 99–118. DOI: 10.1023/a:1022115604225.

Claussen, M., Brovkin, V., Ganopolski, A., Kubatzki, C., Petoukhov, V., & Rahmstorf, S. (1999a). A new model for climate system analysis: Outline of the model and application to palaeoclimate simulations. *Environmental Modeling and Assessment*, *4*(4), 209–216. DOI: 10.1023/a:1019016418068.

Claussen, M., Dallmeyer, A., & Bader, J. (2017). Theory and modeling of the African Humid Period and the Green Sahara. In *Oxford*

research encyclopedia of climate science (pp. 1–40). Oxford University Press. DOI: 10.1093/acrefore/9780190228620.013.532.

Claussen, M., & Gayler, V. (1997). The greening of the Sahara during the mid-Holocene: Results of an interactive atmosphere-biome model. *Global Ecology and Biogeography Letters*, *6*(5), 369. DOI: 10.2307/2997337.

Claussen, M., Kubatzki, C., Brovkin, V., Ganopolski, A., Hoelzmann, P., & Pachur, H.-J. (1999b). Simulation of an abrupt change in Saharan vegetation in the Mid-Holocene. *Geophysical Research Letters*, *26*(14), 2037–2040. DOI: 10.1029/1999gl900494.

Claussen, M., Mysak, L., Weaver, A., Crucifix, M., Fichefet, T., Loutre, M.-F., Weber, S., Alcamo, J., Alexeev, V., Berger, A., Calov, R., Ganopolski, A., Goosse, H., Lohmann, G., Lunkeit, F., Mokhov, I., Petoukhov, V., Stone, P., & Wang, Z. (2002). Earth system models of intermediate complexity: Closing the gap in the spectrum of climate system models. *Climate Dynamics*, *18*(7), 579–586. DOI: 10.1007/s00382-001-0200-1.

Coe, M. T., & Bonan, G. B. (1997). Feedbacks between climate and surface water in northern Africa during the middle Holocene. *Journal of Geophysical Research: Atmospheres*, *102*(D10), 11087–11101. DOI: 10.1029/97JD00343.

COHMAP Members. (1988). Climatic changes of the last 18,000 years: Observations and model simulations. *Science*, *241*(4869), 1043–1052. DOI: 10.1126/science.241.4869.1043.

Collins, J. A., Prange, M., Caley, T., Gimeno, L., Beckmann, B., Mulitza, S., Skonieczny, C., Roche, D., & Schefuß, E. (2017). Rapid termination of the African Humid Period triggered by northern high-latitude cooling. *Nature Communications*, *8*(1, 1372), 1–11. DOI: 10.1038/s41467-017-01454-y.

Cremaschi, M., Zerboni, A., Spötl, C., & Felletti, F. (2010). The calcareous tufa in the Tadrart Acacus Mt. (SW Fezzan, Libya). *Palaeogeography, Palaeoclimatology, Palaeoecology*, *287*(1-4), 81–94. DOI: 10.1016/j.palaeo.2010.01.019.

Crocker, A. J., Naafs, B. D. A., Westerhold, T., James, R. H., Cooper, M. J., Röhl, U., Pancost, R. D., Xuan, C., Osborne, C. P., Beerling, D. J., & Wilson, P. A. (2022). Astronomically controlled aridity in the Sahara since at least 11 million years ago. *Nature Geoscience*, *15*(8), 671–676. DOI: 10.1038/s41561-022-00990-7.

D'Agostino, R., Bader, J., Bordoni, S., Ferreira, D., & Jungclaus, J. (2019). Northern Hemisphere monsoon response to mid-Holocene orbital forcing and greenhouse gas-induced global warming. *Geophysical Research Letters*, *46*(3), 1591–1601. DOI: 10.1029/2018GL081589.

Dallmeyer, A., Claussen, M., Lorenz, S. J., & Shanahan, T. M. (2020). The end of the African Humid Period as seen by a transient comprehensive Earth system model simulation of the last 8000

years. *Climate of the Past*, *16*(1), 117–140. DOI: 10.5194/cp-16-117-2020.

deMenocal, P. B. (1995). Plio-Pleistocene African climate. *Science*, *270*(5233), 53–59. DOI: 10.1126/science.270.5233.53.

deMenocal, P. B., Ruddiman, W. F., & Pokras, E. M. (1993). Influences of jigh- and low-latitude processes on African terrestrial climate: Pleistocene eolian records from equatorial Atlantic Ocean Drilling Program Site 663. *Paleoceanography*, *8*(2), 209–242. DOI: 10.1029/93PA02688.

deMenocal, P. B., Ortiz, J., Guilderson, T., Adkins, J., Sarnthein, M., Baker, L., & Yarusinsky, M. (2000). Abrupt onset and termination of the African Humid Period: Rapid climate responses to gradual insolation forcing. *Quaternary Science Reviews*, *19*(1-5), 347–361. DOI: 10.1016/s0277-3791(99)00081-5.

Dickinson, R. E., Henderson-Sellers, A., & Kennedy, P. J. (1993). Biosphere-Atmosphere Transfer Scheme (BATS) version 1e as coupled to the NCAR Community Climate Model. *NCAR Technical Note*, (387+STR), 1–72.

Drake, N. A., Blench, R. M., Armitage, S. J., Bristow, C. S., & White, K. H. (2011). Ancient watercourses and biogeography of the Sahara explain the peopling of the desert. *Proceedings of the National Academy of Sciences*, *108*(2), 458–462. DOI: 10.1073/pnas.1012231108.

Drake, N. A., Breeze, P. S., & Parker, A. (2013). Palaeoclimate in the Saharan and Arabian Deserts during the Middle Palaeolithic and the potential for hominin dispersals. *Quaternary International*, *300*, 48–61. DOI: 10.1016/j.quaint.2012.12.018.

Drake, N. A., Lem, R. E., Armitage, S. J., Breeze, P. S., Francke, J., El-Hawat, A. S., Salem, M. J., Hounslow, M. W., & White, K. (2018). Reconstructing palaeoclimate and hydrological fluctuations in the Fezzan Basin (southern Libya) since 130 ka: A catchment-based approach. *Quaternary Science Reviews*, *200*, 376–394. DOI: 10.1016/j.quascirev.2018.09.042.

Drake, N. A., Candy, I., Breeze, P. S., Armitage, S. J., Gasmi, N., Schwenninger, J. L., Peat, D., & Manning, K. (2022). Sedimentary and geomorphic evidence of Saharan megalakes: A synthesis. *Quaternary Science Reviews*, *276*(107318), 1–20. DOI: 10.1016/j.quascirev.2021.107318.

Dupont, L. A., Railsback, L. B., Liang, F., Brook, G. A., Cheng, H., & Edwards, R. L. (2022). Episodic deposition of stalagmites in the northeastern Democratic Republic of the Congo suggests Equatorial Humid Periods during insolation maxima. *Quaternary Science Reviews*, *286*(107552), 1–19. DOI: 10.1016/j.quascirev.2022.107552.

Dupont, L. M. (1993). Vegetation zones in NW Africa during the Brunhes chron reconstructed from marine palynological data.

Quaternary Science Reviews, *12*(3), 189–202. DOI: 10.1016/0277-3791(93)90053-0.

Duque-Villegas, **M.**, Claussen, M., Brovkin, V., & Kleinen, T. (2022). Effects of orbital forcing, greenhouse gases and ice sheets on Saharan greening in past and future multi-millennia. *Climate of the Past*, *18*(8), 1897–1914. DOI: 10.5194/cp-18-1897-2022.

Ehrmann, W., Schmiedl, G., Beuscher, S., & Krüger, S. (2017). Intensity of African humid periods estimated from Saharan dust fluxes. *PloS ONE*, *12*(1, e0170989), 1–18. DOI: 10.1371/journal.pone.0170989.

Ehrmann, W., & Schmiedl, G. (2021). Nature and dynamics of North African humid and dry periods during the last 200,000 years documented in the clay fraction of Eastern Mediterranean deep-sea sediments. *Quaternary Science Reviews*, *260*(106925), 1–17. DOI: 10.1016/j.quascirev.2021.106925.

El-Shenawy, M. I., Kim, S.-T., Schwarcz, H. P., Asmerom, Y., & Polyak, V. J. (2018). Speleothem evidence for the greening of the Sahara and its implications for the early human dispersal out of sub-Saharan Africa. *Quaternary Science Reviews*, *188*, 67–76. DOI: 10.1016/j.quascirev.2018.03.016.

Emeis, K.-C., Sakamoto, T., Wehausen, R., & Brumsack, H.-J. (2000). The sapropel record of the eastern Mediterranean Sea – results of Ocean Drilling Program Leg 160. *Palaeogeography, Palaeoclimatology, Palaeoecology*, *158*(3-4), 371–395. DOI: 10.1016/S0031-0182(00)00059-6.

EPICA Community Members. (2004). Eight glacial cycles from an Antarctic ice core. *Nature*, *429*(6992), 623–628. DOI: 10.1038/nature02599.

Eyring, V., Bony, S., Meehl, G. A., Senior, C. A., Stevens, B., Stouffer, R. J., & Taylor, K. E. (2016). Overview of the Coupled Model Intercomparison Project Phase 6 (CMIP6) experimental design and organization. *Geoscientific Model Development*, *9*(5), 1937–1958. DOI: 10.5194/gmd-9-1937-2016.

Foley, J. A., Coe, M. T., Scheffer, M., & Wang, G. (2003). Regime shifts in the Sahara and Sahel: Interactions between ecological and climatic systems in Northern Africa. *Ecosystems*, *6*(6), 524–532. DOI: 10.1007/s10021-002-0227-0.

Gaetani, M., Messori, G., Zhang, Q., Flamant, C., & Pausata, F. S. R. (2017). Understanding the mechanisms behind the northward extension of the West African Monsoon during the Mid-Holocene. *Journal of Climate*, *30*(19), 7621–7642. DOI: 10.1175/JCLI-D-16-0299.1.

Ganopolski, A., & Brovkin, V. (2017). Simulation of climate, ice sheets and CO_2 evolution during the last four glacial cycles with an Earth system model of intermediate complexity. *Climate of the Past*, *13*, 1695–1716. DOI: 10.5194/cp-13-1695-2017.

Ganopolski, A., & Calov, R. (2011). The role of orbital forcing, carbon dioxide and regolith in 100 kyr glacial cycles. *Climate of the Past*, *7*(4), 1415–1425. DOI: 10.5194/cp-7-1415-2011.

Ganopolski, A., Calov, R., & Claussen, M. (2010). Simulation of the last glacial cycle with a coupled climate ice-sheet model of intermediate complexity. *Climate of the Past*, *6*(2), 229–244. DOI: 10.5194/cp-6-229-2010.

Ganopolski, A., & Rahmstorf, S. (2001). Rapid changes of glacial climate simulated in a coupled climate model. *Nature*, *409*(6817), 153–158. DOI: 10.1038/35051500.

Ganopolski, A., Rahmstorf, S., Petoukhov, V., & Claussen, M. (1998). Simulation of modern and glacial climates with a coupled global model of intermediate complexity. *Nature*, *391*(6665), 351–356. DOI: 10.1038/34839.

Ganopolski, A., Winkelmann, R., & Schellnhuber, H. J. (2016). Critical insolation–CO_2 relation for diagnosing past and future glacial inception. *Nature*, *529*(7585), 200–203. DOI: 10.1038/nature16494.

Ganopolski, A., Petoukhov, V., Rahmstorf, S., Brovkin, V., Claussen, M., Eliseev, A., & Kubatzki, C. (2001). CLIMBER-2: A climate system model of intermediate complexity. part II: Model sensitivity. *Climate Dynamics*, *17*(10), 735–751. DOI: 10.1007/s003820000144.

Gasse, F. (2000). Hydrological changes in the African tropics since the Last Glacial Maximum. *Quaternary Science Reviews*, *19*(1-5), 189–211. DOI: 10.1016/s0277-3791(99)00061-x.

Gasse, F., Téhet, R., Durand, A., Gibert, E., & Fontes, J.-C. (1990). The arid–humid transition in the Sahara and the Sahel during the last deglaciation. *Nature*, *346*(6280), 141–146. DOI: 10.1038/346141a0.

Gaven, C., Hillaire-Marcel, C., & Petit-Maire, N. (1981). A Pleistocene lacustrine episode in southeastern Libya. *Nature*, *290*(5802), 131–133. DOI: 10.1038/290131a0.

Geyh, M. A., & Thiedig, F. (2008). The Middle Pleistocene Al Mahrúqah Formation in the Murzuq Basin, northern Sahara, Libya evidence for orbitally-forced humid episodes during the last 500,000 years. *Palaeogeography, Palaeoclimatology, Palaeoecology*, *257*(1-2), 1–21. DOI: 10.1016/j.palaeo.2007.07.001.

Giorgetta, M. A., Jungclaus, J., Reick, C. H., Legutke, S., Bader, J., Böttinger, M., Brovkin, V., Crueger, T., Esch, M., Fieg, K., Glushak, K., Gayler, V., Haak, H., Hollweg, H. D., Ilyina, T., Kinne, S., Kornblueh, L., Matei, D., Mauritsen, T., … Stevens, B. (2013). Climate and carbon cycle changes from 1850 to 2100 in MPI-ESM simulations for the Coupled Model Intercomparison Project phase 5. *Journal of Advances in Modeling Earth Systems*, *5*(3), 572–597. DOI: 10.1002/jame.20038.

Grant, K. M., Grimm, R., Mikolajewicz, U., Marino, G., Ziegler, M., & Rohling, E. J. (2016). The timing of Mediterranean sapropel deposition relative to insolation, sea-level and African monsoon changes. *Quaternary Science Reviews*, *140*, 125–141. DOI: 10.1016/j.quascirev.2016.03.026.

Grant, K. M., Rohling, E. J., Westerhold, T., Zabel, M., Heslop, D., Konijnendijk, T., & Lourens, L. (2017). A 3 million year index for North African humidity/aridity and the implication of potential pan-African Humid periods. *Quaternary Science Reviews*, *171*, 100–118. DOI: 10.1016/j.quascirev.2017.07.005.

Grant, K. M., Amarathunga, U., Amies, J. D., Hu, P., Qian, Y., Penny, T., Rodriguez-Sanz, L., Zhao, X., Heslop, D., Liebrand, D., Hennekam, R., Westerhold, T., Gilmore, S., Lourens, L. J., Roberts, A. P., & Rohling, E. J. (2022). Organic carbon burial in Mediterranean sapropels intensified during Green Sahara Periods since 3.2 Myr ago. *Communications Earth & Environment*, *3*(11), 1–9. DOI: 10.1038/s43247-021-00339-9.

Greve, R. (1997). A continuum–mechanical formulation for shallow polythermal ice sheets. *Philosophical Transactions of the Royal Society of London, Series A*, *355*(1726), 921–974. DOI: 10.1098/rsta.1997.0050.

Groner, V. P., Raddatz, T., Reick, C. H., & Claussen, M. (2018). Plant functional diversity affects climate–vegetation interaction. *Biogeosciences*, *15*(7), 1947–1968. DOI: 10.5194/bg-15-1947-2018.

Grove, A. T., & Warren, A. (1968). Quaternary landforms and climate on the south side of the Sahara. *The Geographical Journal*, *134*(2), 194. DOI: 10.2307/1792436.

Harrison, S. P., & Bartlein, P. J. (2012). Records from the past, lessons for the future. In A. Henderson-Sellers & K. McGuffie (Eds.), *The future of the world's climate* (II, pp. 403–436). Elsevier Science. DOI: 10.1016/b978-0-12-386917-3.00014-2.

Harrison, S. P., Bartlein, P. J., Izumi, K., Li, G., Annan, J., Hargreaves, J., Braconnot, P., & Kageyama, M. (2015). Evaluation of CMIP5 palaeo-simulations to improve climate projections. *Nature Climate Change*, *5*(8), 735–743. DOI: 10.1038/nclimate2649.

Hays, J. D., Imbrie, J., & Shackleton, N. J. (1976). Variations in the Earth's orbit: Pacemaker of the ice ages. *Science*, *194*(4270), 1121–1132. DOI: 10.1126/science.194.4270.1121.

Haywood, A. M., Valdes, P. J., Aze, T., Barlow, N., Burke, A., Dolan, A. M., von der Heydt, A. S., Hill, D. J., Jamieson, S. S. R., Otto-Bliesner, B. L., Salzmann, U., Saupe, E., & Voss, J. (2019). What can palaeoclimate modelling do for you? *Earth Systems and Environment*, *3*(1), 1–18. DOI: 10.1007/s41748-019-00093-1.

Hély, C., Lézine, A.-M., Ballouche, A., Cour, P., Duzer, D., Guinet, P., Jahns, S., Maley, J., Mercuri, A. M., Pons, A., Ritchie, J. C., Salzmann, U., Schulz, E., Campo, M. V., & Waller, M. P. (2014).

Holocene changes in African vegetation: Tradeoff between climate and water availability. *Climate of the Past*, *10*(2), 681–686. DOI: 10.5194/cp-10-681-2014.

Hoffmann, D. L., Rogerson, M., Spötl, C., Luetscher, M., Vance, D., Osborne, A. H., Fello, N. M., & Moseley, G. E. (2016). Timing and causes of North African wet phases during the last glacial period and implications for modern human migration. *Scientific Reports*, *6*(1, 36367), 1–7. DOI: 10.1038/srep36367.

Holden, P. B., Edwards, N. R., Rangel, T. F., Pereira, E. B., Tran, G. T., & Wilkinson, R. D. (2019). PALEO-PGEM v1.0: A statistical emulator of Pliocene–Pleistocene climate. *Geoscientific Model Development*, *12*(12), 5137–5155. DOI: 10.5194/gmd-12-5137-2019.

Holmes, J., & Hoelzmann, P. (2017). The Late Pleistocene-Holocene African Humid Period as evident in lakes. In *Oxford research encyclopedia of climate science* (pp. 1–39). Oxford University Press. DOI: 10.1093/acrefore/9780190228620.013.531.

Hopcroft, P. O., & Valdes, P. J. (2021). Paleoclimate-conditioning reveals a North Africa land–atmosphere tipping point. *Proceedings of the National Academy of Sciences*, *118*(45, e2108783118), 1–7. DOI: 10.1073/pnas.2108783118.

Hopcroft, P. O., Valdes, P. J., Harper, A. B., & Beerling, D. J. (2017). Multi vegetation model evaluation of the Green Sahara climate regime. *Geophysical Research Letters*, *44*(13), 6804–6813. DOI: 10.1002/2017gl073740.

Jolly, D., Harrison, S. P., Damnati, B., & Bonnefille, R. (1998). Simulated climate and biomes of Africa during the late Quaternary. *Quaternary Science Reviews*, *17*(6-7), 629–657. DOI: 10.1016/s0277-3791(98)00015-8.

Joussaume, S., Taylor, K. E., Braconnot, P., Mitchell, J. F. B., Kutzbach, J. E., Harrison, S. P., Prentice, I. C., Broccoli, A. J., Abe-Ouchi, A., Bartlein, P. J., Bonfils, C., Dong, B., Guiot, J., Herterich, K., Hewitt, C. D., Jolly, D., Kim, J. W., Kislov, A., Kitoh, A., … Wyputta, U. (1999). Monsoon changes for 6000 years ago: Results of 18 simulations from the Paleoclimate Modeling Intercomparison Project (PMIP). *Geophysical Research Letters*, *26*(7), 859–862. DOI: 10.1029/1999gl900126.

Jungandreas, L., Hohenegger, C., & Claussen, M. (2021). Influence of the representation of convection on the mid-Holocene West African Monsoon. *Climate of the Past*, *17*(4), 1665–1684. DOI: 10.5194/cp-17-1665-2021.

Jungandreas, L., Hohenegger, C., & Claussen, M. (2023). How does the explicit treatment of convection alter the precipitation–soil hydrology interaction in the mid-Holocene African humid period? *Climate of the Past*, *19*(3), 637–664. DOI: 10.5194/cp-19-637-2023.

Jungclaus, J. H., Fischer, N., Haak, H., Lohmann, K., Marotzke, J., Matei, D., Mikolajewicz, U., Notz, D., & von Storch, J. S. (2013). Characteristics of the ocean simulations in the Max Planck Institute Ocean Model (MPIOM) the ocean component of the MPI-Earth system model. *Journal of Advances in Modeling Earth Systems*, *5*(2), 422–446. DOI: 10.1002/jame.20023.

Kaboth-Bahr, S., Gosling, W. D., Vogelsang, R., Bahr, A., Scerri, E. M. L., Asrat, A., Cohen, A. S., Düsing, W., Foerster, V., Lamb, H. F., Maslin, M. A., Roberts, H. M., Schäbitz, F., & Trauth, M. H. (2021). Paleo-ENSO influence on African environments and early modern humans. *Proceedings of the National Academy of Sciences*, *118*(23, e2018277118), 1–6. DOI: 10.1073/pnas.2018277118.

Kapsch, M.-L., Mikolajewicz, U., Ziemen, F., & Schannwell, C. (2022). Ocean response in transient simulations of the last deglaciation dominated by underlying ice-sheet reconstruction and method of meltwater distribution. *Geophysical Research Letters*, *49*(e2021GL096767), 1–11. DOI: 10.1029/2021gl096767.

Killick, R., Fearnhead, P., & Eckley, I. A. (2012). Optimal detection of changepoints with a linear computational cost. *Journal of the American Statistical Association*, *107*(500), 1590–1598. DOI: 10.1080/01621459.2012.737745.

Kinne, S., O'Donnel, D., Stier, P., Kloster, S., Zhang, K., Schmidt, H., Rast, S., Giorgetta, M., Eck, T. F., & Stevens, B. (2013). MAC-v1: A new global aerosol climatology for climate studies. *Journal of Advances in Modeling Earth Systems*, *5*(4), 704–740. DOI: 10.1002/jame.20035.

Kleinen, T., Gromov, S., Steil, B., & Brovkin, V. (2021). Atmospheric methane underestimated in future climate projections. *Environmental Research Letters*, *16*(094006), 1–12. DOI: 10.1088/1748-9326/ac1814.

Kleinen, T., Gromov, S., Steil, B., & Brovkin, V. (2023). Atmospheric methane since the last glacial maximum was driven by wetland sources. *Climate of the Past*, *19*(5), 1081–1099. DOI: 10.5194/cp-19-1081-2023.

Köhler, P., Nehrbass-Ahles, C., Schmitt, J., Stocker, T. F., & Fischer, H. (2017). A 156 kyr smoothed history of the atmospheric greenhouse gases CO_2, CH_4, and N_2O and their radiative forcing. *Earth System Science Data*, *9*(1), 363–387. DOI: 10.5194/essd-9-363-2017.

Kowalski, K., van Neer, W., Bocheński, Z., Młynarski, M., Rzebik-Kowalska, B., Szyndlar, Z., Gautier, A., Schild, R., Close, A. E., & Wendorf, F. (1989). A last interglacial fauna from the eastern Sahara. *Quaternary Research*, *32*(3), 335–341. DOI: 10.1016/0033-5894(89)90099-9.

Krinner, G., Lézine, A.-M., Braconnot, P., Sepulchre, P., Ramstein, G., Grenier, C., & Gouttevin, I. (2012). A reassessment of lake

and wetland feedbacks on the North African Holocene climate. *Geophysical Research Letters*, *39*(7, L07701), 1–6. DOI: 10.1029/2012gl050992.

Kröpelin, S., Verschuren, D., Lézine, A.-M., Eggermont, H., Cocquyt, C., Francus, P., Cazet, J.-P., Fagot, M., Rumes, B., Russell, J. M., Darius, F., Conley, D. J., Schuster, M., von Suchodoletz, H., & Engstrom, D. R. (2008). Climate-driven ecosystem succession in the Sahara: The past 6000 years. *Science*, *320*(5877), 765–768. DOI: 10.1126/science.1154913.

Kuper, R., & Kröpelin, S. (2006). Climate-controlled Holocene occupation in the Sahara: Motor of Africa's evolution. *Science*, *313*(5788), 803–807. DOI: 10.1126/science.1130989.

Kutzbach, J. E. (1981). Monsoon climate of the early Holocene: Climate experiment with the Earth's orbital parameters for 9000 years ago. *Science*, *214*(4516), 59–61. DOI: 10.1126/science.214.4516.59.

Kutzbach, J. E., Bonan, G., Foley, J., & Harrison, S. P. (1996). Vegetation and soil feedbacks on the response of the African monsoon to orbital forcing in the early to middle Holocene. *Nature*, *384*(6610), 623–626. DOI: 10.1038/384623a0.

Kutzbach, J. E., Guan, J., He, F., Cohen, A. S., Orland, I. J., & Chen, G. (2020). African climate response to orbital and glacial forcing in 140,000-y simulation with implications for early modern human environments. *Proceedings of the National Academy of Sciences*, *117*(5), 2255–2264. DOI: 10.1073/pnas.1917673117.

Kutzbach, J. E., & Guetter, P. J. (1986). The influence of changing orbital parameters and surface boundary conditions on climate simulations for the past 18 000 years. *Journal of the Atmospheric Sciences*, *43*(16), 1726–1759. DOI: 10.1175/1520-0469(1986)043<1726:TIOCOP>2.0.CO;2.

Kutzbach, J. E., Harrison, S. P., & Coe, M. T. (2001). Land-ocean-atmosphere interactions and monsoon climate change. In *Global biogeochemical cycles in the climate system* (pp. 73–86). Elsevier. DOI: 10.1016/b978-012631260-7/50008-x.

Kutzbach, J. E., Liu, X., Liu, Z., & Chen, G. (2008). Simulation of the evolutionary response of global summer monsoons to orbital forcing over the past 280,000 years. *Climate Dynamics*, *30*(6), 567–579. DOI: 10.1007/s00382-007-0308-z.

Kutzbach, J. E., & Liu, Z. (1997). Response of the African monsoon to orbital forcing and ocean feedbacks in the Middle Holocene. *Science*, *278*(5337), 440–443. DOI: 10.1126/science.278.5337.440.

Kutzbach, J. E., & Otto-Bliesner, B. L. (1982). The sensitivity of the African-Asian monsoonal climate to orbital parameter changes for 9000 years B.P. in a low-resolution general circulation model. *Journal of the Atmospheric Sciences*, *39*(6), 1177–1188. DOI: 10.1175/1520-0469(1982)039<1177:tsotaa>2.0.co;2.

Kutzbach, J. E., & Street-Perrott, F. A. (1985). Milankovitch forcing of fluctuations in the level of tropical lakes from 18 to 0 kyr BP. *Nature*, *317*(6033), 130–134. DOI: 10.1038/317130a0.

Larrasoaña, J. C. (2021). A review of West African monsoon penetration during Green Sahara periods – implications for human evolution and dispersals over the last three million years. *Oxford Open Climate Change*, *1*(1, kgab011), 1–19. DOI: 10.1093/oxfclm/kgab011.

Larrasoaña, J. C., Roberts, A. P., & Rohling, E. J. (2013). Dynamics of green Sahara periods and their role in hominin evolution. *PLoS ONE*, *8*(10, e76514), 1–12. DOI: 10.1371/journal.pone.0076514.

Larrasoaña, J. C., Roberts, A. P., Rohling, E. J., Winklhofer, M., & Wehausen, R. (2003). Three million years of monsoon variability over the northern Sahara. *Climate Dynamics*, *21*(7-8), 689–698. DOI: 10.1007/s00382-003-0355-z.

Levis, S., Bonan, G. B., & Bonfils, C. (2004). Soil feedback drives the mid-Holocene North African monsoon northward in fully coupled CCSM2 simulations with a dynamic vegetation model. *Climate Dynamics*, *23*(7-8), 791–802. DOI: 10.1007/s00382-004-0477-y.

Lézine, A.-M. (2017). Vegetation at the time of the African Humid Period. In *Oxford research encyclopedia of climate science* (pp. 1–25). Oxford University Press. DOI: 10.1093/acrefore/9780190228620.013.530.

Lézine, A.-M., & Casanova, J. (1991). Correlated oceanic and continental records demonstrate past climate and hydrology of North Africa (0-140 ka). *Geology*, *19*(4), 307. DOI: 10.1130/0091-7613(1991)019<0307:COACRD>2.3.CO;2.

Lézine, A.-M., Hély, C., Grenier, C., Braconnot, P., & Krinner, G. (2011). Sahara and Sahel vulnerability to climate changes, lessons from Holocene hydrological data. *Quaternary Science Reviews*, *30*(21-22), 3001–3012. DOI: 10.1016/j.quascirev.2011.07.006.

Lisiecki, L. E., & Raymo, M. E. (2005). A Pliocene-Pleistocene stack of 57 globally distributed benthic δ^{18}O records. *Paleoceanography*, *20*(1, PA1003), 1–17. DOI: 10.1029/2004pa001071.

Liu, Z., Harrison, S. P., Kutzbach, J. E., & Otto-Bliesner, B. L. (2004). Global monsoons in the mid-Holocene and oceanic feedback. *Climate Dynamics*, *22*(2-3), 157–182. DOI: 10.1007/s00382-003-0372-y.

Liu, Z., Wang, Y., Gallimore, R., Notaro, M., & Prentice, I. C. (2006). On the cause of abrupt vegetation collapse in North Africa during the Holocene: Climate variability vs. vegetation feedback. *Geophysical Research Letters*, *33*(22, L22709), 1–6. DOI: 10.1029/2006gl028062.

Lourens, L. J., Wehausen, R., & Brumsack, H. J. (2001). Geological constraints on tidal dissipation and dynamical ellipticity of

the Earth over the past three million years. *Nature*, *409*(6823), 1029–1033. DOI: 10.1038/35059062.

Lunt, D. J., Abe-Ouchi, A., Bakker, P., Berger, A., Braconnot, P., Charbit, S., Fischer, N., Herold, N., Jungclaus, J. H., Khon, V. C., Krebs-Kanzow, U., Langebroek, P. M., Lohmann, G., Nisancioglu, K. H., Otto-Bliesner, B. L., Park, W., Pfeiffer, M., Phipps, S. J., Prange, M., ... Zhang, Z. S. (2013). A multi-model assessment of last interglacial temperatures. *Climate of the Past*, *9*(2), 699–717. DOI: 10.5194/cp-9-699-2013.

Lüthi, D., Floch, M. L., Bereiter, B., Blunier, T., Barnola, J.-M., Siegenthaler, U., Raynaud, D., Jouzel, J., Fischer, H., Kawamura, K., & Stocker, T. F. (2008). High-resolution carbon dioxide concentration record 650,000–800,000 years before present. *Nature*, *453*(7193), 379–382. DOI: 10.1038/nature06949.

Manning, K., & Timpson, A. (2014). The demographic response to Holocene climate change in the Sahara. *Quaternary Science Reviews*, *101*, 28–35. DOI: 10.1016/j.quascirev.2014.07.003.

Marzin, C., Braconnot, P., & Kageyama, M. (2013). Relative impacts of insolation changes, meltwater fluxes and ice sheets on African and Asian monsoons during the Holocene. *Climate Dynamics*, *41*(9-10), 2267–2286. DOI: 10.1007/s00382-013-1948-9.

Masson-Delmotte, V., Schulz, M., Abe-Ouchi, A., Beer, J., Ganopolski, A., González Rouco, J. F., Jansen, E., Lambeck, K., Luterbacher, J., Naish, T., Osborn, T., Otto-Bliesner, B. L., Quinn, T., Ramesh, R., Rojas, M., Shao, X., & Timmermann, A. (2013). Information from paleoclimate archives. In T. F. Stocker, D. Qin, G.-K. Plattner, M. M. B. Tignor, S. K. Allen, J. Boschung, A. Nauels, Y. Xia, V. Bex, & P. M. Midgley (Eds.), *Climate change 2013: The physical science basis. contribution of working group i to the fifth assessment report of the intergovernmental panel on climate change* (pp. 383–464). Cambridge University Press. DOI: 10.1017/CBO9781107415324.013.

Mauritsen, T., Bader, J., Becker, T., Behrens, J., Bittner, M., Brokopf, R., Brovkin, V., Claussen, M., Crueger, T., Esch, M., et al. (2019). Developments in the MPI-M Earth System Model version 1.2 (MPI-ESM1.2) and its response to increasing CO2. *Journal of Advances in Modeling Earth Systems*, *11*(4), 998–1038. DOI: 10.1029/2018MS001400.

McGee, D., & deMenocal, P. B. (2017). Climatic changes and cultural responses during the African Humid Period recorded in multiproxy data. In *Oxford research encyclopedia of climate science* (pp. 1–45). Oxford University Press. DOI: 10.1093/acrefore/9780190228620.013.529.

McGee, D., deMenocal, P. B., Winckler, G., Stuut, J.-B. W., & Bradtmiller, L. I. (2013). The magnitude, timing and abruptness of changes in North African dust deposition over the last

20,000 yr. *Earth and Planetary Science Letters*, *371*, 163–176. DOI: 10.1016/j.epsl.2013.03.054.

Meccia, V. L., & Mikolajewicz, U. (2018). Interactive ocean bathymetry and coastlines for simulating the last deglaciation with the Max Planck Institute Earth System Model (MPI-ESM-v1. 2). *Geoscientific Model Development*, *11*(11), 4677–4692. DOI: 10.5194/gmd-11-4677-2018.

Meinshausen, M., Nicholls, Z. R. J., Lewis, J., Gidden, M. J., Vogel, E., Freund, M., Beyerle, U., Gessner, C., Nauels, A., Bauer, N., Canadell, J. G., Daniel, J. S., John, A., Krummel, P. B., Luderer, G., Meinshausen, N., Montzka, S. A., Rayner, P. J., Reimann, S., ... Wang, R. H. J. (2020). The shared socio-economic pathway (SSP) greenhouse gas concentrations and their extensions to 2500. *Geoscientific Model Development*, *13*(8), 3571–3605. DOI: 10.5194/gmd-13-3571-2020.

Menviel, L., Govin, A., Avenas, A., Meissner, K. J., Grant, K. M., & Tzedakis, P. C. (2021). Drivers of the evolution and amplitude of African Humid Periods. *Communications Earth & Environment*, *2*(237), 1–11. DOI: 10.1038/s43247-021-00309-1.

Mikolajewicz, U., Ziemen, F., Cioni, G., Claussen, M., Fraedrich, K. F., Heidkamp, M., Hohenegger, C., de la Cuesta, D. J., Kapsch, M.-L., Lemburg, A., Mauritsen, T., Meraner, K., Röber, N., Schmidt, H., Six, K. D., Stemmler, I., Tamarin-Brodsky, T., Winkler, A., Zhu, X., & Stevens, B. (2018). The climate of a retrograde rotating Earth. *Earth System Dynamics*, *9*, 1191–1215. DOI: 10.5194/esd-9-1191-2018.

Milankovitch, M. (1941). *Kanon der Erdbestrahlung und seine Anwendung auf das Eiszeitenproblem* (Vol. 33). Königlich Serbische Akademie.

Nicholson, S. E., & Flohn, H. (1980). African environmental and climatic changes and the general atmospheric circulation in late Pleistocene and Holocene. *Climatic Change*, *2*(4), 313–348. DOI: 10.1007/bf00137203.

Nicoll, K. (2004). Recent environmental change and prehistoric human activity in Egypt and Northern Sudan. *Quaternary Science Reviews*, *23*(5-6), 561–580. DOI: 10.1016/j.quascirev.2003.10.004.

Notaro, M., Wang, Y., Liu, Z., Gallimore, R., & Levis, S. (2008). Combined statistical and dynamical assessment of simulated vegetation-rainfall interactions in North Africa during the mid-Holocene. *Global Change Biology*, *14*(2), 347–368. DOI: 10.1111/j.1365-2486.2007.01495.x.

O'Mara, N. A., Skonieczny, C., McGee, D., Winckler, G., Bory, A. J.-M., Bradtmiller, L. I., Malaizé, B., & Polissar, P. J. (2022). Pleistocene drivers of Northwest African hydroclimate and vegetation. *Nature Communications*, *13*(3552), 1–11. DOI: 10.1038/s41467-022-31120-x.

Osman, M. B., Tierney, J. E., Zhu, J., Tardif, R., Hakim, G. J., King, J., & Poulsen, C. J. (2021). Globally resolved surface temperatures since the Last Glacial Maximum. *Nature*, *599*(7884), 239–244. DOI: 10.1038/s41586-021-03984-4.

Otto-Bliesner, B. L., Braconnot, P., Harrison, S. P., Lunt, D. J., Abe-Ouchi, A., Albani, S., Bartlein, P. J., Capron, E., Carlson, A. E., Dutton, A., Fischer, H., Goelzer, H., Govin, A., Haywood, A., Joos, F., LeGrande, A. N., Lipscomb, W. H., Lohmann, G., Mahowald, N., … Zhang, Q. (2017). The PMIP4 contribution to CMIP6 – Part 2: Two interglacials, scientific objective and experimental design for Holocene and Last Interglacial simulations. *Geoscientific Model Development*, *10*(11), 3979–4003. DOI: 10.5194/gmd-10-3979-2017.

Otto-Bliesner, B. L., Brady, E. C., Zhao, A., Brierley, C. M., Axford, Y., Capron, E., Govin, A., Hoffman, J. S., Isaacs, E., Kageyama, M., Scussolini, P., Tzedakis, P. C., Williams, C. J. R., Wolff, E., Abe-Ouchi, A., Braconnot, P., Buarque, S. R., Cao, J., de Vernal, A., … Zheng, W. (2021). Large-scale features of Last Interglacial climate: Results from evaluating the lig127k simulations for the Coupled Model Intercomparison Project (CMIP6) – Paleoclimate Modeling Intercomparison Project (PMIP4). *Climate of the Past*, *17*(1), 63–94. DOI: 10.5194/cp-17-63-2021.

Pachur, H.-J., & Hoelzmann, P. (1991). Paleoclimatic implications of late Quaternary lacustrine sediments in Western Nubia, Sudan. *Quaternary Research*, *36*(3), 257–276. DOI: 10.1016/0033-5894(91)90002-m.

Pachur, H.-J., & Hoelzmann, P. (2000). Late Quaternary palæoecology and palæoclimates of the eastern Sahara. *Journal of African Earth Sciences*, *30*(4), 929–939. DOI: 10.1016/s0899-5362(00)00061-0.

Past Interglacials Working Group of PAGES. (2016). Interglacials of the last 800,000 years. *Reviews of Geophysics*, *54*(1), 162–219. DOI: 10.1002/2015rg000482.

Pausata, F. S. R., Messori, G., & Zhang, Q. (2016). Impacts of dust reduction on the northward expansion of the African monsoon during the Green Sahara period. *Earth and Planetary Science Letters*, *434*, 298–307. DOI: 10.1016/j.epsl.2015.11.049.

Pausata, F. S. R., Gaetani, M., Messori, G., Berg, A., de Souza, D. M., Sage, R. F., & deMenocal, P. B. (2020). The greening of the Sahara: Past changes and future implications. *One Earth*, *2*(3), 235–250. DOI: 10.1016/j.oneear.2020.03.002.

Peltier, W. R. (1994). Ice age paleotopography. *Science*, *265*(5169), 195–201. DOI: 10.1126/science.265.5169.195.

Perez-Sanz, A., Li, G., González-Sampériz, P., & Harrison, S. P. (2014). Evaluation of modern and mid-Holocene seasonal precipitation of the Mediterranean and northern Africa in the CMIP5

simulations. *Climate of the Past*, *10*(2), 551–568. DOI: 10.5194/cp-10-551-2014.

Petit, J. R., Jouzel, J., Raynaud, D., Barkov, N. I., Barnola, J.-M., Basile, I., Bender, M., Chappellaz, J., Davis, M., Delaygue, G., Delmotte, M., Kotlyakov, V. M., Legrand, M., Lipenkov, V. Y., Lorius, C., PÉpin, L., Ritz, C., Saltzman, E., & Stievenard, M. (1999). Climate and atmospheric history of the past 420,000 years from the Vostok ice core, Antarctica. *Nature*, *399*(6735), 429–436. DOI: 10.1038/20859.

Petit-Maire, N. (1996). Climatic change and cultural change in the Sahara over the last 130 Ka. In A. N. Angelakis & A. S. Issar (Eds.), *Diachronic climatic impacts on water resources* (pp. 1–7, Vol. 36). Springer Berlin Heidelberg. DOI: 10.1007/978-3-642-61084-4_1.

Petoukhov, V., Ganopolski, A., Brovkin, V., Claussen, M., Eliseev, A., Kubatzki, C., & Rahmstorf, S. (2000). CLIMBER-2: A climate system model of intermediate complexity. part I: Model description and performance for present climate. *Climate Dynamics*, *16*(1), 1–17. DOI: 10.1007/pl00007919.

Pokras, E. M., & Mix, A. C. (1985). Eolian evidence for spatial variability of late Quaternary climates in tropical Africa. *Quaternary Research*, *24*(2), 137–149. DOI: 10.1016/0033-5894(85)90001-8.

Pokras, E. M., & Mix, A. C. (1987). Earth's precession cycle and Quaternary climatic change in tropical Africa. *Nature*, *326*(6112), 486–487. DOI: 10.1038/326486a0.

Prell, W. L., & Kutzbach, J. E. (1987). Monsoon variability over the past 150,000 years. *Journal of Geophysical Research*, *92*(D7), 8411–8425. DOI: 10.1029/JD092iD07p08411.

Quade, J., Dente, E., Armon, M., Dor, Y. B., Morin, E., Adam, O., & Enzel, Y. (2018). Megalakes in the Sahara? a review. *Quaternary Research*, *90*(2), 253–275. DOI: 10.1017/qua.2018.46.

Rachmayani, R., Prange, M., & Schulz, M. (2015). North African vegetation–precipitation feedback in early and mid-Holocene climate simulations with CCSM3-DGVM. *Climate of the Past*, *11*(2), 175–185. DOI: 10.5194/cp-11-175-2015.

Railsback, L. B., Gibbard, P. L., Head, M. J., Voarintsoa, N. R. G., & Toucanne, S. (2015). An optimized scheme of lettered marine isotope substages for the last 1.0 million years, and the climatostratigraphic nature of isotope stages and substages. *Quaternary Science Reviews*, *111*, 94–106. DOI: 10.1016/j.quascirev.2015.01.012.

Rea, D. K. (1994). The paleoclimatic record provided by eolian deposition in the deep sea: The geologic history of wind. *Reviews of Geophysics*, *32*(2), 159–195. DOI: 10.1029/93rg03257.

Reick, C. H., Raddatz, T., Brovkin, V., & Gayler, V. (2013). Representation of natural and anthropogenic land cover change in

MPI-ESM. *Journal of Advances in Modeling Earth Systems*, *5*(3), 459–482. DOI: 10.1002/jame.20022.

Reick, C. H., Gayler, V., Goll, D., Hagemann, S., Heidkamp, M., Nabel, J. E. M. S., Raddatz, T., Roeckner, E., Schnur, R., & Wilkenskjeld, S. (2021). *JSBACH 3 - The land component of the MPI Earth System Model: Documentation of version 3.2* (Vol. 240). Max Planck Institute for Meteorology. DOI: 10.17617/2.3279802.

Renssen, H., Brovkin, V., Fichefet, T., & Goosse, H. (2003). Holocene climate instability during the termination of the African Humid Period. *Geophysical Research Letters*, *30*(4, 1184), 1–4. DOI: 10.1029/2002gl016636.

Riddick, T., Brovkin, V., Hagemann, S., & Mikolajewicz, U. (2018). Dynamic hydrological discharge modelling for coupled climate model simulations of the last glacial cycle: The MPI-DynamicHD model version 3.0. *Geoscientific Model Development*, *11*(10), 4291–4316. DOI: 10.5194/gmd-11-4291-2018.

Ritchie, J. C., Eyles, C. H., & Haynes, C. V. (1985). Sediment and pollen evidence for an early to mid-Holocene humid period in the eastern Sahara. *Nature*, *314*(6009), 352–355. DOI: 10.1038/314352a0.

Rohling, E. J., Marino, G., & Grant, K. M. (2015). Mediterranean climate and oceanography, and the periodic development of anoxic events (sapropels). *Earth-Science Reviews*, *143*, 62–97. DOI: 10.1016/j.earscirev.2015.01.008.

Rossignol-Strick, M. (1983). African monsoons, an immediate climate response to orbital insolation. *Nature*, *304*(5921), 46–49. DOI: 10.1038/304046a0.

Rossignol-Strick, M. (1985). Mediterranean Quaternary sapropels, an immediate response of the African monsoon to variation of insolation. *Palaeogeography, Palaeoclimatology, Palaeoecology*, *49*(3-4), 237–263. DOI: 10.1016/0031-0182(85)90056-2.

Rossignol-Strick, M., Nesteroff, W., Olive, P., & Vergnaud-Grazzini, C. (1982). After the deluge: Mediterranean stagnation and sapropel formation. *Nature*, *295*(5845), 105–110. DOI: 10.1038/295105a0.

Sarnthein, M. (1978). Sand deserts during glacial maximum and climatic optimum. *Nature*, *272*(5648), 43–46. DOI: 10.1038/272043a0.

Scerri, E. M. L. (2017). The North African Middle Stone Age and its place in recent human evolution. *Evolutionary Anthropology*, *26*(3), 119–135. DOI: 10.1002/evan.21527.

Scerri, E. M. L., Drake, N. A., Jennings, R., & Groucutt, H. S. (2014). Earliest evidence for the structure of Homo sapiens populations in Africa. *Quaternary Science Reviews*, *101*, 207–216. DOI: 10.1016/j.quascirev.2014.07.019.

Scerri, E. M. L., Thomas, M. G., Manica, A., Gunz, P., Stock, J. T., Stringer, C., Grove, M., Groucutt, H. S., Timmermann, A., Rightmire, G. P., d'Errico, F., Tryon, C. A., Drake, N. A., Brooks, A. S., Dennell, R. W., Durbin, R., Henn, B. M., Lee-Thorp, J., deMenocal, P. B., ... Chikhi, L. (2018). Did our species evolve in subdivided populations across Africa, and why does it matter? *Trends in Ecology & Evolution*, *33*(8), 582–594. DOI: 10.1016/j.tree.2018.05.005.

Scussolini, P., Bakker, P., Guo, C., Stepanek, C., Zhang, Q., Braconnot, P., Cao, J., Guarino, M.-V., Coumou, D., Prange, M., Ward, P. J., Renssen, H., Kageyama, M., Otto-Bliesner, B. L., & Aerts, J. C. J. H. (2019). Agreement between reconstructed and modeled boreal precipitation of the Last Interglacial. *Science Advances*, *5*(11, eaax7047), 1–11. DOI: 10.1126/sciadv.aax7047.

Scussolini, P., Eilander, D., Sutanudjaja, E. H., Ikeuchi, H., Hoch, J. M., Ward, P. J., Bakker, P., Otto-Bliesner, B. L., Guo, C., Stepanek, C., Zhang, Q., Braconnot, P., Guarino, M.-V., Muis, S., Yamazaki, D., Veldkamp, T. I. E., & Aerts, J. C. J. H. (2020). Global river discharge and floods in the warmer climate of the Last Interglacial. *Geophysical Research Letters*, *47*(e2020GL089375), 1–12. DOI: 10.1029/2020gl089375.

Shanahan, T. M. (2018). Quaternary climate variation in West Africa. In *Oxford research encyclopedia of climate science* (pp. 1–41). Oxford University Press. DOI: 10.1093/acrefore/9780190228620.013.526.

Shanahan, T. M., McKay, N. P., Hughen, K. A., Overpeck, J. T., Otto-Bliesner, B. L., Heil, C. W., King, J., Scholz, C. A., & Peck, J. (2015). The time-transgressive termination of the African Humid Period. *Nature Geoscience*, *8*(2), 140–144. DOI: 10.1038/ngeo2329.

Singarayer, J. S., & Burrough, S. L. (2015). Interhemispheric dynamics of the African rainbelt during the late Quaternary. *Quaternary Science Reviews*, *124*, 48–67. DOI: 10.1016/j.quascirev.2015.06.021.

Skonieczny, C., McGee, D., Winckler, G., Bory, A., Bradtmiller, L. I., Kinsley, C. W., Polissar, P. J., Pol-Holz, R. D., Rossignol, L., & Malaizé, B. (2019). Monsoon-driven Saharan dust variability over the past 240,000 years. *Science Advances*, *5*(1, eaav1887), 1–8. DOI: 10.1126/sciadv.aav1887.

Smith, J. R., Giegengack, R., Schwarcz, H. P., McDonald, M. M. A., Kleindienst, M. R., Hawkins, A. L., & Churcher, C. S. (2004). A reconstruction of Quaternary pluvial environments and human occupations using stratigraphy and geochronology of fossil-spring tufas, Kharga Oasis, Egypt. *Geoarchaeology*, *19*(5), 407–439. DOI: 10.1002/gea.20004.

Specht, N. F., Claussen, M., & Kleinen, T. (2022). Simulated range of mid-Holocene precipitation changes from extended lakes and

wetlands over North Africa. *Climate of the Past*, *18*(5), 1035–1046. DOI: 10.5194/cp-18-1035-2022.

Stein, U., & Alpert, P. (1993). Factor separation in numerical simulations. *Journal of the Atmospheric Sciences*, *50*(14), 2107–2115. DOI: 10.1175/1520-0469(1993)050<2107:fsins>2.0.co;2.

Stevens, B., Giorgetta, M., Esch, M., Mauritsen, T., Crueger, T., Rast, S., Salzmann, M., Schmidt, H., Bader, J., Block, K., Brokopf, R., Fast, I., Kinne, S., Kornblueh, L., Lohmann, U., Pincus, R., Reichler, T., & Roeckner, E. (2013). Atmospheric component of the MPI-M Earth system model: ECHAM6. *Journal of Advances in Modeling Earth Systems*, *5*(2), 146–172. DOI: 10.1002/jame.20015.

Stocker, T. F., Mysak, L. A., & Wright, D. G. (1992). A zonally averaged, coupled ocean-atmosphere model for paleoclimate studies. *Journal of Climate*, *5*(8), 773–797. DOI: 10.1175/1520-0442(1992)005<0773:azacoa>2.0.co;2.

Street, F. A., & Grove, A. T. (1976). Environmental and climatic implications of late Quaternary lake-level fluctuations in Africa. *Nature*, *261*(5559), 385–390. DOI: 10.1038/261385a0.

Tarasov, L., Dyke, A. S., Neal, R. M., & Peltier, W. R. (2012). A data-calibrated distribution of deglacial chronologies for the North American ice complex from glaciological modeling. *Earth and Planetary Science Letters*, *315*, 30–40. DOI: 10.1016/j.epsl.2011.09.010.

Tarasov, L., Hughes, A., Gyllencreutz, R., Lohne, O. S., Mangerud, J., & Svendsen, J.-I. (2014). The global GLAC-1C deglaciation chronology, melwater pulse 1-a, and a question of missing ice. *IGS Symposium on Contribution of Glaciers and Ice Sheets to Sea-Level Change*.

Tarasov, L., & Peltier, W. R. (2002). Greenland glacial history and local geodynamic consequences. *Geophysical Journal International*, *150*(1), 198–229. DOI: 10.1046/j.1365-246x.2002.01702.x.

Texier, D., de Noblet, N., Harrison, S. P., Haxeltine, A., Jolly, D., Joussaume, S., Laarif, F., Prentice, I. C., & Tarasov, P. (1997). Quantifying the role of biosphere-atmosphere feedbacks in climate change: Coupled model simulations for 6000 years BP and comparison with palaeodata for northern Eurasia and northern Africa. *Climate Dynamics*, *13*(12), 865–881. DOI: 10.1007/s003820050202.

Thompson, A. J., Skinner, C. B., Poulsen, C. J., & Zhu, J. (2019). Modulation of mid-Holocene African rainfall by dust aerosol direct and indirect effects. *Geophysical Research Letters*, *46*(7), 3917–3926. DOI: 10.1029/2018GL081225.

Tierney, J. E., deMenocal, P. B., & Zander, P. D. (2017a). A climatic context for the out-of-Africa migration. *Geology*, *45*(11), 1023–1026. DOI: 10.1130/G39457.1.

Tierney, J. E., Pausata, F. S. R., & deMenocal, P. B. (2017b). Rainfall regimes of the Green Sahara. *Science Advances*, *3*(1, e1601503), 1–9. DOI: 10.1126/sciadv.1601503.

Tierney, J. E., Zhu, J., King, J., Malevich, S. B., Hakim, G. J., & Poulsen, C. J. (2020a). Glacial cooling and climate sensitivity revisited. *Nature*, *584*(7822), 569–573. DOI: 10.1038/s41586-020-2617-x.

Tierney, J. E., Poulsen, C. J., Montañez, I. P., Bhattacharya, T., Feng, R., Ford, H. L., Hönisch, B., Inglis, G. N., Petersen, S. V., Sagoo, N., Tabor, C. R., Thirumalai, K., Zhu, J., Burls, N. J., Foster, G. L., Goddéris, Y., Huber, B. T., Ivany, L. C., Turner, S. K., … Zhang, Y. G. (2020b). Past climates inform our future. *Science*, *370*(6517, eaay3701), 1–9. DOI: 10.1126/science.aay3701.

Timm, O., Köhler, P., Timmermann, A., & Menviel, L. (2010). Mechanisms for the onset of the African Humid Period and Sahara greening 14.5–11 ka BP. *Journal of Climate*, *23*(10), 2612–2633. DOI: 10.1175/2010JCLI3217.1.

Tjallingii, R., Claussen, M., Stuut, J.-B. W., Fohlmeister, J., Jahn, A., Bickert, T., Lamy, F., & Röhl, U. (2008). Coherent high- and low-latitude control of the northwest African hydrological balance. *Nature Geoscience*, *1*(10), 670–675. DOI: 10.1038/ngeo289.

Tuenter, E., Weber, S. L., Hilgen, F. J., & Lourens, L. J. (2003). The response of the African summer monsoon to remote and local forcing due to precession and obliquity. *Global and Planetary Change*, *36*(4), 219–235. DOI: 10.1016/s0921-8181(02)00196-0.

Tuenter, E., Weber, S. L., Hilgen, F. J., Lourens, L. J., & Ganopolski, A. (2005). Simulation of climate phase lags in response to precession and obliquity forcing and the role of vegetation. *Climate Dynamics*, *24*(2-3), 279–295. DOI: 10.1007/s00382-004-0490-1.

Turney, C. S. M., & Jones, R. T. (2010). Does the Agulhas Current amplify global temperatures during super-interglacials? *Journal of Quaternary Science*, *25*(6), 839–843. DOI: 10.1002/jqs.1423.

Vamborg, F. S. E., Brovkin, V., & Claussen, M. (2011). The effect of a dynamic background albedo scheme on Sahel/Sahara precipitation during the mid-Holocene. *Climate of the Past*, *7*(1), 117–131. DOI: 10.5194/cp-7-117-2011.

Vernekar, A. D. (1972). Long-Period Global Variations of Incoming Solar Radiation. In *Long-Period Global Variations of Incoming Solar Radiation* (pp. 1–128, Vol. 12). American Meteorological Society. DOI: 10.1007/978-1-935704-34-8_1.

Waelbroeck, C., Labeyrie, L., Michel, E., Duplessy, J. C., McManus, J. F., Lambeck, K., Balbon, E., & Labracherie, M. (2002). Sea-level and deep water temperature changes derived from benthic foraminifera isotopic records. *Quaternary Science Reviews*, *21*(1-3), 295–305. DOI: 10.1016/s0277-3791(01)00101-9.

Wagner, B., Vogel, H., Francke, A., Friedrich, T., Donders, T., Lacey, J. H., Leng, M. J., Regattieri, E., Sadori, L., Wilke, T., Zanchetta, G., Albrecht, C., Bertini, A., Combourieu-Nebout, N., Cvetkoska, A., Giaccio, B., Grazhdani, A., Hauffe, T., Holtvoeth, J., … Zhang, X. (2019). Mediterranean winter rainfall in phase with African monsoons during the past 1.36 million years. *Nature*, *573*(7773), 256–260. DOI: 10.1038/s41586-019-1529-0.

Wang, P. X., Wang, B., Cheng, H., Fasullo, J., Guo, Z. T., Kiefer, T., & Liu, Z. (2014). The global monsoon across timescales: Coherent variability of regional monsoons. *Climate of the Past*, *10*(6), 2007–2052. DOI: 10.5194/cp-10-2007-2014.

Watrin, J., Lézine, A.-M., & Hély, C. (2009). Plant migration and plant communities at the time of the "green Sahara". *Comptes Rendus Geoscience*, *341*(8-9), 656–670. DOI: 10.1016/j.crte.2009.06.007.

Webb III, T., & Kutzbach, J. E. (1998). An introduction to 'Late Quaternary climates: Data syntheses and model experiments'. *Quaternary Science Reviews*, *17*(6-7), 465–471. DOI: 10.1016/s0277-3791(98)00008-0.

Weber, S. L., & Tuenter, E. (2011). The impact of varying ice sheets and greenhouse gases on the intensity and timing of boreal summer monsoons. *Quaternary Science Reviews*, *30*(3-4), 469–479. DOI: 10.1016/j.quascirev.2010.12.009.

Weldeab, S., Lea, D. W., Schneider, R. R., & Andersen, N. (2007). 155,000 years of West African Monsoon and ocean thermal evolution. *Science*, *316*(5829), 1303–1307. DOI: 10.1126/science.1140461.

Westerhold, T., Marwan, N., Drury, A. J., Liebrand, D., Agnini, C., Anagnostou, E., Barnet, J. S. K., Bohaty, S. M., Vleeschouwer, D. D., Florindo, F., Frederichs, T., Hodell, D. A., Holbourn, A. E., Kroon, D., Lauretano, V., Littler, K., Lourens, L. J., Lyle, M., Pälike, H., … Zachos, J. C. (2020). An astronomically dated record of Earth's climate and its predictability over the last 66 million years. *Science*, *369*(6509), 1383–1387. DOI: 10.1126/science.aba6853.

Wilkinson, R. D. (2010, October). Bayesian calibration of expensive multivariate computer experiments. In L. Biegler, G. Biros, O. Ghattas, M. Heinkenschloss, D. Keyes, B. Mallick, Y. Marzouk, L. Tenorio, B. van Bloemen Waanders, & K. Willcox (Eds.), *Large-scale inverse problems and quantification of uncertainty* (pp. 195–215). Wiley. DOI: 10.1002/9780470685853.ch10.

Yacoub, A. N., Sylvestre, F., Moussa, A., Hoelzmann, P., Alexandre, A., Dinies, M., Chalié, F., Vallet-Coulomb, C., Paillès, C., Darius, F., Sonzogni, C., Couapel, M., Mazur, J.-C., & Kröpelin, S. (2023). The African Holocene Humid Period in the Tibesti mountains (central Sahara, Chad): Climate reconstruction inferred from fossil diatoms and their oxygen isotope composition. *Quater-*

nary Science Reviews, *308*(108099), 1–17. DOI: 10.1016/j.quascirev.2023.108099.

Zhao, Y., Braconnot, P., Marti, O., Harrison, S. P., Hewitt, C., Kitoh, A., Liu, Z., Mikolajewicz, U., Otto-Bliesner, B. L., & Weber, S. L. (2005). A multi-model analysis of the role of the ocean on the African and Indian monsoon during the mid-Holocene. *Climate Dynamics*, *25*(7-8), 777–800. DOI: 10.1007/s00382-005-0075-7.

Ziegler, M., Tuenter, E., & Lourens, L. J. (2010). The precession phase of the boreal summer monsoon as viewed from the eastern Mediterranean (ODP Site 968). *Quaternary Science Reviews*, *29*(11-12), 1481–1490. DOI: 10.1016/j.quascirev.2010.03.011.

LIST OF FIGURES

LIST OF TABLES

ACKNOWLEDGEMENTS

I am grateful for the opportunity and the support that has allowed me to complete the work in this thesis. I have been so fortunate to immerse myself in an interesting topic for consecutive years. I thank my supervisors Martin Claussen, Victor Brovkin and Thomas Kleinen for their constant support and patience to reply countless emails, and for guiding me through technical and theoretical complexities of modelling the Earth system. Their wide-angle view on the problem at hand was always encouraging, by constantly stressing how small bits of results mattered for the big picture.

Many thanks also to Gerhard Schmiedl for leading interesting discussions during advisory meetings and the invitations to learn more about the data motivating our research. This work owes a lot also to the feedback I got during research group meetings, by Anne Dallmeyer, Jürgen Bader, Roberta D'Agostino, Pin-hsin Hu, Nora Specht, Leonore Jungandreas, Josephine Wong, Koushikh Karunakar, Manuel Chevalier and Christian Reick. I would also like to thank colleagues in the research group CLICCS–A4 at the University of Hamburg, for their feedback and discussions.

Many thanks to Antje Weitz, Cornelia Kampmann and Michaela Born, who not only work tirelessly to keep the doctoral program running smoothly, but also were always ready with encouraging smiles and advice. My gratitude extends to the entire research school, whose graduate students represented me in corporate meetings, gave me valuable input during institute retreats, and planned social activities. Especial thanks to Diego Jiménez de la Cuesta, Laura Paccini, Geet George, David Marcolino Nielsen, Zoé Rehder, Arjun Kumar, Lennart Ramme, Iana Strigunova, Daniel Burt, Clara Henry, Jacqueline Behncke, Luca Schmidt, Moritz Günther, John Ssebandeke, Markus Ritschel, Jiawei Bao, and Hans Segura. And to Meike Schickhoff, Pin-hsin Hu, Nora Specht, István Dunkl, Constanze Reinken and Jun Liu for all the help and nice times. Also thanks to Jairo Segura, Janine Börker, Paul Keil, Hauke Schmidt and football fans for all the fun.

And none of this would come to be without the unwavering support from my family. Muchísimas gracias a toda mi familia. Siento su inagotable apoyo en cada paso. Gracias a mi papá y mi mamá, gracias a Simón, y gracias a Irma, Darío, Lore, Adrián y Mati. Por último y por encima de todo, gracias infinitas a mi Mel, que estuvo siempre a mi lado y es quien le da sentido a todo lo que hago.

This document was typeset using
the typographical look-and-feel
`classicthesis` developed by
André Miede and Ivo Pletikosić.